Thèse de doctorat

Université de Limoges

Université de Limoges

École Doctorale Bio-Santé (ED 524)

Faculté de Sciences et Techniques – XLIM Équipe BioEM

Thèse pour obtenir le grade de

Docteur de l'Université de Limoges

Discipline – Biologie, médicine et santé

Présentée et soutenue par

Ryan Burke

Le 19 décembre 2017

Investigating the role of voltage-gated ion channels in pulsed electric field effects in excitable and non-excitable cell lines

Thèse dirigée par Dr. Philippe Leveque

Co-dirigée par Dr. Sylvia Bardet

JURY :

Président du jury	
Mme. Catherine YARDIN	Professeur des universités, Praticien hospitalier
Rapporteurs	
M. Justin TEISSIE	Directeur de recherche CNRS, émérite
M. Yann PERCHERANCIER	Chargé de recherche CNRS, HDR
Examinateurs	
M. Mounir TAREK	Directeur de recherche CNRS
Mme Sylvia BARDET	Maître de conférences, Université de Limoges
M. Philippe LEVEQUE	Directeur de recherche CNRS

Structure of the thesis

All experiments described in this thesis were conducted over the period of 2014 – 2017. They were carried out primarily in the Bioelectromagnetics lab at XLIM Research Institute in Limoges, France. Another portion of the data presented in this thesis was the result of a collaboration with the group at the Biocybernetics lab at the University of Ljubljana.

The thesis is outlined as follows:

- Chapter 1 provides a review of the literature and describes the general methodology for this thesis.
- Chapter 2 is the first experimental section that employs advanced biostatistics to examine how well data can be predicted using common parameters present in current electrophysical models of electropermeabilization.
- Chapter 3 looks at the effects of nanosecond pulsed electric fields on the transmembrane potential in U87 glioblastoma cells. Using a host of pharmacological modulators of ion channel activity, the role of voltage-gated ion channels is explored.
- Chapter 4 is the result of a collaborative exchange with the University of Ljubljana. We look at the effect of pulsed electric fields, ranging from 10 ns to 10 ms, on membrane potential and membrane permeability of several cell lines.
- Chapter 5 begins with a brief summary of each chapter, and then moves into a more global discussion of how our results contribute to the current literature.

Acknowledgements

There are so many people that I wish to thank for their inspiration, support and guidance.

I would like to thank Dr. Michael Persinger who was my thesis supervisor during my B.Sc. and M.Sc. candidacy. You have inspired me in ways you will never know. You demanded excellence and creativity and pushed me to grow beyond what I imagined possible. I am grateful, maybe above all, for your emphasis on developing a very strong knowledge of biostatistics. There is no tool more important or more powerful in science than the ability to properly measure and interpret experimental data.

Thank you to Dr. Philippe Leveque. Despite being overwhelmed with a tremendous work load, you took me on as your student half way through my Ph.D. Thank you for all of your guidance and support. If I could go back in time, I would have selected you as my supervisor for my entire Ph.D.

I am grateful to several colleagues who I am happy to call friends. Lynn, Maarten and Stine, you all have helped so much. What an honor to have worked with you. I wish you all prosperity and happiness in your future endeavors.

Thank you to my amazing family. Mom, you are one of the most inspiring people I have ever known. I am here because of you. Thank you for everything you have ever done for your family. I cherish you. Dad, I can't begin to express how much I miss you. You taught me what it means to be a man. You taught me to pursue my dreams and to never give up. This thesis is dedicated to your memory. Cancer took you from us, and I hope that my humble contribution to the field of cancer research would have made you proud. Tom, you are such an amazing brother. Although you're my younger brother, I have always looked up to your incredible work ethic. I am so proud of the man you have grown into. You deserve nothing but excellence. Les, I hope you realize that I love you so much. You too are an amazing man and I am so happy for you and your beautiful family. I have the best brothers ever! I love you all!

To the love of my life, Melanie. You have no idea how much you mean to me. You put all of your dreams on hold for me to be here today. When faced with the idea of selling everything you own and flying across the ocean far away from your family friends, you didn't hesitate for one second. There is no luckier man than I. You are truly a remarkable woman! I feel blessed for every moment we share and I look forward to the next chapter of our lives. From the bottom of my heart, thank you.

Abstract (English)

The use of pulsed electric fields (PEF) in medical and biotechnology sectors has become increasingly prevalent over the last few decades. Research has shown that by adjusting the duration of the PEF we can predict what effects will be observed. Whereas PEF in the micro-to-millisecond range have been used to permeabilize the cell membrane and enhance drug or protein uptake, nanosecond PEF (nsPEF) have demonstrated unique effects on intracellular organelles. Both PEF and nsPEF have demonstrated therapeutic potential for a variety of human pathologies, including the treatment of cancer. Using live-cell imaging, this thesis investigated, *in vitro,* the effects of pulsed fields ranging in duration from 10 ns to 10 ms on cancerous (U87 glioblastoma multiforme) and non-cancerous cell lines (mouse hippocampal neurons (HT22) and Chinese hamster ovary (CHO) cells). Previously published results have demonstrated that cancerous cells have a greater sensitivity to applied electric fields than healthy cells do. Our results are in agreement with these findings, insofar as the U87 cells underwent a significantly greater depolarization of their transmembrane potential following a single electric pulse at all durations. In a parallel set of experiments, despite having similar electric field thresholds for membrane permeabilization, the U87 cells demonstrated significantly enhanced YO-PRO uptake compared to the other cells lines. Although U87 cells underwent the greatest change in both membrane depolarization and membrane permeabilization, they also showed the fastest membrane resealing constant, which was approximately 30 seconds faster than other cell lines. To elucidate some of the underlying mechanisms by which U87 cells respond to electric fields, a series of experiments looked at the role of transmembrane ion channels. Several recent studies have reported that PEFs can act directly on voltage-gated ion channels. Using a variety of specific and broad acting pharmacological ion channel modulators, we demonstrated that we could almost entirely inhibit the electric field-induced membrane depolarization in U87 cells by blocking certain cationic channels. These results were quite specific, such that the big conductance potassium (BK) channel, L- and T-type calcium channels, and the non-specific cationic channel, TRPM8, were able to inhibit depolarization while blocking other ion channels produced no significant

change. The work in this thesis showed that the malignant U87 cell line showed a greater sensitivity to electric fields from ranging from 10 ns – 10 ms when compared to the non-cancerous cell lines that were investigated. Potential improvements to current treatment protocols have been proposed based on the findings presented herein.

Résumé (Français)

L'utilisation de champs électriques pulsés (PEF) dans les secteurs de la médecine et de la biotechnologie est devenue de plus en plus courante au cours des dernières décennies. La recherche a montré qu'en ajustant la durée du PEF, nous pouvons prédire quels effets seront observés. Alors que les PEF dans la gamme micro - milliseconde ont été utilisés pour perméabiliser la membrane cellulaire et améliorer l'absorption de médicament ou de protéine, le PEF nanoseconde (nsPEF) a démontré des effets uniques sur les organites intracellulaires. Les deux PEF et nsPEF ont démontré un potentiel thérapeutique pour une variété de pathologies humaines, y compris le traitement du cancer. Utilisant l'imagerie des cellules vivantes, cette thèse a étudié in vitro les effets de champs pulsés d'une durée de 10 ns à 10 ms sur des lignées cancéreuses (U87 glioblastome multiforme) et non cancéreuses (neurones hippocampes de souris (HT22) et cellules ovariennes du hamster chinois (CHO)). Des résultats publiés antérieurement ont démontré que les cellules cancéreuses sont plus sensibles aux champs électriques que les cellules saines. Nos résultats sont en accord avec ces résultats, dans la mesure où les cellules U87 ont subi une dépolarisation significativement plus importante de leur potentiel transmembranaire après une seule impulsion électrique à toutes les durées. Dans un ensemble d'expériences parallèles, malgré des seuils de champ électrique similaires pour la perméabilisation membranaire, les cellules U87 ont démontré une absorption significativement améliorée de YO-PRO par rapport aux autres lignées cellulaires. Bien que les cellules U87 aient subi le plus grand changement dans la dépolarisation membranaire et la perméabilisation membranaire, elles ont également montré la constante de rescellement de la membrane la plus rapide, qui était environ 30 secondes plus rapide que les autres lignées cellulaires. Pour élucider certains des mécanismes sous-jacents par lesquels les cellules U87 répondent aux champs électriques, une série d'expériences a examiné le rôle des canaux ioniques transmembranaires. Plusieurs études récentes ont rapporté que les PEF peuvent agir directement sur les canaux ioniques voltage-dépendants. En utilisant divers modulateurs de canaux ioniques pharmacologiques spécifiques et à action large, nous avons

démontré que nous pouvions presque entièrement inhiber la dépolarisation membranaire induite par le champ électrique dans les cellules U87 en bloquant certains canaux cationiques. Ces résultats étaient assez spécifiques, tels que le canal de potassium de grande conductance (BK), les canaux calciques de type L et T, et le canal cationique non spécifique, TRPM8, étaient capables d'inhiber la dépolarisation tandis que le blocage d'autres canaux ioniques ne produisait aucun changement significatif. . Les travaux de cette thèse ont montré que la lignée cellulaire maligne U87 présentait une plus grande sensibilité aux champs électriques allant de 10 ns à 10 ms par rapport aux lignées cellulaires non cancéreuses étudiées. Des améliorations potentielles aux protocoles de traitement actuels ont été proposées sur la base des résultats présentés ici.

Table of Contents

Table of figures

Chapter 1:

General Introduction

1.1 Pulsed electric fields

The last few decades have seen an increased interest in the study of pulsed electric fields, which has been particularly evident in medical and biotechnology sectors. They have been shown to have broad applications in the food processing industry [1–3], for cryopreservation of cell lines [4–6], enhancing gene or drug uptake by cells [7–10], and induce cell death through necrotic or apoptotic pathways [11–13].

Understanding how electric fields influence cell behavior is important when considering how to improve or expand current treatment options. The following section will begin by taking a closer look at the cell and its intracellular contents, but more specifically at the membranes that surround them, where electric fields are expected to interact.

1.2 Biological membranes

Understanding how a cell interacts with its environment begins with the very boundary that separates them, which of course is its membrane. The cell membrane (Fig. 1.1) is composed of a series of polar lipid molecules that have hydrophobic and hydrophilic regions organized into a bilayer [14]. This structure displays self-organizing properties in an aqueous environment that results in a boundary condition separating the cytoplasm from extracellular fluids. A very similar arrangement of amphipathic lipid molecules within the cell serves to separate organelles from the cytoplasm. These membranes are critical for selective transport into and out of the cell.

In addition to the phospholipid bilayer, a host of other lipids, proteins and carbohydrates can be identified. These molecules are highly variable in their distribution along the membrane, each serving different functions ranging from signaling molecules to structural support to name a couple. Transmembrane protein channels are of particular interest to our topic and will be discussed in more detail.

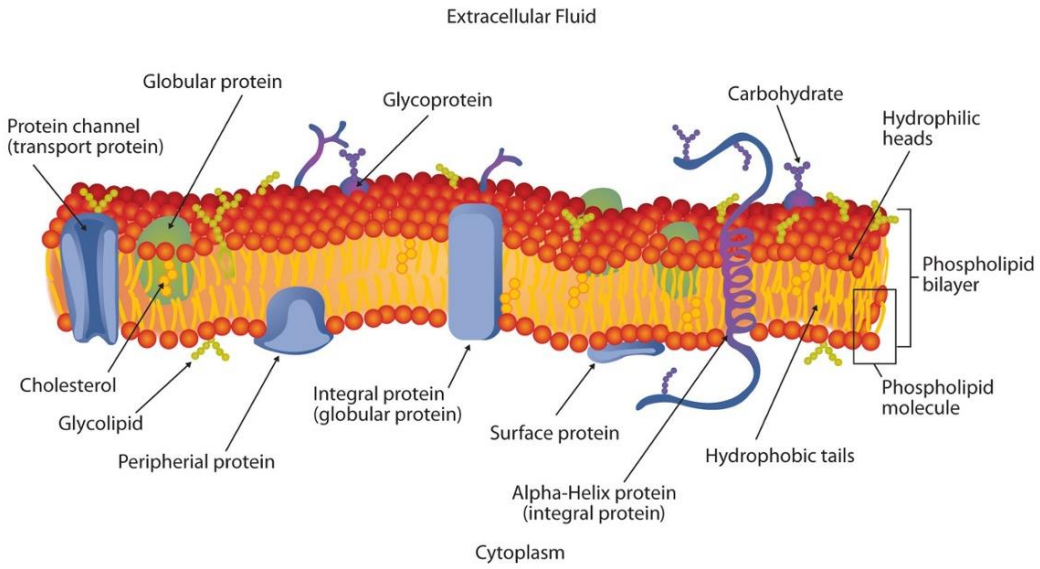

Figure 1.1 – Structure of cell membrane. The cell membrane is a highly complex structure whose fundamental unit is the phospholipid molecule (bottom right of the figure). The amphipathic structure of this molecule results in the formation of a bilayer in aqueous solution. Embedded within the membrane, multiple additional lipids, proteins and carbohydrates serve to communicate with the external environment. Figure taken from: https://www.thinglink.com/scene/634047922140348418.

1.3 Transmembrane proteins

Transmembrane proteins, to a large degree, dictate the function of the cell. Some serve as signal conduits, whereby extracellular molecules interact with the protein leading to a specific intracellular effect [15]. Others serve as selectivity filters responsible for modulating, either passively or actively, the passage of ions. These ion channels are highly variable and are critical for many cell processes.

Ion channels fluctuate between open and closed states, and these states can be influenced through multiple mechanisms (Fig 1.2). Some examples include voltage-gated channels, mechanically-gated channels, or ligand-gated channels. Upon activation, these channels become permeable to specific ions. They can be highly specific, meaning they allow just one type of ion to pass, or charge-specific allowing either cations or anions to pass.

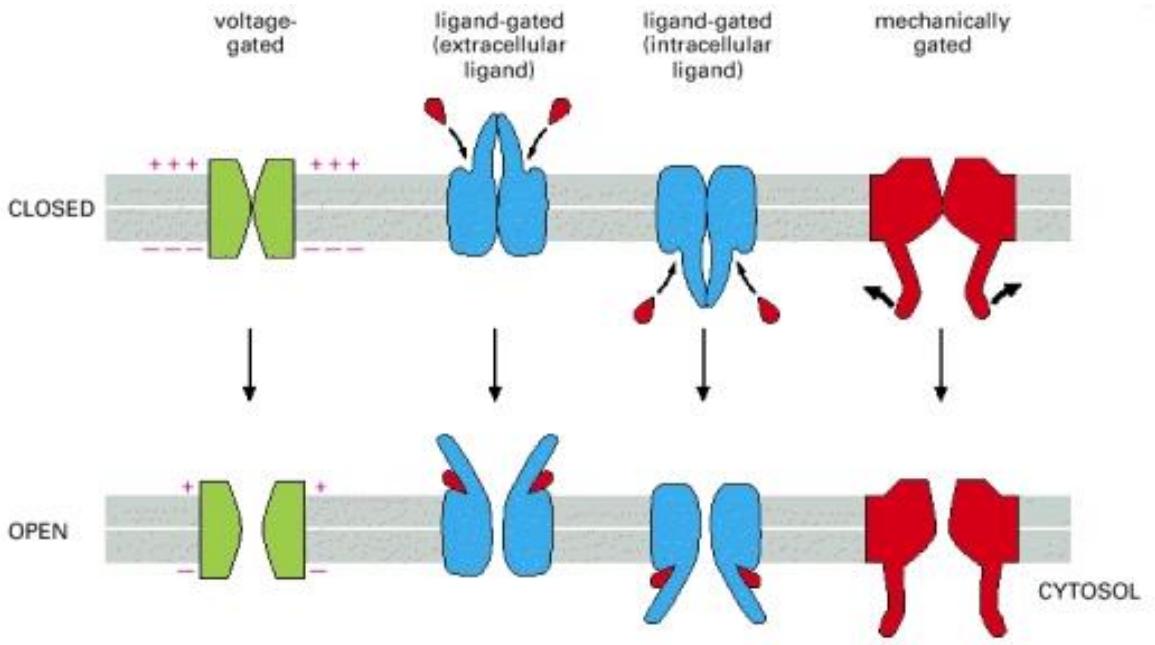

Figure 1.2 – Ion channels are classified by the stimulus which modulates their activity. Voltage-gated channels can be activated by fluctuations in a cells transmembrane potential. Ligand-gated channels are activated through signal molecules that bind on extra- or intracellular sites of the channel. Mechanically-gated channels are modulated through changes in shape associated a physical stimulus. Image taken from Molecular biology of the cell, 4th edition at https://www.ncbi.nlm.nih.gov/books/NBK26910/.

The selective nature of these ion channels is responsible for the generation of a transmembrane potential, which is equally present and varies among intracellular organelles as it is across the plasma membrane. The chemical basis of this voltage-gradient, known as the resting membrane potential, is the uneven distribution of ions inside and outside of the cell [16]. The electrical properties of ions, combined with the conductive properties of protein channels and the insulating properties of the membranes lipid bilayer, have allowed the cell to be modeled as an electric circuit. This has been useful when studying electrical communication between cells for example, but also when developing treatment strategies to modulate cell activity.

1.4 Describing the cell as an electrical circuit

In the 1950's Alan Hodgkin and Andrew Huxley proposed a model to describe the ionic mechanisms responsible for the propagation of electrical impulses along a giant squid axon. As a general overview (Fig. 1.3), the Hodgkin-Huxley model represents the lipid bilayer as parallel capacitors capable of storing charge and ion channels as variable resistors capable of passing current. The transmembrane potential is generated across the cell membrane and fluctuates according to the activity of the ion channels.

This model has been invaluable in understanding certain biological phenomena such as electrochemical communication between cells, particularly between electrically excitable cells in nervous and muscular tissues. Another application for this model extends into fields interested in modulating cellular activity using applied electric fields.

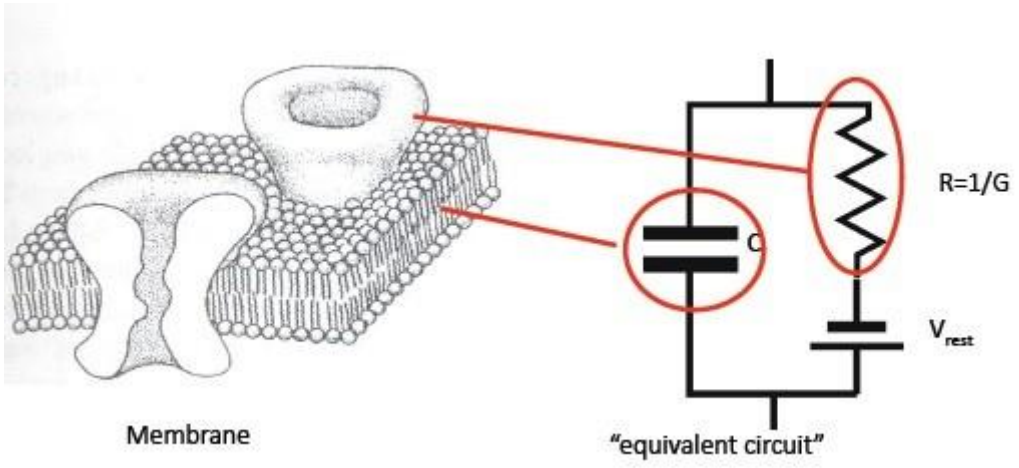

Figure 1.3 – The equivalent electric circuit model of the cell membrane. In this model, the lipid bilayer is represented as a pair of parallel capacitors and the transmembrane ion channels are represented as variable resistors. Image adapted from Lehigh University Bioengineers page, https://lehighbioe.wordpress.com/2012/10/23/the-cell-membrane-as-a-circuit/.

1.5 Electric field interaction with the cell membrane

When cells are exposed to an electric field, an electric force is generated, which acts on ions both inside the cell and in the external media. Because ions are charged molecules, this force causes them to move along the electric field lines. Whereas the extra- and intracellular solutions are conductive, the cells lipid membrane is non-conductive. As a result these ions will accumulate along the membrane and generate a large transmembrane potential. At a certain point, which is approximately 1 V [17, 18], the induced voltage exceeds the membrane capacitance and breakdown of the membrane occurs. When considering the diameter of the membrane is approximately 10 nm, the electric field strength associated with this threshold is on the order of a MV/cm. This process, which is termed electroporation or electropermeabilization is associated with enhanced membrane permeability.

To describe this effect, the Schwan equation (Eq. 1.1) was developed. This equation is limited to modeling a spherical cell, and states that the induced membrane potential (Vm) is proportional to the radius of the cell (R) and the applied electric field (E), and will not be uniform along the cell membrane (Fig. 1.4). Extensions of this model have been developed to help understand more complex models, such as irregular-shaped cells that can't be accurately described as spherical or ellipsoid.

$$V_m = \frac{3}{2} ER\, cos\theta$$

Equation 1.1 Schwan equation (steady-state). This describes the effect of an applied electric field (E) on the transmembrane potential (Vm) given a cell radius of (R) as a function of the angle (θ).

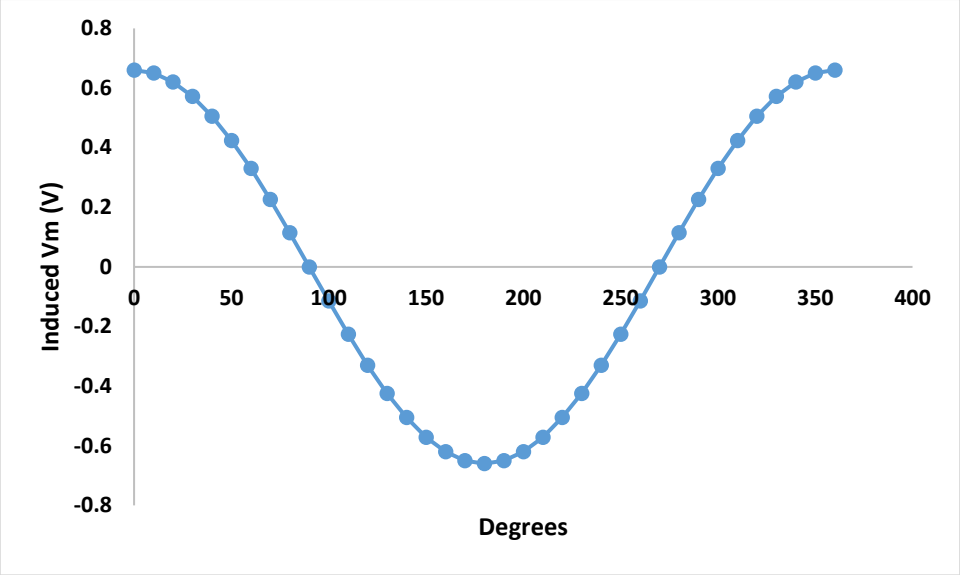

Figure 1.4 – The induced membrane potential varies along the cell membrane. This is an example of the Schwan equation applied to a spherical cell with a radius of 10 μm and an applied field intensity of 44 kV/cm.

More recently, there has been a shift in methodology toward understanding the biomolecular events occurring when an electric field interacts with a lipid bilayer. Molecular dynamics (MD) simulations have helped to clarify some of the events associated with electropermeabilization, and have allowed us to visualize the dynamics associated with membrane breakdown [19–23]. Up to now, limitations in the computational power have restricted MD to a period less than 1 millisecond following pulse delivery [24]; however, a multitude of effects have been reported over much longer time periods. These effects appear to be highly dependent on several factors such as; pulse duration, electric field strength, number of pulses, and frequency of pulses delivered.

1.6 Factors influencing outcome following membrane exposure to an electric field

It is generally accepted that the initial step in membrane breakdown following PEF exposure is the magnitude of the induced transmembrane potential [17, 18]. Thus, it is unsurprising that electric field strength would play an important role in this process. Finding

the threshold for this response has been the subject of many investigations seeking to exploit this consequence of PEF application. Achieving this threshold; however, is highly dependent on the duration of the pulse delivered, such that eliciting a response using a shorter pulse would require a stronger electric field than the same response using a longer pulse. For example, using pulses ranging from 1 ns to 100 ms to stimulate gastrocnemius muscles, an applied voltage of 4.5 kV was required for a 1.8 ns pulse to elicit a similar response to a 100 ms pulse delivered at 0.02 kV [25].

In addition to the electric field intensity and pulse duration, other important features are; the number of pulses and the frequency at which they are delivered. These factors were explored in [26], where nsPEF were investigated for their ability to cause swelling in Jurkat cells. Single nsPEF were compared to 10 & 50 nsPEF. After 20 seconds significantly enhanced swelling was seen as a function of number of pulses. In the same study, frequency of pulses was explored, where swelling was measured after exposure to 10 pulses at 1 Hz or 10 pulses at 1 kHz. Similarly, significantly more swelling was observed in the group of cells exposed to 10 nsPEF at 1 kHz when compared to the 1 Hz and the control groups.

In a study looking at Yo-Pro uptake in U87 cells following nsPEFs [27] the authors report a significant enhancement in Yo-Pro uptake as a function of both number & frequency of pulses delivered. Here, a single 10 nsPEF (1 p) was compared to 10 pulses (10 p) at 1 Hz, 10 Hz, and 100 Hz, and 100 pulses (100 p) at 1 Hz, 10 Hz, and 100 Hz. The results can be summarized as follows: The greatest Yo-Pro uptake was observed – 100 p 100 Hz > 100 p 10 Hz > 100 p 1 Hz > 10 p 100 Hz > 10 p 10 Hz > 10 p 1 Hz > 1 p > control.

A noteworthy feature is evident when considering pulse shape in the context of the literature presented above. In [28], using μsPEFs it was reported that the electric field intensity required to permeabilize 50 % of the cells was reduced by 20 % when the authors used symmetrical bipolar pulses. The working hypotheses for these results propose that i) the polar asymmetry following a unipolar pulse is counterbalanced when a bipolar pulse is delivered and ii) bipolar pulses increase the odds that a non-spherical cell are permeabilized.

In contrast to this research, several articles show a dampened effect when bipolar nanosecond pulses are used. In [29], the addition of a second phase (of opposite polarity) cancelled the effect of the initial monopolar phase in both intracellular calcium mobilization and cell survival. These results persisted in spite of a doubling of total energy delivered to cells, and was not dependent on pulse duration (60 ns or 300 ns), amplitude (15 – 60 kV/cm) or number of pulses delivered (1 – 60). This dampening effect gradually decreased as the delay between the bipolar pulses increased. A similar dampening effect was observed for calcium uptake [30] as well as measures of plasma membrane integrity Calcium Green-1, Propidium Iodide and FM1-43 [31] when comparing bipolar effects to monopolar effects.

Although some explanations were put forth to explain the differences between μs and ns bipolar pulses, the duration of the pulse is critical and is based on a biological constant known as the membrane charging constant, which will be discussed in further detail in the next section.

1.6 The role of pulse duration in PEF effects

Recall that the induced transmembrane potential is due to the accumulation of ions along the cells membrane. This process obviously requires time, and is referred to as the charging time, or charging constant. Although it varies slightly between cells, the charging time is on the order of a few hundred nanoseconds [32–34]. Pulse durations that are longer than the charging constant will have very different effects those that are shorter.

The following sections will examine the different effects expected when using pulsed electric fields of various durations. For simplicity, pulses that are longer than the charging time will be referred to as pulsed electric fields (or PEF), and those that are shorter will be referred to as nanosecond pulsed electric fields (or nsPEF).

1.7 PEF effects and applications

At longer durations, in the micro- or millisecond range, PEF have been shown to be effective at delivering drugs, proteins, and DNA across the cell membrane [35–41]. By adjusting the number, frequency and intensity of the pulses one can reversibly or irreversibly permeabilize the plasma membrane.

1.7.1 Irreversible electropermeabilization (IRE)

Irreversible electropermeabilization (IRE) has been studied as a purely electrical treatment for tumors [13, 42–45]. Here, the cell is unable to repair the damage imposed by the electric field. A review of this technique [46] looked at results from 106 patients over a period ranging from 3 – 18 months. Efficacy of treatment ranged from 67 – 100% over this period.

Most recently, another human trial has shown promising results [47]. In this study, 30 patients were treated with liver tumors. They were monitored for 6 months following treatment where treatment success was defined as no evidence of residual tumors in the ablated area from CT and ultrasound scans. After 3 and 6 months, success was achieved in 79% and 66% of the patients, respectively.

1.7.2 Reversible electropermeabilization

Contrary to IRE, reversible electropermeabilization utilizes the ability of the membrane to repair itself as an advantage. Of the two, reversible electropermeabilization has been most thoroughly investigated, and offers a greater number of potential therapies. Gene electrotransfer (GET) is one such application, where DNA is introduced into the cell and makes it possible to regulate the production of a desired transgene. A very thorough review [39] highlights the vast number of disorders that can potentially be treated, including Parkinson's disease, HIV/AIDS and cancer to name a few.

A more recent review of clinical GET trials highly the broad potential for this therapy [48]. In this review, the author summarizes the results of more than 50 clinical trials (some of which are ongoing) where GET has proven to be a safe and effective method to treat various

cancers by stimulating immune activity or disrupting angiogenesis in tumors; as well as a role in DNA vaccines for HIV, Hepatitis, Human papilloma virus, and Hantaviruses.

Electrochemotherapy (ECT) is another application for reversible electropermeabilization, where chemotherapeutics (or high concentrations of calcium) can be injected systemically or locally followed by electropulsation of the tumor. Here drugs such as bleomycin and cisplatin have been selected for their combination of low membrane permeability and high cytotoxicity, and when combined with electropulsation, the toxicity of these agents has been significantly enhanced [49–51].

Recently, a case study looked at the effects of calcium electroporation and electrochemotherapy on a patient with malignant melanoma [52]. This patient had numerous metastases (Fig. 1.5) yet 12 months following treatment complete leveling was observed in both treated and non-treated lesions. The fact that non-treated tumors responded highlights the potential role of the immune system in mediating this response. Biopsies taken upon completion of the follow-up period revealed an absence of malignant cells.

1.8 nsPEF effects and applications

When pulse durations shorter than the charging constant are applied, the plasma membrane no longer shields the intracellular environment [32, 33], and very different effects can be expected. Effects such as mitochondrial depolarization [53, 54], caspase activation [55, 56] and nuclear condensation [57, 58]; all effects typical of cell death by apoptosis, have been reported. Additional effects such as cytoskeleton disruptions, including microtubule [27] and actin [59] assembly have also been reported.

Figure 1.5 – Results from a case study of a patient with malignant melanoma. The top two images were taken prior to treatment using electrochemotherapy and calcium electroporation. In these images multiple cutaneous metastases are evident. The bottom two images were taken 16 months following treatment. A complete leveling was observed in both treated and non-treated metastases. Biopsies of the pigmented lesions were found to be non-malignant. Results and images from [52]

Whereas intracellular effects are specific to nsPEF, there is a lot of evidence suggesting additional effects occur on the plasma membrane. For example, membrane permeability was found to be enhanced following nsPEF exposure, where YO-PRO [27] and bleomycin [60] uptake into the cell was observed. In an experiment using giant unilamellar vesicles, a single nsPEF resulted in the delivery of siRNA molecules into the cytoplasm [61].

It has been hypothesized that these ultra-short fields may exert effects directly on transmembrane protein channels in the plasma membrane [62]. Experimental evidence exists that supports this, where nanosecond pulses have resulted in direct activation of voltage-gated channels [63–65].

While nsPEF have demonstrated very unique effects compared to PEF, there is still a need for clinical data to validate the translation of these effects in human trials. The first human trial using nsPEF for cancer treatment was published in 2014 [66]. In this study a total of 10 tumors were treated with nsPEF on 3 patients with basal cell carcinoma. Of the tumors treated, seven were completely free of cancerous cells, two had partially regressed, and one recurred 10 weeks after treatment. An example of tumor treatment in this study can be seen in Fig. 1.6 below.

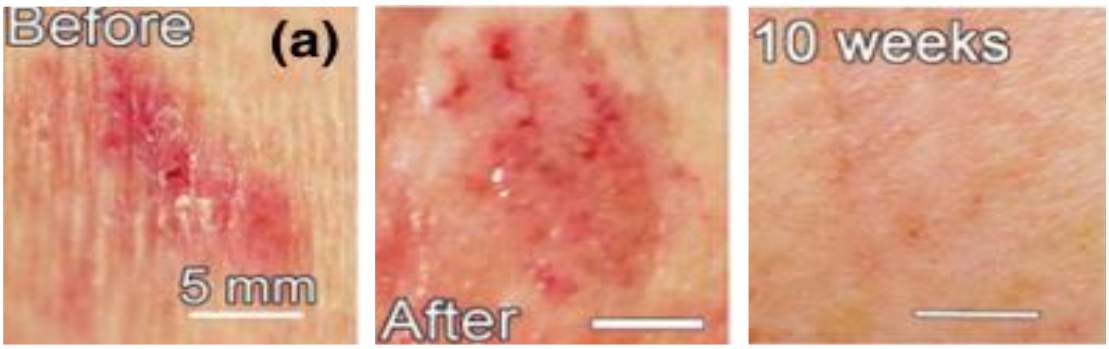

Figure 1.6 – In-human trial for treatment of basal cell carcinoma with nsPEF. An example from [66], where the first human trial was conducted testing nsPEF efficacy on skin cancer. Three patients were treated using nsPEF and followed for several weeks following treatment. Images above are a representative example of the effects observed. The first and second images were taken pre- and immediately post-nsPEF exposure. The final image was taken 10 weeks post-treatment where there was no evidence of tumor recurrence. This was confirmed by histological analysis of biopsy.

Despite all of the promising research using PEF and nsPEF, this field is still continuing to evolve. Many questions still remain with respect to the mechanism of action of PEF/nsPEF

effects on biological systems. Understanding these mechanisms will help us overcome some of the limitations present in this field of study.

1.9 Limitations of PEF/nsPEF as a clinical treatment

The major limitations facing experimentation using pulsed electric fields (PEF/nsPEF) for treating humans are time and money. An abundance of research demonstrates the potential of electrically based therapies. Recently, the handbook of electroporation was published [67] containing a comprehensive series of chapters from various contributing authors highlighting studies from modeling and simulations to *in vitro* work right up to clinical applications. Despite the amount of research, very few countries offer treatments using pulsed electric fields.

As a result, patients who could benefit from these treatments aren't even being given the option. And those who may be aware will have to make the choice between paying from their own pockets and choosing those treatment options that are covered by health insurance policies. That is why I say time and money are the major limitations. More money is required to generate further research, and this takes time. With that said, it is an honor contribute in the most humble way to this ever-growing field hoping that I can add to the current body of knowledge.

The pulse generators, as well as the fluorescent indicators of transmembrane potential and membrane permeability, used for these experiments will be discussed in detail in the following section.

1.10 General methods

The following section will provide a detailed overview of some of the techniques and equipment used throughout the work presented in this thesis. Attention will be given to explaining the cell lines used and how they were maintained; the different pulse generators and electrodes used; the fluorescence microscopes used and which fluorescent indicators were selected; the methods involved in extraction of data from images, and the statistical

methodology applied. Part of the work described in this thesis was the result of a collaboration with the University of Ljubljana. My contribution to this collaboration involved data collection and statistical analyses. Whereas we investigated the role of pulse durations ranging from 10 ns to 10 ms, the majority of the work presented in this thesis focuses on 10 nsPEF, which is the primary focus of our lab.

1.11 Culture and maintenance of cell lines

1.11.1 Cell lines and maintenance

Three cell lines were used for the experiments that will be presented. Chinese hamster ovary (CHO) cells (European Collection of Authenticated Cell Cultures ECACC, cells CHO-K1, cat. no. 85051005, obtained directly from the repository), U87-MG human glioblastoma cells (ECACC, Public Health England, cat. no. 89081402) and HT22 immortalized mouse hippocampal neurons (The Salk Institute, La Jolla, CA) were grown in an incubator at 37 °C at 5 % CO_2 for 2-5 days before experiments. HT22 cells were used in their non-differentiated and differentiated states. The procedure used to differentiate these cells will be explained further in section 1.11.2

Experiments were completed in laboratories in Limoges, France and Ljubljana, Slovenia. In Limoges, depending on the experimental setup, cells were grown in one of two ways. They were either grown on Poly-Lysine (Sigma-Aldrich, Germany) coated 22 mm glass coverslips in 35 mm Petri dishes (VWR International, USA); or they were grown in 35 mm glass FluoroDishes (World precision instruments, USA). In the former condition, the 22 mm glass coverslip was transferred into a customized plastic ring which could be mounted onto the microscope. In Ljubljana, cells were grown in 40 mm Petri dishes (TPP, Austria). To ensure these subtle differences in methodology were not significantly influencing the results, experimental results were compared between labs.

For growth and maintenance of cell lines, CHO cells were grown in Ham-F12 media (Sigma-Aldrich, Germany), U87 cells in MEM (Sigma-Aldrich, Germany) and the HT22 cells

in DMEM (Sigma-Aldrich, Germany) growth medium. All growth media were supplemented with 10% fetal bovine serum (Gibco, France or Sigma-Aldrich, Germany, cat. no. F9665), L-glutamine (StemCell, Canada) and antibiotics.

1.11.2 Differentiation of HT22 cells

HT22 cells were used in their non-differentiated and terminally differentiated forms. In order for HT22 cells to be differentiated, DMEM growth media had to be replaced with Neurobasal media (Thermofisher, USA, cat. no. 21103-049), and supplemented with 0.5 mM L-glutamine and 1 mL B-27 (Thermofisher, USA, cat. no. 17504-044) for every 50 mL Neurobasal media. Cells were maintained in this differentiation medium for 24 – 48 hours prior to experimentation.

1.12 Exposure of cells to electric pulses

Cells were exposed to different pulse durations (10 ns, 550 ns, 1 μs, 10 μs, 100 μs, 1 ms, and 10 ms). To accommodate experiments using these pulse durations, three different pulse generators were used. For 10 ns pulses, a commercially available nsPEF generator (FPG 10-1NM-T, FID Technology, Germany) with 50 Ω output impedance was used. The 10 ns pulse durations (13.6 ns full width at half magnitude (FWHM) duration and a 5.2 ns rise time) were applied with electric field intensities ranging from 16.5 – 52.0 kV/cm. A high-voltage measurement device (tap-off) connected to a digital phosphor oscilloscope (DPO 4104, Tektronix, USA) was used to visualize the time-domain measurements of each pulse. Pulses were delivered to cells by positioning the electrodes (Fig. 1.7 a), comprised of two stainless-steel electrodes (1.2 mm gap) with a 50 Ω impedance resistive load in parallel, using a micromanipulator (MP28, Sutter Instruments USA). The applied electric field was numerically determined [27]. Numerical modelling of the electrode delivery system was performed with a Finite-Difference Time-Domain (FDTD) based electromagnetic solver, and a finest spatial mesh of 100 μm.

For pulse exposures of 550 ns and 1 µs, a laboratory prototype nanosecond generator with H-bridge MOSFET amplifier architecture and additional peripheral circuitry for voltage adjustments and safety was used. Voltage could reach 1 kV with an accuracy of 3 %. For pulse exposures of 10 µs – 10 ms a commercially available BetaTech electroporator (Electro cell B10, Betatech, France) was used, and the current was measured with either current probe CP030 (Teledyne LeCroy, USA) or a Pearson current monitor (Model 2877, Pearson Electronics Inc., USA). Pulses longer than 10 ns were applied using either stainless-steel wire electrodes with a 4 mm intra-electrode distance and 1.29 mm diameter (16 gauge needle) or Pt/Ir wire electrodes with 5 mm intra-electrode distance and 0.75 mm diameter (Fig. 1.7 b). The numerical calculations show that the electric field in the middle of the electrodes is approximately homogeneous [68]. To compare the results obtained with both electrodes, we approximated the electric field between the electrodes as E = U / d, where U is the applied voltage and d the distance between the electrodes. We adapted the applied voltage to achieve the same electric field and acquired images in the middle of the two electrodes.

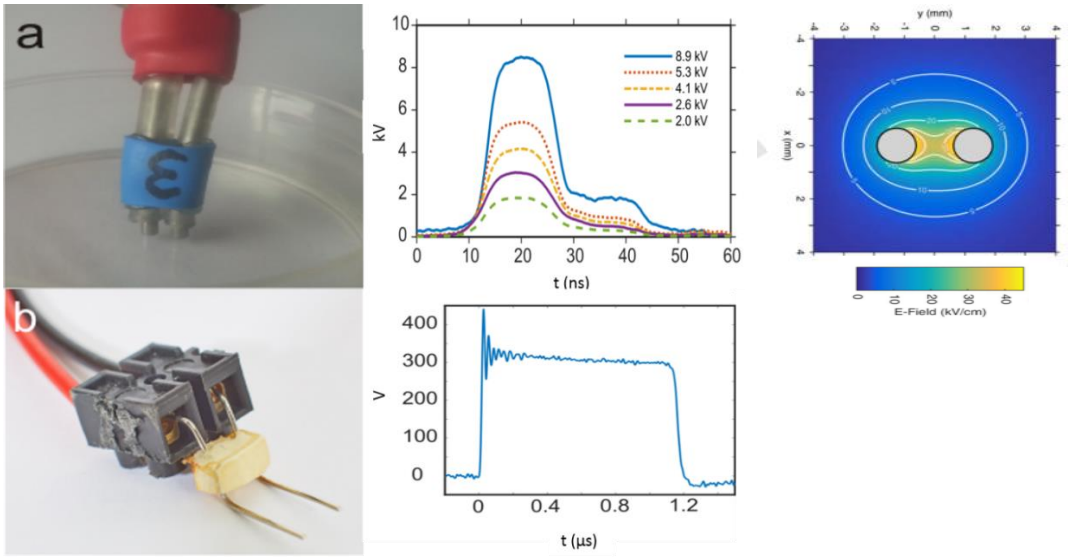

Figures 1.7 (a-b) Photos of the electrodes, used for experiments. A - Electrodes used for delivering 10 ns pulses; B - electrodes used for delivering pulses longer than 500 ns. Respective traces for 10-ns and 1-µs pulses delivered are to the right of electrode images, along with a numerical simulation of the nsPEF field distribution.

1.13 Fluorescence imaging

Experiments conducted in Limoges were performed on a DMI6000 confocal microscope (Leica Microsystems, Germany) using a 63x oil immersion objective (for experiments measuring membrane potential) or a 20x objective (for experiments measuring membrane permeability). A Spectra 7 light engine (Lumencor, USA) was used for fluorescence excitation, whereas the emitted light was captured with an electron-multiplying charge-coupled device camera (EMCCD Evolve 512, Rope, USA). Fig. 1.8 shows the imaging setup.

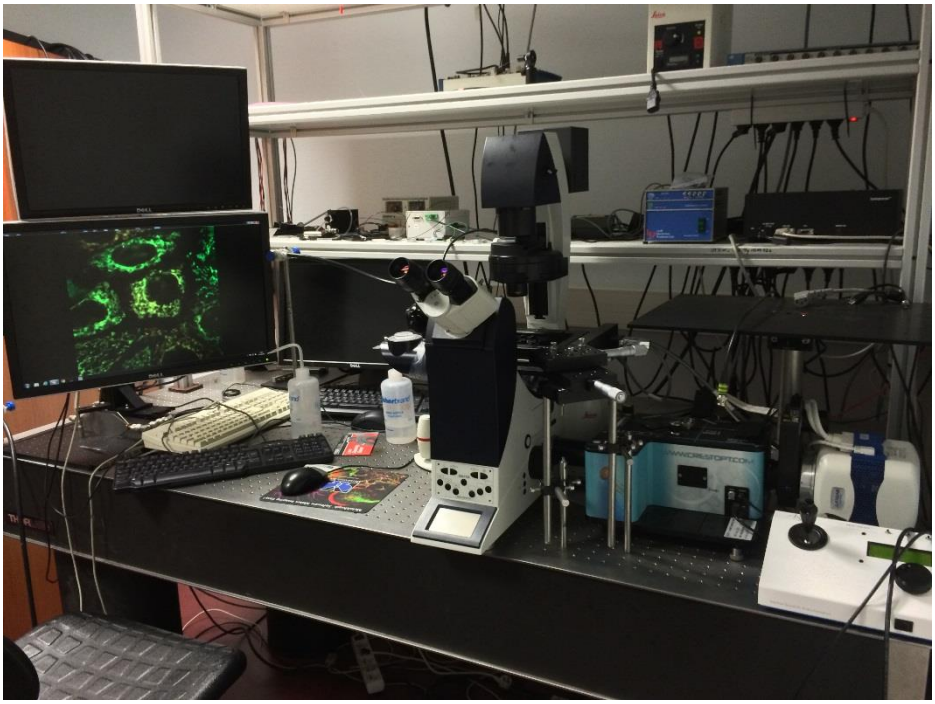

Figure 1.8 – Fluorescence imaging setup. An image of the workstation where the nsPEF experiments were performed.

In Ljubljana, an inverted microscope AxioVert 200 (Zeiss, Germany) was used for experiments with a 20x (when measuring membrane permeability) or 40x (when measuring membrane potential) objective. Samples were excited using a high-speed polychromator (Visitron systems GmbH, Germany), and the emitted fluorescence was acquired with a VisiCam 1280 CCD camera (Visitron, Germany).

1.14 Fluorescent indicators for measuring transmembrane potential and membrane permeability

1.14.1 Measuring membrane permeability

Selecting a fluorescent dye for measuring membrane permeability was straightforward because there are only a few that are commonly used in the literature. Generally, membrane integrity is measured using either propidium iodide (PI) or YO-PRO (YP). There are multiple studies using these dyes; however, when directly compared [69], YP was found to be a more sensitive measure for membrane permeability than PI (Fig. 1.9). This difference was attributed to the size of the molecule, insofar as YO-PRO has much less steric hindrance associated with its planar configuration. For that reason it was used for the permeability experiments presented in this thesis. In all cases, it was used at a concentration of 1 μM.

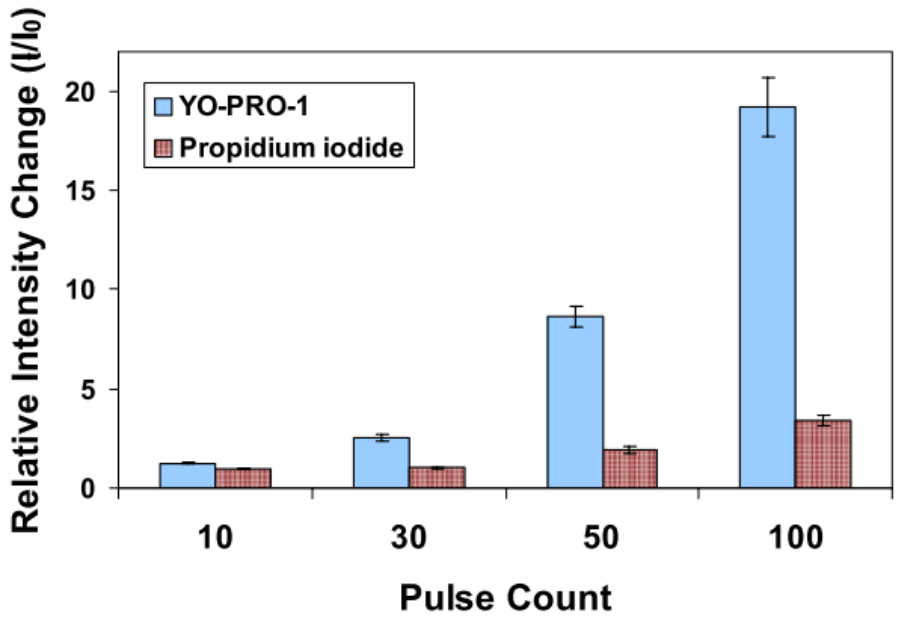

Figure 1.9 – Direct comparison of YP and PI uptake following nsPEF exposure. These results demonstrate the difference in sensitivities between YP and PI for measurement of membrane integrity. Image taken from [69].

1.14.2 Measuring transmembrane potential

Selecting a voltage probe, on the other hand, required more consideration. Typically voltage-sensors are divided into two slow- or fast-probes. Depending on cell type (excitable vs non-excitable) or on the experimental objectives, both voltage-sensors have advantages and disadvantages. A summary of their differences is available below in Table 1.1.

The major difference between slow and fast probes is the mechanism by which they permit the measurement of V_m. (Fig. 1.10). Slow probes, also called Nernstian probes, undergo V_m - dependent changes in their transmembrane distribution. These probes typically are considered when looking for long-term changes (seconds to minutes) in membrane potential that is due to alterations in ionic permeability of the membrane.

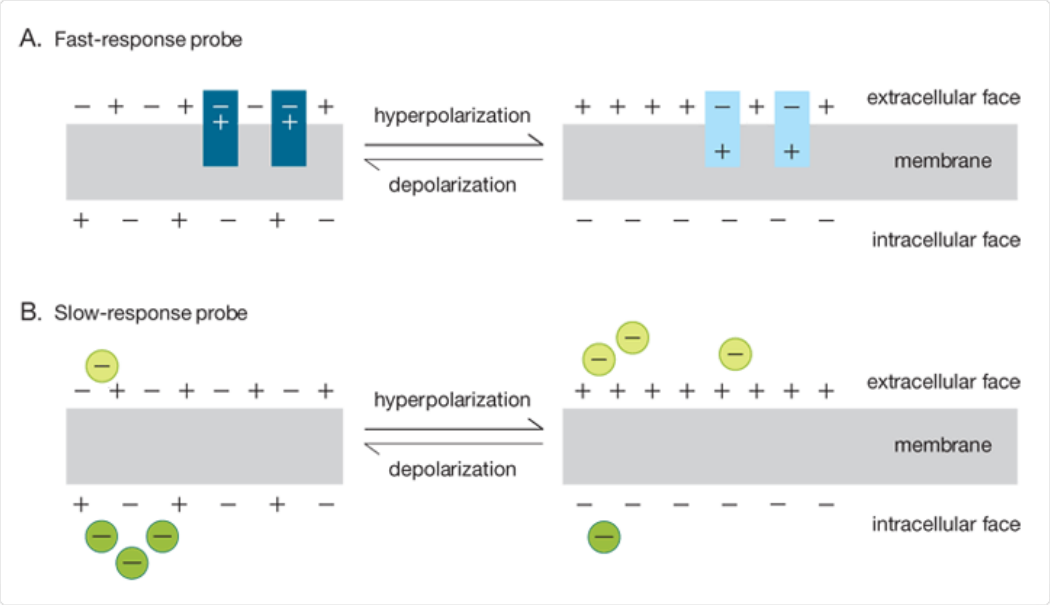

Figure 1.10 – Fast-response vs slow-response voltage-probes. A In response to a change in the local electric field, fast-response probes undergo a change in the electronic configuration. This structural change leads to changes in the fluorescent properties of the molecule. **B** Slow-response probes undergo a transmembrane redistribution that is dependent on the membrane potential. Source for the figure - *https://www.thermofisher.com/fr/fr/home/references/molecular-probes-the-handbook/probes-for-membrane-potential/introduction-to-potentiometric-probes.html*

Whereas the optical response time for slow probes prevents the study of single action potentials in excitable cells such as neurons and muscle cells, the magnitude of response is much greater than fast-response probes, in some cases approaching 100 x more sensitive (~ 1% change per mV). This allows for the measurement of subtler changes in V_m over time.

Fast-probes, or electrochromic probes, are typically selected when the interest is in very rapid changes in membrane potential. These probes undergo a change in the electronic structure of the molecule when the surrounding electric field is changed. This change in structure results in a change in fluorescent properties. Because the change in fluorescence does not depend on translocation across the membrane, the optical response time is extremely fast. Contrary to the slow probes, the cost of the rapid response is a significant reduction in sensitivity (~ 2 – 10% change per 100 mV).

	Slow	**Fast**
How they work	Membrane potential-dependent change in their transmembrane distribution results in change in fluorescence	A change in surrounding electric field results in a change in the electronic structure of the probe which changes the fluorescent properties of the molecule
Magnitude of change	~ 1% change per mV	~ 2-10% change per 100 mV
Optical response	Suitable for detection of average membrane potential changes (from respiratory activity, ion-channel permeability, drug binding etc.)	Suitable for detection of transient, rapid changes in potential (ms) in neurons and cardiac cells
Examples	Carbocyanines and rhodamines (cations); and oxonols (anions)	AminoNaphthylEthenylPyridium (ANEP) dyes; Förster resonance energy transfer (FRET) sensors; FluoVolt*

Table 1.1 – Describing fast vs slow voltage probes. Comparing the pros and cons of various types of probe based on their mechanism of action, magnitude of change and optical response. * FluoVolt has magnitude of change closer to 25% per 100mV.

A commercially available slow probe, known as plasma membrane potential indicator (PMPI); a commercially available fast-probe, FluoVolt; and a genetically encoded fast probe, ArcLight were tested and compared to determine how they responded to a single nsPEF. Experiments were performed to determine which would be more appropriate for our experiments.

ArcLight is part of the rapidly evolving family of genetically encoded voltage sensors. This next generation technology is made possible due to a fusion of a voltage sensor found in the sea squirt, *Ciona intestinalis,* with a fluorescent protein (GFP) found in the jelly fish, *Aequorea victoria* [70]. DNA transfection into the host cell and subsequent expression is made possible using a baculovirus which is unable to replicate in mammalian cells [71–73]. First described in 2012, ArcLight has been considered a revolutionary step forward in fast-response probes and genetically encoded voltage sensors in particular because of its relatively large magnitude of response, which has been reported to approach 35% per 100 mV change in transmembrane potential [70].

Despite this large magnitude of response when compared to other fast voltage-probes, when ArcLight-transfected U87 cells were exposed to a 34 kV/cm nsPEF, the relative change was quite minimal. With such a minimal response taken with the relative inconvenience associated with the time taken to transfect the cells, this probe was not considered ideal for the purpose of our intended experiments.

The second fast-response voltage-sensing probe, FluoVolt, is considered to be the next generation for electrochromes not included in the genetically encoded family. Because of the commercial nature of this voltage-sensitive dye, the chemical structure is unknown. Lifetechnologies, the company who distributes this dye, states that its optical resolution is in the sub millisecond timescale and exhibits a magnitude of response up to 25% per 100 mV change in membrane potential.

Although easy to use, requiring a simple mixing procedure along with a 15 – 30 minute incubation period, the response observed following a 34 kV/cm nsPEF was similar to that

achieved with ArcLight. A recent article [65] using nanosecond pulsed electric fields confirmed that the resultant response of FluoVolt, in this case to a 3 kV/cm, 200 ns PEF was closer to 5% than the 25 % expected. This level of response would not be adequate to determine potentially subtle effects following application of various ion channel modulators.

The commercially available slow-response probe, PMPI, was determined to be the most capable for answering the questions we set out to answer, and will be addressed in the following section. This probe, also of unknown chemical structure because of its commercial nature, was able to reliably respond with a magnitude around 20 - 30x greater than the other probes tested. Because of the kinetics of this dye, such that an increase in fluorescence is associated with a depolarization of the transmembrane potential, the chemical family could be determined.

Three types of slow-response probes exist: Carbocyanines, rhodamines, and oxonols. The two former families are cationic species. Because they are positively charged, these molecules tend to be used more for monitoring mitochondrial membrane potential whose resting potential is significantly more negative than that of the cell's plasma membrane [74, 75]. Oxonol dyes, on the other hand, are anionic species which do not label mitochondria or other intracellular organelles. This is the choice family of dyes for monitoring changes in plasma membrane potential *in vitro* [76].

When compared with ArcLight and FluoVolt, PMPI has the advantage of a significantly greater sensitivity to our nsPEF conditions. Moreover, it requires a simple dilution (0.5 μL/ mL) into the imaging solution and a 30 minute incubation period prior to use. Finally, PMPI has been relatively well tested and validated as an appropriate tool for the optical measurement of transmembrane potential, even when compared to patch-clamp electrophysiology [77–80]. Taken together, this voltage-sensitive dye was selected to investigate nsPEF effects on V_m in the experiments to be presented.

1.15 Image acquisition

Images were acquired using MetaFluor software (Molecular Devices, USA) in Limoges and with MetaMorph software (Molecular Devices, USA) in Ljubljana. Prior to experimentation the growth media was replaced with Live cell imaging solution (Molecular probes-A14291DJ) with the addition of 20 % D - glucose at a concentration of 1.0 mg/mL. Images were acquired every 30 seconds for experiments using PMPI, and every 3 seconds for those using YO-PRO. Where electropulsation occurred, a 5 minute baseline of fluorescence was collected for PMPI experiments, and a 30 second baseline for YO-PRO experiments.

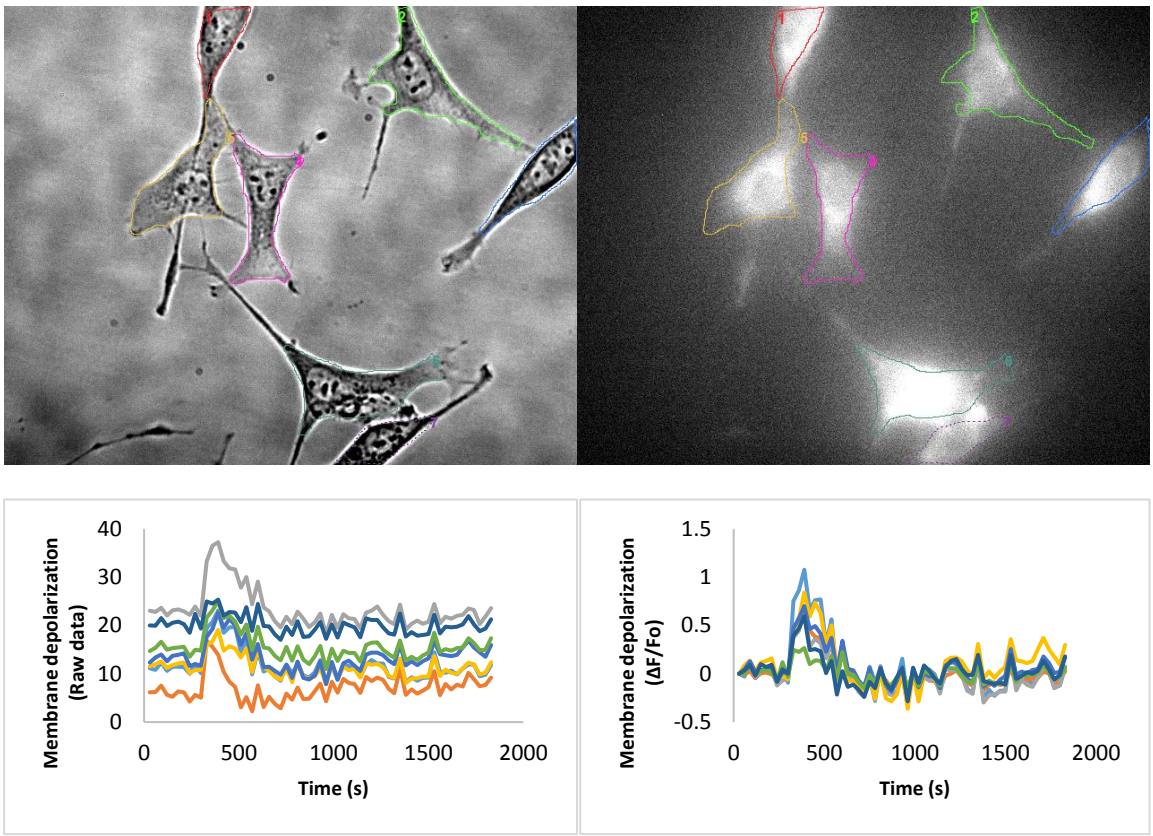

Figure 1.11 – Example of image processing and data extraction. The ROI's are traced around the perimeter of each cell membrane in the brightfield image (top left). These ROI's are then copied and pasted into the fluorescence image series (top right). Both the raw fluorescence data (bottom left) and relative fluorescence data (bottom right) is extracted for statistical analyses.

An example of image analysis using HT22 undifferentiated cells in Image Analyst MKII software (Fig. 1.11). The initial step involves tracing the perimeter of the visible region of each cell membrane which will be the regions of interest (ROIs) when extracting data. Following this step, the ROIs were copied from the bright field image and then pasted into the fluorescence image series. An additional ROI is traced in an area of the fluorescence image series where no movement is observed. This final ROI will serve to remove the background noise by subtracting its value from the entire image series. Finally, the raw and relative ($\Delta F/F_o$) data is extracted and exported for statistical analysis. This was an example where PMPI was used. YO-PRO experiments were handled in the same manner.

1.16 Statistical analysis

Following image analysis and extraction of data, statistical analyses were performed using IBM SPSS 19 or SigmaPlot v.11. Multiple types of statistical tests were performed throughout this thesis, all of which were parametric tests. Therefore, certain assumptions pertaining to the dataset had to be met for these tests to be properly used and interpreted. The following assumptions are required for all tests used in this thesis. Additional assumptions are required depending on the statistical test used. For a review on the more specific assumptions, refer to [81].

1.16.1 Independence of data

Because the experimental questions looked at differences between groups, the assumption of independence had to be met. This assumption simply states that the observations were collected on different subjects. This can be slightly difficult in *in vitro* studies since we are often comparing different effects on the same cell line. Therefore, to ensure the design was as balanced as possible, data was collected and repeated on different days ensuring that the assumption of independence was met.

1.16.2 Normal distribution

Since parametric tests are based off the normal distribution, it is important to ensure that the data collected within groups is normally distributed. To measure normality, several measures should be evaluated; including plotting the frequency distribution, evaluating the shape of the data using values of kurtosis and skewness, analyzing P-P plots to determine if the data collected was comparable to a theoretical normal distribution, and using the Kolmogorov-Smirnov (K-S) test which compares the data with a theoretical dataset containing the same mean and standard deviation.

1.16.3 Homogeneity of variance

The final general assumption to be met involved variability in the dependent variable. This requires that the variances within conditions are approximately similar. As an example, suppose we are interested in the electric field threshold for a 10 ns PEF. To meet this assumption, the variability should be similar for each electric field intensity used. Levene's test is used for this purpose, where a significant result suggests that the variance between conditions is not similar.

1.16.4 Violations of statistical assumptions

Two options are available when the data does not meet the conditions for parametric testing: Either the data can be transformed using one of many available options, or it can be removed from the analysis. The drawback to transforming data is that one must also change any conclusions. For example, if we log transform our data for membrane depolarization, any conclusions must interpreted in the same way. For the purpose of our results, it seems unhelpful to make claims about the effects of PEF on the log transformed membrane depolarization.

Therefore, we are left with the alternative, which is to remove any cases that are significantly influencing the dataset. For the purpose of analyses outliers were defined as cells (ROIs) whose fluorescence was beyond 2 standard deviations from the group mean (+/- 2 SD).

1.16.5 Additional inclusionary criteria

It is worth noting that prior to testing the assumptions, additional criteria was necessary for inclusion. In order to be considered for analysis, the cells being measured could not undergo any excessive movement. This included an automatic exclusion of any cells entering or exiting the field of view after the experiment commenced. Moreover, cells were excluded in the event that other debris entered the image series and altered the measured fluorescence in those ROIs. Finally, a stable baseline was required prior to any experimental manipulation in order for data from that cell to be further considered.

1.16.6 Definition of threshold

Many of the results to be presented will refer to a threshold. Whether it refers to PMPI experiments or YO-PRO experiments, the threshold was defined as the minimum electric field intensity required to produce a response that was significantly different than the control as determined by the statistical test performed. In the case of PMPI experiments, the threshold refers to membrane depolarization, whereas in YO-PRO experiments this refers to membrane permeability. The alpha criteria was set at $\alpha = 0.05$ for all tests.

1.16.7 Statistical terminology and abbreviations

Each statistical test is associated with an abbreviation. Using an ANOVA, the following will help elucidate some of the terminology that will be encountered when reading this text. The first letter, F, is used to represent the ANOVA. If a t-test is used, a t will replace the F; and in the case of a discriminant analysis, a Λ will take its place. In brackets, 2 numbers are seen and these represent the degrees of freedom (between, within groups). Between groups degrees of freedom (df) are calculated by subtracting 1 from the total number of groups tested. This would indicate that 3 groups were tested in the example below. Within groups df relates more to the sample size, where the number of groups is subtracted from the total sample size. Following the same example, this would indicate that the total sample size was 30. The number

14.20 is the obtained F-value, which is compared to a critical F-value and is dependent on the degrees of freedom and the threshold for statistical significance.

$$F\ (2, 27) = 14.20,\ p<0.01,\ \Omega^2 = 0.80$$

The p-value is a measure of statistical significance. If the F-value obtained is greater than the critical F-value, the p-value will represent a statistically significant difference between the groups tested. This value is traditionally set to either 0.05 or 0.01, which suggests that there is a 5 % or 1 % probability that the measured significance is false. The final number is the effect size Ω^2. This value represents the proportion of change in your dependent variable due to the experimental manipulations of the independent variable. The value 0.80 means that 80 percent of the variability in your dependent variable is due to the experimental manipulation. Additional abbreviations will be encountered for parameters such as; sample size (n), average (X), and standard error (SE).

1.17 Objectives and hypotheses for this Thesis

As a general overview of this chapter, whether the cell or the intracellular organelles are targeted, ultimately the membranes surrounding them are influenced using pulsed electric fields. Depending on the desired effect, pulse durations can be used which are greater than or less than the membrane charging constant. When pulse durations are greater than the charging time, we observe effects at the level of the plasma membrane. Conversely, shorter pulse durations have the ability to penetrate the plasma membrane and influence intracellular organelles.

The research presented in this thesis investigated pulse durations ranging from 10 nanoseconds up to 10 milliseconds on several cell lines. The major point of interest will be to study the potential for these fields to act on transmembrane proteins, specifically ion channels. Three experimental chapters will be presented. Because our lab specializes in nsPEF exposure, the bulk of the data will be centered on these effects. The longer pulse durations were used in

the final experimental chapter, which was a collaborative venture between our lab and the University of Ljubljana.

The first chapter presents a statistical perspective on the results of nsPEF-induced membrane depolarization. Here we examined experiments on 500 cells over 3 years and attempted to use factors common in electrophysical models, such as cell size, shape, orientation to the electric field, and density of cells exposed to determine how well these parameters could predict the observed depolarization response.

The second chapter investigates the potential for nsPEF to modulate ion channel activity in U87 cells. Here, a vast number of broad and specific modulators of a variety of ion channels were used to determine whether they could influence the depolarizing response following electric field exposure. The null hypothesis being, if the depolarizing response to these fields was predominately due to electroporation of the plasma membrane, blocking individual ion channels should not significantly alter the effect.

Finally, knowledge gained from these chapters was applied to several cell lines in a collaborative project with the University of Ljubljana. Both excitable and non-excitable cell lines were selected to determine effects of pulse durations ranging from 10 ns to 10 ms on membrane depolarization. Membrane permeability was an additional parameter explored for these experiments. The goal for this chapter was to determine whether an electric field intensity could be found that was able to permeabilize the cells without significantly altering the transmembrane potential. The application of such a pulse would be to permeabilize cells targeted during electrochemotherapy treatment, while minimizing pain associated with electrically exciting surrounding nervous tissue. A manuscript has been submitted for this collaboration and is currently under review. The results presented in this thesis will include only those that I directly contributed to.

Chapter 2:

A comparative analysis of the theoretical and experimental interactions of PEF with cells *in vitro*

2.1 Introduction

Despite decades of research into the effects of PEF on biological systems, the mechanisms by which electric fields interact with cells are not fully understood. The present consensus relies on the combination of mathematical models and computer simulation to describe and predict experimental data.

A pioneer in this field of research, H. P. Schwan, was the first to mathematically describe the interactions between electric fields and biological systems in the late 1950's [82]. This relationship is summarized in Fig. 2.1 below, where the induced transmembrane potential, (V_m), is expected to be proportional to the applied electric field (E) and the cell radius (R). The cosine function predicts that V_m will be non-uniformly affected along the cell membrane, such that the greatest effects would be predicted at areas of the membrane adjacent to the electrodes. Moreover, it suggests that when two cells are exposed to an electric field of equal intensity, the greatest effects on V_m will be observed in the larger cell.

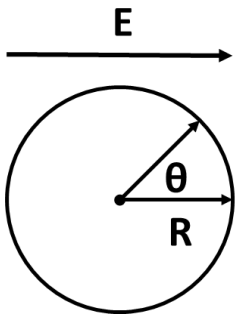

$$V_m = \frac{3}{2} ER\ cos\theta$$

Figure 2.1 – Schwan equation (steady - state). This steady-state equation predicts the induced transmembrane potential (V_m) on a cell with a radius (R) following the application of an electric field with an intensity (E). The cosine function (θ) suggests the effect will be influenced by the angle at which it interacts with the membrane.

An important issue to consider with the steady-state Schwan equation is that it does not consider the time required to superimpose an external electric field on the cell's resting membrane potential. This has become especially important as pulse durations have become

shorter than the time constant for charging the plasma membrane. For that to be considered, a modification of Schwan's equation incorporates the pulse duration (t) and the membrane charging time (τ_m) (Eq 2.1).

$$V_m = \frac{3}{2} ER\ cos\theta\ (1 - e^{\left(\frac{-t}{\tau_m}\right)})$$

Equation 2.1 - Schwan equation (first - order). Extension of the Schwan equation that incorporates time (t), and the membrane charging constant (τ_m).

One limitation with the Schwan equation is that the more a cell deviates from a spherical shape, the less it becomes applicable. With that said, regardless of the shape of the cell, experimental data has demonstrated repeatedly when fluorescent markers with high temporal resolution are used, the greatest effects are observed at membrane regions adjacent to the electrodes [83–86].

An excellent example of this was published recently, when a genetically encoded calcium indicator, GCamP, was used in experiments using nsPEF [87]. In Fig. 2.2 the authors delivered 100 x 10 ns pulses at either 10 Hz (top series) or 1 Hz (bottom series) with an electric field intensity of 44 kV/cm. In both conditions, although the time dynamics differ, a wave of calcium can be seen entering the cell moving along the electric field gradient from the anode to the cathode.

Sometimes, however, we find unanticipated results in the literature. Theory would predict [88] that, under the same conditions, the cell with a larger radius should be more influenced by the electric field than the smaller one. Yet we find results that show a positive relationship [88], an inverse [89], or no relationship [90, 91] between the size of a cell and the observed effects.

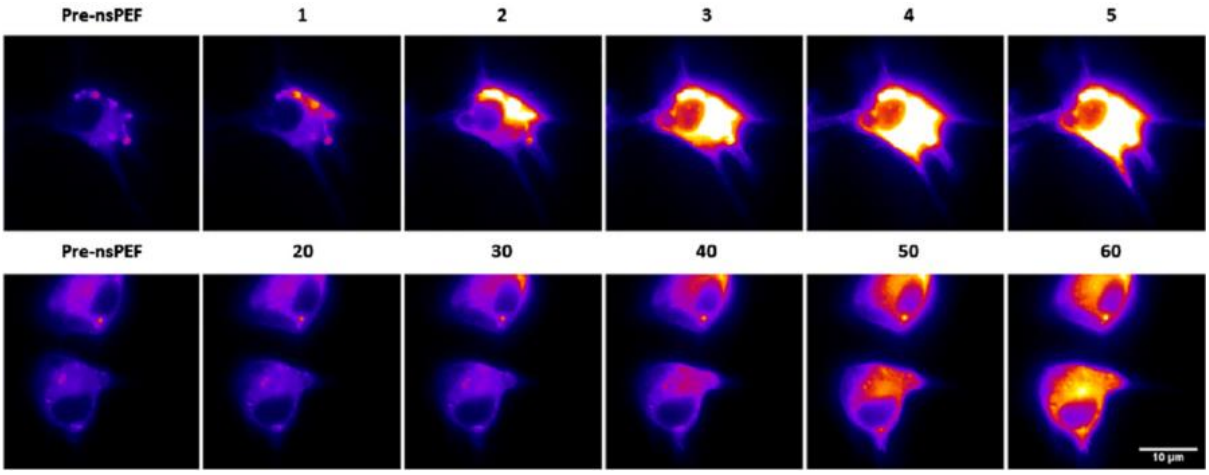

Figure 2.2 – Calcium wave entering the cell from the anodic pole following nsPEF. The top series shows results following 100 x 10 nsPEF, delivered at 100 Hz and an electric field intensity of 44 kV/cm. The bottom exposed cells to the same parameters except the pulses were delivered at 1 Hz. The numbers above the images are measure of time in seconds. Figure adapted from [87].

It is possible that there are some methodological differences that could shed some light on this discrepancy. For example, there were different cell types used in those experiments, which included yeast, rodent and human cell lines. All cells exhibit fairly characteristic growth patterns and rates, specific to their cell type. Since the density of cells being exposed is expected to play a significant role in the observed effect [86, 92], perhaps this factor could have contributed to the variation in results when considering the size of the cell. Despite the models describing the influence of cell density on PEF effects, I was unable to find any published articles that attempted to experimentally account for this parameter.

The objective for this section will be to determine how factors such as cell size, shape, orientation and density can predict membrane depolarization in U87 cells exposed to a single 10 ns PEF. Although analytical and numerical models for these parameters have been described [85, 86, 92], (Fig. 2.3) there have been no studies which have tried to experimentally determine how all of these factors simultaneously influenced the induced transmembrane

potential. For these analyses, additional factors such as temperature, medium conductivity, electric field intensity, pulse shape and duration have all been held constant to reduce as many extraneous variables as possible. One would expect that a significant contribution to the induced transmembrane potential following a PEF will be accounted for by variables such as; cell size, shape, the angle at which the PEF interacts with the cells major axis, and the density of cells in the field of view.

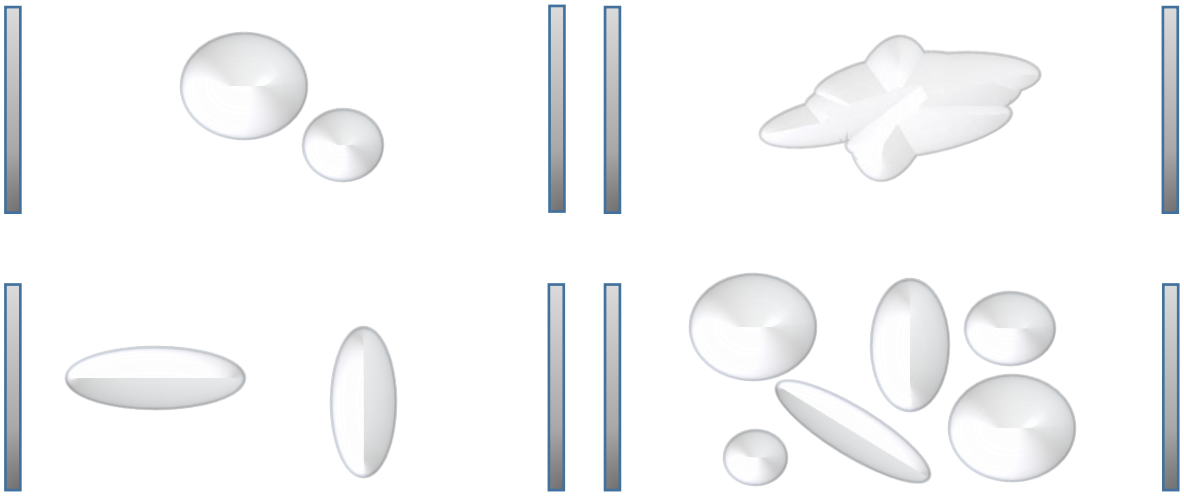

Figure 2.3 – Theoretical interaction of an electric field and a cell membrane. Factors such as cell size (top left), shape (top right), orientation to the electric field (bottom left), and density of cells (bottom right) will influence the observed response following PEF.

2.2 Methods

2.2.1 Determining size, shape and orientation of cells to PEF

2.2.1.1 Calibration of images

In order to measure the size of a cell, images had to be calibrated. This was accomplished using Image J software along with a calibration slide. The slide contained 15 micron beads, and when loaded into Image J, a line was traced across the diameter of the bead. A measurement of the line provided a value in pixels, and since the diameter of the bead

was known, we obtained a value of pixels / μm. This value was then applied to all subsequent images.

2.2.1.2 Determining size of the cell

The size or area of a given cell was determined using the same protocol as in 2.4.3, where a line was traced around the visible perimeter of the plasma membrane. This procedure was repeated for all cells in the field of view, and then added to the ROI manager in Image J. From here the measurements for size (μm²) were extracted and loaded into SPSS for analysis.

2.2.1.3 Determining shape of a cell

The cells used in these analyses were attached to the glass dish, which means that they each varied in shape to a certain degree. Image J offers a measurement of circularity, which is described in equation 2.2 below. This provides a unitless value with a range from 0 to 1, with 1 indicating a perfect circle.

$$Circularity = 4\pi\, x\, \frac{Area}{Perimeter^2}$$

Equation 2.2 - Determining the shape of a cell. A predetermined parameter provided by image J software providing a measure of sphericity. Unitless values are computed from 0 – 1, where 1 indicates a perfect circle.

2.2.1.4 Determining the angle of the cell with respect to the applied electric field

The ROI manager in Image J also provides a measurement of angle. This is a calculation that initially measures the long and short axes of the plasma membrane, and then measures the angle in degrees between the x axis of the image and the cell's long axis. Once this data was extracted, a correction was made for the positioning of the electrodes.

2.2.1.5 Determining the density of cells in a given image

After each cell had been traced a final ROI was traced around the entire field of view, which was also added to the ROI manager. The density of cells per unit area (cells / μm²) was

then calculated simply by dividing the number of cells in the field of view by the area of the image.

2.2.2 Statistical analyses

The statistical tests used in this chapter were based on the assumptions of a parametric dataset. As such, various criteria had to be met prior to performing these tests. These assumptions have been outlined in the general methods section of the introductory chapter and are detailed in [81].

2.3 Results

From a large sample size of 500 U87 cells collected over a multitude of experiments and over a three year period, variables such as cell size (μm^2), circularity of cell (1 indicating a perfect sphere), angle (degrees) relative to the direction of the applied electric field, and density of cells in the field of view (cells per μm^2) were extracted. These factors were subsequently entered as predictors into a linear multiple regression. The outcome variable was relative change in membrane potential, which was measured using PMPI.

Two variables were able to account for a small proportion of the change in V_m following nsPEF. Circularity ($n = 500$, $X = 0.78$, $SD = 0.10$, $p < 0.01$) and density ($n = 500$, $X = 0.0015$, $SD = 0.0008$, $p = 0.02$) entered the statistically significant model [$F(2 , 497) = 6.65$, $p < 0.01$, $\Omega^2 = 0.02$]. The relationship can be represented by (Eq. 2.3). This equation, as would be expected, highlights a positive relationship with circularity and a negative relationship with cell density. In other words, the greatest change in V_m post nsPEF would be expected under conditions where fewer cells were present and when those cells were more spherical than irregularly shaped.

$$V_m = 88.4x - 9157.9y + 54.9$$

Equation 2.3 – Equation describing relationship between cell shape and density with PEF-induced membrane depolarization. Here, V_m is measured as relative change in PMPI fluorescence; x refers to the shape (circularity); and y refers to density.

It is interesting that the statistically significant model was only able to account for approximately 2 % of the change in Vm following nsPEF exposure. In other words, that majority of the variability in membrane depolarization is unaccounted for using the factors entered into the regression. Moreover, factors such as cell size and orientation to the electric field failed to significantly contribute to the model.

After carefully looking through the data, something became apparent that wasn't noticed during the initial analysis. When considering the baseline fluorescence, there was a clear grouping of data points (Fig 2.4). To test if this represented two statistically different groups, a sequence of tests was performed. To begin, a cluster analysis was performed on the baseline fluorescence data. Consistent with our observations, the results from the cluster analysis divided the data into 2 groups, where 465 cells were in the first group and the other 35 cells were in the second group.

Using the groups generated from the cluster analysis, a discriminant function analysis was performed to determine if these groups were truly statistically different from one another. The results from this test revealed a discriminant function that explained 92% of the variance between groups. This function significantly differentiated the baseline fluorescence data [$\Lambda = 0.15, \chi^2(1) = 946.82, p < 0.01$].

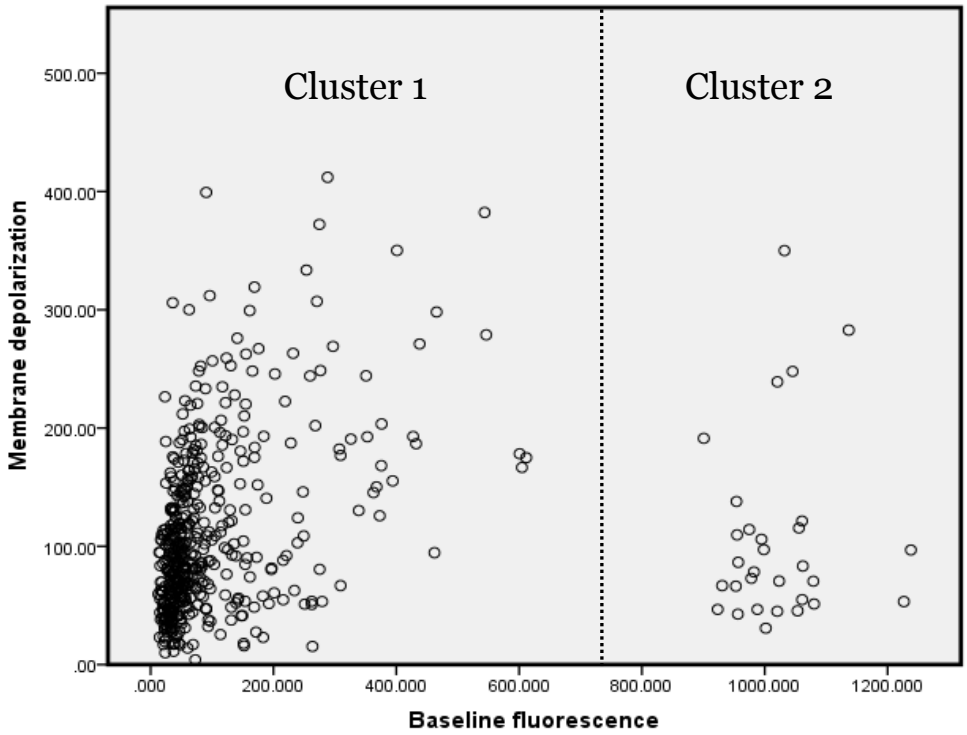

Figure 2.4 - Investigating pattern in baseline fluorescence. Two distinct clusters are easily distinguishable when examining baseline fluorescence values. X (average of first 5 minutes pre-pulse) and y (first 2.5 minutes post-pulse) values are given in raw fluorescence values.

These results suggest that there were two populations of cells that were significantly different from one another despite having identical experimental protocols. Moreover, these cells weren't clustered temporally, meaning they represent two distinct populations that have been collected over several years. What could be different about these cells then? Referring to table 2.1 and 2.2 below, you will find descriptive statistics for the two groups along with a correlation table which describes their relationship with the factors used in the multiple regressions.

	Sample size (n)	Minimum	Maximum	Mean	Standard deviation
Cluster 1					
Area (µm²)	465	15.09	538.62	87.05	58.56
Baseline fluorescence	465	12.55	465.64	88.48	84.38
Circularity	465	0.36	0.96	0.77	0.10
Angle (degrees)	465	0.25	179.76	95.66	51.50
Density (#/µm²)	465	$9.70\ 10^{-5}$	$2.\ 10^{-3}$	$1.54\ 10^{-3}$	$8.54\ 10^{-4}$
Cluster 2					
Area (µm²)	35	33.33	363.48	126.24	74.08
Baseline fluorescence	35	543.81	1237.91	958.54	172.66
Circularity	35	0.65	0.90	0.80	0.08
Angle (degrees)	35	0.13	177.49	92.32	46.94
Density (#/µm²)	35	$2.91\ 10^{-4}$	$2.82\ 10^{-3}$	$1.48\ 10^{-3}$	$4.56\ 10^{-4}$

Table 2.1 - Descriptive statistics for the two populations of cells grouped by baseline fluorescence. For each parameter investigated, this table provides the sample size (n), minimum, maximum, and mean values, as well as the standard deviation for both clusters of cells.

Fluorescence change	Area (µm2)	Fluorescence baseline	Circularity	Angle (degrees)	Density (#/µm2)
Cluster 1	0.106	0.424	0.123	0.029	-0.107
Cluster 2	-0.160	-0.446	0.069	0.238	-0.072

Table 2.2 - Pearson correlation table from the multiple regression test divided into clusters. Values in bold indicate a statistically significant correlation between those values and the change in fluorescence using an alpha of 0.05.

Interpretation of the above two tables provides insight into the difference between groups. Beginning with the descriptive statistics (Table 2.1), aside from the different baseline fluorescence values, the average values from all other factors are essentially identical. Important differences are seen, however, when we refer to the correlation table (Table 2.2). Despite being the same cells treated in the exact same way, the first cluster is comprised of cells that are depolarized more as the size of the cell increases; which is contrasted in the second cluster, where depolarization is more pronounced as the size of the cell decreases.

The same pattern follows when considering the baseline values. Keeping in mind that the baseline values are representative of the resting membrane potential, cells in cluster 1 have a tendency to be more influenced by exposure to the nsPEF as the baseline fluorescence increases (less negative resting membrane potential); whereas cells in cluster 2 tend to be more influenced as the baseline fluorescence decreases (more negative resting membrane potential).

2.4 Discussion

Since the 1950's, electrophysical models have described the interaction between an applied electric field and a biological membrane. These have been extremely useful in designing experiments and interpreting results. Yet, despite multiple discrepancies between

theoretical predictions and experimental data in the literature, the established theory has not been challenged.

Of course these models are based off well established physical laws of electromagnetism described eloquently by Maxwell in the mid 1800's; however, application of these theories into biology tends to require that a cell is reduced from a complex living thing to a capacitor floating in conductive solution.

Molecular dynamics (MD) simulations have been a technological breakthrough that allow us to investigate electric field effects on the individual molecules making up a cell. Yet despite this incredible tool, the programs that determine the output are all designed based off the same fundamental theories. One advantage of MD is modeling a dynamic structure as opposed to the static electrophysical resistor-capacitor model. The cost of this, however, is the requirement for tremendous computational power limiting our search to a small fraction of the cell membrane and for a very short period of time.

The goal of this chapter was to investigate how theoretical models hold up against a large experimental dataset. Membrane potential was selected as the outcome variable because according to the literature, the induced transmembrane potential is the first step in a series of biological events following electropulsation [17, 18].

The results from this section suggest that under these conditions, there appears to be additional variables that are contributing to the nsPEF-induced membrane depolarization. Factors such as cell size, shape, orientation to the electric field and the density of cells being exposed failed to account for more than 90 % of variability in membrane depolarization following nsPEF exposure.

So, what other factors could account for this variability? One possibility could include ion channels. This idea was first explored almost 30 years ago [93], where microsecond pulses were found to influence the activity of Na^+/K^+ pump in human erythrocytes. Later, evidence was presented suggesting ms-PEF may induce electro-conformational damage to voltage-gate

channels [94]. Despite these findings, researching the potential role of ion channels in PEF-effects has just recently began to resurge. Several studies have now shown that voltage-gated ion channels can be activated by nsPEF [63–65].

Directly related to the activity of voltage-gated channels, the cell cycle could provide additional clues regarding variability in data from PEF experiments. Cells constantly oscillate through periods of de- and hyperpolarization, associated with changes in ion channel conductivity, that have been directly correlated with specific phases of the cell cycle [95–97].

When we consider results [89] demonstrating that membrane permeability was significantly greater following PEF exposure of cells in the S – M phase of the cell cycle compared to those in the G1 phase, it may not be spurious that we found two statistically distinct groups of cells clustered by baseline fluorescence (resting membrane potential). Furthermore, the 90/10 split between clusters is in line with the proportion of time primary carcinomas [98], and specifically U87 cells [99], spend in G1 phase versus S, G2 and M phases. Even If we assume that our clusters are representative of groups of cells divided into G1 and S – M phases, several key differences make it is difficult to compare our results to those in [89]; namely different pulse durations (μs vs ns), measured outcomes (permeability vs membrane potential), and cell type used (yeast vs human cells).

With that said, more attention should be given to expanding our understanding of electric field – cell membrane interactions. This is most important when we are looking at cell effects over longer periods of time. Combining the results presented here, along with some of the recent research discussed above, the influence of PEFs on transmembrane ion channels and perhaps even the role of cell cycle effects seem like good candidates for future studies.

Chapter 3:

Nanosecond pulsed electric fields depolarize transmembrane potential via voltage-gated K^+, Ca^{2+} and TRPM8 channels in U87 glioblastoma cells.

(Based on published manuscript)

3.1 Introductory Remarks

The following chapter is based on the manuscript [100]. It is worth noting that additional experiments have been included here that were not present in the manuscript. When considering the effects of PEF on complex living cells, the most fundamental process to begin our investigations would be the transmembrane potential (V_m). The reason it is imperative to understand the interaction of an electric field with the cell's resting membrane potential is because the superposition of the applied electric field on the cells V_m is considered to be the initial factor influencing cell behavior [17, 18] .

nsPEFs have a variety of applications in the biomedical and biotechnology industries. Cancer treatment has been at the forefront of investigations thus far as nsPEFs permeabilize cellular and intracellular membranes leading to apoptosis and necrosis. nsPEFs may also influence ion channel gating and have the potential to modulate cell physiology without poration of the membrane. This phenomenon was explored using live cell imaging and a sensitive fluorescent probe of transmembrane voltage in the human glioblastoma cell line, U87 MG, known to express a number of voltage-gated ion channels. The specific ion channels involved in the nsPEF response were screened using a membrane potential imaging approach and a combination of pharmacological antagonists and ion substitutions. It was found that a single 10ns pulsed electric field of 34 kV/cm depolarizes the transmembrane potential of cells by acting on specific voltage-sensitive ion channels; namely the voltage and $Ca2^{+}$ gated BK potassium channel, L- and T-type calcium channels, and the TRPM8 transient receptor potential channel.

3.2 Introduction

Nanosecond pulsed electric fields (nsPEFs) have been exploited in applications such as cancer therapy [66, 101, 102], and have demonstrated promise in improving gene delivery when combined with conventional pulses [103, 104]. *In vitro* experiments [27, 69, 105–107]

along with support from mathematical modeling [32, 62, 108] have demonstrated that nsPEFs cause changes in cell physiology by permeabilization of the plasma membrane and intracellular organelles. Results have also been demonstrated *in vivo* with considerable nsPEF effects on tumor growth [55] and vascular perfusion [109]. A prominent mechanistic working model developed from MD simulations suggests that nsPEF permeabilization is mediated by the reorganization of water molecules at the lipid membrane interface by the electric field-induced orientation of their dipoles, leading to the formation of pores [110].

Few experimental studies or simulations have considered the potential role of transmembrane pore-forming protein complexes and channels in nsPEF effects. A wide variety of such ion channels exist in the plasma membrane that can influence membrane permeability to ions and small molecules and can be gated by a wide range of stimuli ranging from ligands (ionotropic receptors), voltage (voltage-gated ion channels), mechanical perturbation (mechanosensitive ion channels) or changes in temperature (transient receptor potential channels (TRPs)).

In vitro studies have primarily investigated the permeabilization of the plasma membrane by nsPEF using the translocation of small membrane-impermeant fluorescent molecules, fluorescent ion sensors, or electrophysiology. The latter, more direct approach of measuring plasma membrane impedance using the patch-clamp technique was used to probe membrane resistance following the application of nsPEFs (60 ns, 12 kV/cm), revealing a threefold decrease in membrane resistance 80 - 120 seconds following pulse delivery with a gradual recovery over 15 minutes [105]. Several ion channel pore blockers and ion substitutions were used in these experiments to examine the selectivity and specificity of the membrane permeability to various ionic species. Although this study did support MD theory of membrane permeabilization, the authors were careful to differentiate permeabilization and poration, and concluded that there was not sufficient evidence to confirm the creation of aqueous pores.

A subsequent study examined the size and lifetime of nanopores at the level of the plasma membrane. These experiments compared the effects of nsPEF (600 ns, 0.75-10.2 kV/cm) on the uptake of small fluorescent molecules (YO-PRO, propidium iodide PI) vs the uptake of Thallium (Tl^+) [111]. This investigation followed previous studies [69, 112] which demonstrated that more intense electric field strengths were required to observe PI uptake versus YO-PRO uptake. It was concluded that the larger PI molecules were occluded from pores where the smaller YO-PRO molecules passed through. Because of its small size (< 1 nm), Tl^+ uptake showed the presence of even smaller nanopores from which YO-PRO and PI would be excluded. The results from this study, combined with previous findings, suggested that nsPEF exposure led to pores smaller than 1 nanometer.

Some studies have considered the possibility that such short pulsed electric fields could influence ion channel behavior. This alternative to electroporation was first explored in bovine chromaffin cells using a pulse protocol of 5 ns, 50 kV/cm [64]. By using several pharmacological inhibitors of calcium and sodium channels, it was shown that a combination of L- N- and P/Q-type calcium channel blockers abolished the nsPEF-induced influx of calcium into cells, suggesting the involvement of voltage-gated calcium channels.

In a separate study, the effects of PEF's was examined on several cell lines [63] using a pulse duration of 500 picoseconds at 190 kV/cm, with a range of pulses up to 100 at a frequency of 200 Hz or 1 kHz. When applying these pulse parameters to CHO cells, which served as a negative control due to the lack of voltage-gated channels, no effects were observed while measuring $[Ca^{2+}]_i$ with Fura-2. Yet when tested on cell lines known to contain voltage-gated channels, such as GH3 and NG108, the same protocol resulted in a significant increase in $[Ca^{2+}]_i$. To demonstrate this effect was not due to electroporation of the plasma membrane, voltage-gated calcium channel blockers, verapamil (L-type) and w-Conotoxin (N-type) were utilized. While these pharmacological inhibitors could partially block the calcium response when used separately, as a cocktail they could block 85 - 100 % of the observed PEF response.

These results imply that the calcium increase caused by ultrashort pulsed electric fields was mediated by voltage-gated calcium channels.

The distinction between direct permeabilization effects on the plasma membrane and changes in ion permeability mediated by voltage-gated ion channels is important, given that many cancers are known to express voltage-gated ion channels [113, 114]. We therefore chose to investigate the influence of nsPEFs on the human glioblastoma cell line (U87), as it expresses many types of ion channels that are characterized at the level of gene expression [115] and in detailed electrophysiological recordings [116, 117]. Our working hypothesis was that if nsPEF-induced membrane permeabilization was due to electroporation and the formation of nanopores, the response would not be inhibited by specific pharmacological inhibitors of ion channels. We tested this hypothesis using a fluorescent indicator of transmembrane potential to screen a wide range of ion channel inhibitors for their ability to inhibit a plasma membrane depolarization response caused by a single, 10 ns pulsed electric field of 34 kV/cm.

3.3 Materials and Methods

3.3.1 Pharmacological manipulation of ion channel activity

Multiple ion channel agonists/antagonists were used to monitor their effects on nsPEF-induced membrane depolarization. These drugs were selected based on their ability to block channels known to be present in this cell line [97, 116–121]. All ion channel modulators were purchased from Sigma Aldrich and are summarized by activity in table 3.1 below.

Product	Concentration	Mechanism of action	Incubation period
Calcium channel modulators			
A784168	10 μM	TRPV1 blocker	15 minutes
AMTB Hydrate	50 μM	TRPM8 channel blocker	15 minutes
BAPTA-AM	10 μM, 30 μM	IC Ca2+ chelator	45 minutes
Cyclopiazonic acid	1 μM	Ca-ATPase blocker/depletes ER	10 minutes
Ethylene glycol tetraacetic acid (EGTA)	1.8 mM (replaced $CaCl_2$)	EC Ca2+ chelator	15 minutes
Gadolinium	10 μM	Broad calcium and TRP channel antagonist	15 minutes
HC-030031	3 μM to 300 μM	TRPA1 blocker	15 minutes
Ionomycin	10μM	Ca^{2+} ionophore	Added prior to imaging
Lanthanum chloride ($LaCl_3$)	100 μM	Broad calcium channel antagonist	15 minutes
M8-B	2 nM to 50 μM	TRPM8 channel blocker	15 minutes
Mibefradil	20 μM	T-type VGCC blocker	15 minutes
Nifedipine	10 μM	L-type VGCC blocker	15 minutes
Ruthenium Red	100 μM	Broad calcium channel antagonist	15 minutes
2-APB	100 μM	TRPC blocker	15 minutes
Potassium channel modulators			
Barium chloride (BaCl2)	2.5 mM (replaced KCl)	KIR channel blocker	15 minutes
Clotrimazole	30 μM	IK channel blocker	15 minutes
Glibenclamide	50 μM	ATP-dependent K^+ channel blocker	15 minutes
Iberiotoxin	10 nM	BK channel blocker	15 minutes

Paxilline	100 μM	BK channel blocker	15 minutes
Penitrem A	100 nM to 10 μM	BK channel blocker	15 minutes
Phloretin	30 – 1000 μM	BK activator	Added prior to imaging
Tetraethylammonium chloride (TEA)	5 mM to 100 mM	Voltage-gated K^+ channel blocker	15 minutes
Sodium channel modulators			
Amiloride HCl	200 μM	Na+ channel blocker; ASIC blocker; mechanogated ion channel blocker	15 minutes
Tetrodotoxin (TTX)	1 μM	Voltage-gated Na+ channel blocker	15 minutes
Choline Chloride	140 mM	Used to replace sodium in imaging media	15 minutes
N-methyl-D-glucamine (NMDG)	140 mM	Used to replace sodium in imaging media	15 minutes

Table 3.1 - List of pharmacological agents used throughout this investigation. Product names are given along with the concentrations used and their mechanism of action. For clarification of abbreviations: TRP = transient receptor potential, IC = intracellular, EC = extracellular, CaMKII = Calcium/calmodulin-dependent protein kinase II, VGCC = voltage-gated calcium channel, K_{IR} = inward-rectifying potassium channel, IK = intermediate conductance calcium-dependent potassium channel, BK = big conductance calcium-dependent potassium channel, ASIC = acid-sensing ion channel.

3.3.2 Calibration of PMPI voltage-dye

In order to obtain information regarding membrane potential from fluorescence data the fluorophore (PMPI) needed to be calibrated. Cells were incubated in the same method as above; however, several imaging solutions were made where the concentration of NaCl was replaced by increasing amounts of KCl (2.5 mM, 25 mM, 50 mM, 100 mM, and 140 mM). An

estimate of membrane potential was then computed by applying the Goldmann equation and comparing the fluorescence data at various K^+ concentrations with the calculated membrane potential at those concentrations. Although semi-quantitative in nature, this method allowed for a general estimate of the changes in membrane potential over time following exposure to nsPEF.

The results from the calibration were compared to separate results calibrating PMPI using patch-clamp electrophysiology (section 3.4.1). Here, cells were exposed to a voltage-ramp while PMPI fluorescence was measured. With these results, we were able to compare both quantitative and semi-quantitative measures of transmembrane potential and use this data to estimate the magnitude of depolarization following electric field exposure.

3.3.3 Statistical analyses

Statistical analysis was performed using IBM SPSS 19. Assumptions were met for analysis using parametric tests. More detail on the individual statistical analyses can be found in the general methods section of the introductory chapter, in addition to [81].

3.4 Results

3.4.1 Calibration of PMPI

The first step in our investigation was to calibrate PMPI. Although semi-quantitative in nature, using different calibration methods it should be possible to determine a change in transmembrane potential in response to a stimulus. This is different than knowing the absolute value of the transmembrane potential at a given moment; however, knowing how much a given manipulation is altering V_m is still useful for interpreting effects. PMPI calibration was performed using potassium [K^+] gradients and additionally using patch-clamp electrophysiology.

3.4.1.1 Potassium calibration

Calibration of the dye using K^+ was achieved by monitoring the change in relative fluorescence over time using varying concentrations of extracellular K^+. For a period of 30 minutes, imaging medium was exchanged every 5 minutes with [K^+] from 2.5 mM to 140 mM (Fig. 3.1). Maximum depolarization of the transmembrane potential occurred following the addition of 100 mM [K^+].

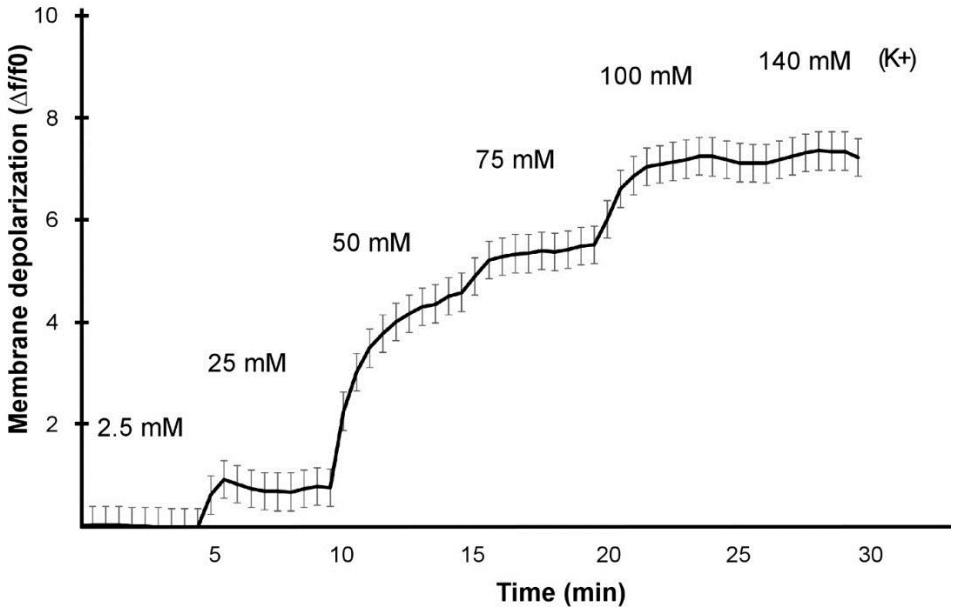

Figure 3.1 - Calibration of PMPI by varying extracellular K^+. Relative fluorescence changes for PMPI were measured over time in response to increases in extracellular [K^+]. Potassium concentration was gradually increased from 2.5 mM to 140 mM with a step occurring every 5 minutes Results are the average from 5 experiments. Error bars represent +/- 2 SE

Because we were most interested in the change in relative fluorescence at different concentrations of extracellular [K^+], a linear regression was performed to determine the relationship between variables. It should be noted that maximum depolarization occurred at 100 mM; therefore, the 140 mM data was not entered into the regression because no useful information could be obtained. The relationship between relative fluorescence and

extracellular [K^+] can be summarized using Eq. 3.1 below in which 96 % of the variability can be explained by the relationship between variables.

$$y = 0.0993x - 0.479\,, R^2 = 0.96$$

Equation 3.1 – Equation describing relationship between extracellular potassium concentration and membrane depolarization between 0 and 100 mM [K^+]. A linear regression was performed to find a relationship between relative fluorescence and the extracellular [K^+].

3.4.1.2 Calibration using electrophysiology

The next step involved a similar approach as above, using patch-clamp electrophysiology. Cells (n = 4) were exposed to a voltage-step ranging from -90 mV to +10 mV for five minutes and the relative fluorescence was recorded. The results obtained from these experiments were best fit using a 2nd order polynomial expression, which is summarized in equation 3.2 below, where the experimental manipulation accounted for 99% of the variability. This equation suggests that every increase in 1 relative fluorescent unit is associated with a membrane depolarization equivalent to 22.7 mV.

$$y = 0.0052x^2 - 0.1198x + 1.0402\,, R^2 = 0.99$$

Equation 3.2 – Equation describing relationship between membrane potential and PMPI fluorescence. A 2nd order polynomial equation was best able to explain the relationship between the transmembrane potential (mV) and the relative fluorescence measured.

PMPI calibration using two methods should allow us to generate a semi-quantitative estimate regarding the PEF effects on V_m. Table 3.2 below provides a comparison of the relative fluorescence changes using K^+ calibration and electrophysiology. The last column

provides an estimation, using the Goldman-Hodgkin-Katz (GHK) equation (Eq 3.3), of the transmembrane potential changes associated with alterations of the extracellular potassium concentration. Results from both electrophysiology and GHK estimation of the V_m are seen in columns 2 & 4. Relative fluorescence changes using PMPI under both calibration methods result in very similar (+/- 4 mV) changes in V_m.

$$V_m = \frac{RT}{F} \ln\left(\frac{p_k\ [K^+]_i + p_{Na}\ [Na^+]_i + p_{Cl}\ [Cl^-]_i}{p_k\ [K^+]_o + p_{Na}\ [Na^+]_o + p_{Cl}\ [Cl^-]_o}\right)$$

Equation 3.3 – Goldmann equation. Describes the predicted membrane potential based on the concentrations of ions inside $[X]_i$ and outside $[X]_o$ of the cell, where X is Na^+, K^+, or Cl^-, in addition to factors such as membrane permeability (p) of a give ion species, The gas constant (R), Faraday's constant (F) and the temperature (T).

Relative fluorescence ($\Delta F/F_o$)	ΔV_m (mV) Ephys	$[K^+]_o$	ΔV_m (mV) GHK estimation
1	22.7	14.9	18
2	29.3	25.0	26
3	34.1	35.0	32
4	38.0	45.1	37
5	41.4	55.2	42
6	44.5	65.2	45
7	47.3	75.3	48
8	49.9	85.4	51

Table 3.2 - Comparison between calibration methods for PMPI. This table summarizes the membrane potential change following nsPEF delivery for both the electrophysiology and potassium calibration.

3.4.2 Determining the threshold of electric field intensity required for nsPEF-induced membrane depolarization.

In order to determine the threshold for membrane depolarization, electric field intensity was varied (16.5 kV/cm, 22 kV/cm, 34 kV/cm, and 44 kV/cm). When comparing the

group means 2.5 minutes post pulse, significant group differences were observed. Applied electric field strengths of 16.5 kV/cm or 22 kV/cm were not significantly different than the no pulse conditions, although the latter was qualitatively different. Both the 34 kV/cm and 44 kV/cm applied field strengths were significantly different than control conditions (Fig. 3.2). In each case, membrane depolarization caused by a single 10 ns pulse was transient, recovering in 15 - 20 minutes.

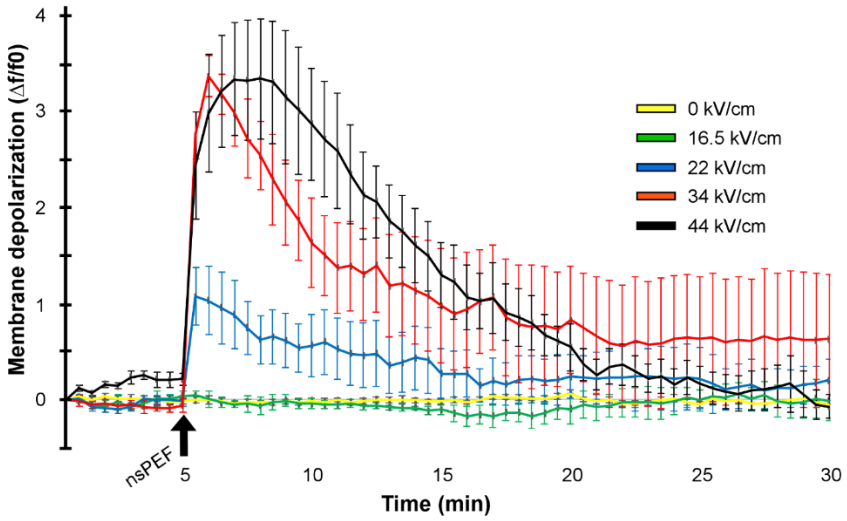

Figure 3.2- Determining the electric field threshold for a single nsPEF to depolarize plasma membrane. An analysis of variance indicated there was a significant difference in relative fluorescence between groups exposed to different electric field strengths [$F(4, 26) = 27.82$, $p < 0.01$, $\Omega^2 = 0.80$]. *Post hoc analysis followed using the Games-Howell method.* Significant membrane depolarization was observed when using applied field strengths of 34 kV/cm [$n = 5$, $X = 2.85$, $SE = 0.17$, $p < 0.01$, $r = 0.99$] and 44 kV/cm [$n = 5$, $X = 2.90$, $SE = 0.56$, $p < 0.01$, $r = 0.97$] when compared to control conditions [$n = 8$, $X = 0.01$, $SE = 0.02$]. When field strength was reduced to either 22 kV/cm [$n = 5$, $X = 0.89$, $SE = 0.31$] or 16.5 kV/cm [$n = 5$, $X = 0.001$, $SE = 0.03$] no significant effect was observed, though a visible qualitative response in the 22 kV/cm condition. Pulse deliver occurred at 5 minutes and is indicated by arrow in figure. Error bars represent +/- 2 SE

3.4.3 Fluorescence imaging of plasma membrane depolarization following a single 34 kV/cm nsPEF.

One of the most conspicuous features of the membrane potential dye (PMPI) is its unequal distribution within the cell. The 2-part dye responds to changes in membrane potential by entering or exiting the cell. During depolarization, the anionic, charged component enters the cell resulting in an increase in fluorescence (Fig. 3.3 a, b). This response is reversed during repolarization as the charged molecules exit the cell and interact with the quenching agent present in the extracellular space thereby decreasing the fluorescence.

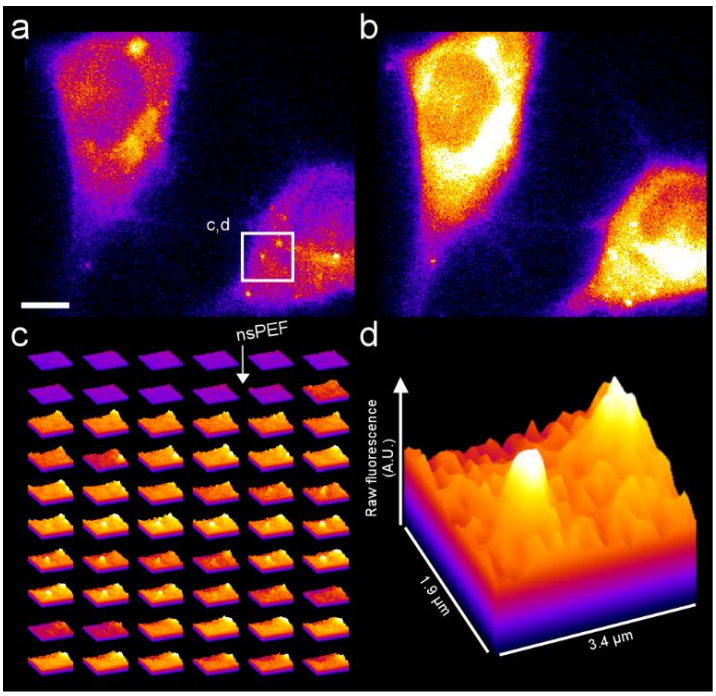

Figure 3.3 - Fluorescence imaging of U87 cells prior to and after delivering a single nsPEF with an electric field intensity of 34 kV/cm. PMPI is a two-part indicator of membrane potential consisting of an anionic, charged component and a quenching agent restricted to the extracellular space. Upon depolarization of the plasma membrane, the charged molecules enter the cytosol and increase in fluorescence intensity. Pseudo-colored images are shown for enhanced contrast. **a** and **b** depict the fluorescence change pre vs. post pulse. **c** is a surface plot montage of the selected region in a framed by the square. The nsPEF was delivered after five minutes, corresponding to the tenth image of the montage marked by the arrow. Maximum depolarization can be seen after 60 seconds and individual regions of

intense depolarization are observed throughout the remainder of the experiment at different time points. **d** is an example taken from the surface plot highlighting the geometry of these punctate regions where depolarization of membrane potential first occurs in response to the nsPEF (x and y axes are given in micrometers, while the z axis is in raw fluorescence changes).

3.4.4 Inhibition of nsPEF depolarizing effect with BK channel blockers.

In order to investigate the role of ion channels in the nsPEF depolarization, multiple ion channel antagonists were tested for their ability to abrogate the response to a single 34 kV/cm nsPEF. If depolarization was mediated by pores, then none of the pharmacological channel-blockers would be expected to inhibit the response. The following section investigates the influence of nsPEF on a subtype of voltage-dependent potassium channels.

U87 cells are known to express several potassium channels, many of which are voltage dependent. Because the observed depolarization was slow, taking place over minutes, non-voltage-gated channel antagonists were also used. Inhibitors of voltage-and-calcium-dependent potassium channels were found to inhibit the depolarization of the plasma membrane caused by a single nsPEF (fig. 3.4 below). When inhibitors of voltage-and-calcium-dependent potassium channels (BK, SK, IK), Inward rectifying potassium channels (K_{IR}) and ATP-dependent potassium channels (K_{ATP}) were compared with nsPEF-only conditions, there was a statistically significant difference in their ability to abrogate the nsPEF depolarization (fig. 3.4 below).

Prior to depolarization, the dye can be seen clustering into small, punctate regions. Although the spatial distribution of labelling varied in each cell, the clusters accounted for roughly 15 - 20 percent of the observable plasma membrane, with the small punctate regions ranging from 0.5 - 1.0 μm in diameter (fig. 3.3 c, d).

Post-hoc analysis using Games-Howell method indicated the source of the significant difference was between the nsPEF only condition and those cells pretreated with 10 μM Penitrem A and 100 mM TEA. No significant differences were observed between nsPEF depolarized cells and cells those treated with any of the other inhibitors. Results are presented in Fig. 3.4 below.

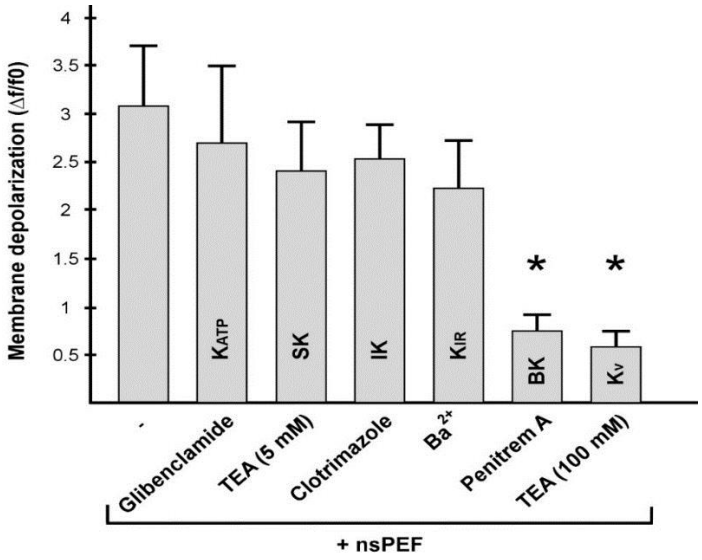

Figure 3.4- Effects of potassium channel blockers on nsPEF-induced membrane depolarization. An analysis of variance indicated there was a significant difference between the mean fluorescence between groups using different potassium blockers [F (6, 64) = 17.09, $p < 0.01$, $\Omega^2 = 0.60$]. *Post hoc analysis using the Games-Howell method revealed the following: w*hen comparing control conditions (nsPEF only) and those with potassium channel blockers, only Penitrem A, a specific BK channel blocker [n = 5, X = 0.75, SE = 0.26, $p < 0.01$, r = 0.96]; and 100 mM TEA, a broad voltage-gated potassium channel blocker (K_V) [n = 16, X = 0.58, SE = 0.26, $p < 0.01$, r = 0.96] significantly inhibited membrane depolarization from a single 34 kV/cm, 10 nsPEF. Inhibiting ATP-dependent (K_{ATP}) channels with Glibenclamide [n = 9, X = 2.73, SE = 0.27], small conductance voltage-and-calcium dependent potassium (SK) channels with 5 mM TEA [n = 5, X = 2.42, SE = 0.18], intermediate conductance voltage-and-calcium dependent potassium (IK) channels with 30 μM Clotrimazole [n = 11, X = 2.55, SE = 0.09], or inward rectifying potassium channels (K_{IR}) with 2.5 mM Barium chloride ($BaCl_2$) [n = 10, X = 2.24, SE = 0.40] produced no significant

differences from controls. Asterisks * represents statistical significance at alpha = 0.05 compared to nsPEF only condition. Error bars represent +/- 2 SE

Whereas the 100 mM TEA condition significantly inhibited the nsPEF-induced depolarization, the 5 mM TEA did not. Since it is known that K_V inhibition at high concentrations (> 10 mM) of TEA are known to include BK channels but not at low concentrations (≤ 10 mM) [116], a range of TEA concentrations were used next to investigate the dose-response of the TEA inhibition of the nsPEF depolarization. A statistically significant trend can be seen, whereby increasing concentrations of TEA inhibited the nsPEF-induced membrane depolarization (Fig. 3.5).

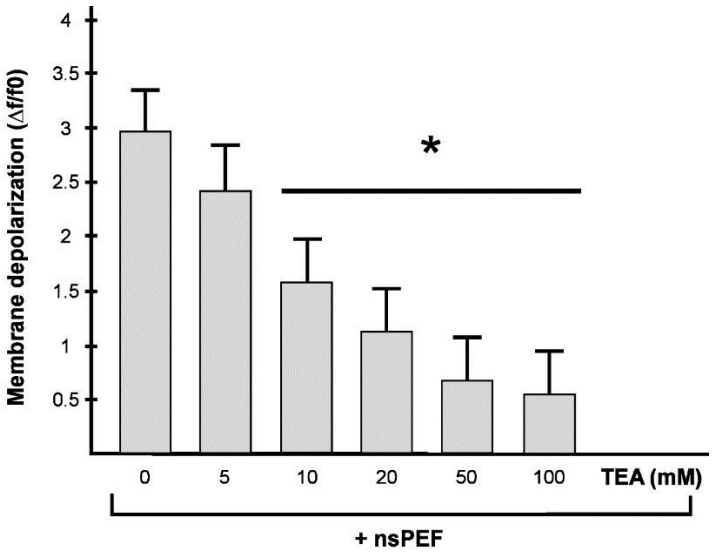

Figure 3.5 - Concentration-dependent inhibition of nsPEF depolarization by TEA. Comparing the nsPEF-induced membrane depolarization measured using increasing concentrations on tetraethyl ammonium (TEA) compared to the control conditions showed significant group differences [$F(5, 46) = 25.32$, $p < 0.01$, $\Omega^2 = 0.72$]. Post hoc analysis using Games-Howell test were conducted. Whereas 5 mM [n = 5, X = 2.42, SE = 0.18] TEA concentrations did not have statistically significant effects on nsPEF-induced depolarization, a linear trend can be seen as concentrations increase reaching statistical significance at 10 mM [n = 7, X = 1.58, SE = 0.15, p = 0.02, r = 0.69], 20 mM [n = 5, X = 1.13, SE = 0.34, p = 0.02, r = 0.87], 50 mM [n = 5, X = 0.68, SE = 0.22, p < 0.01, r = 0.84], and 100 mM [n = 15, X = 0.57,

SE = 0.08, $p < 0.01$, $r = 0.96$] TEA. Asterisks * represents statistical significance at alpha = 0.05 compared to nsPEF only condition. Error bars represent +/- 2 SE

Post-hoc analyses using Games-Howell reveal that statistically significant nsPEF inhibition was observed in conditions using 10 mM, 20 mM, 50 mM, and 100 mM TEA concentrations, but not with conditions using 5 mM TEA.

Since results from experiments using high concentrations of TEA and those using the selective BK channel blocker, Penitrem A, suggest that BK channel blockers can inhibit the nsPEF-induced membrane depolarization; two additional BK channel blockers were investigated: 100 μM Paxilline and 10nM Iberiotoxin. When compared to the nsPEF only condition BK channel block resulted in statistically significant inhibition of nsPEF-induced depolarization (Fig. 3.6a). Post-hoc analysis using Games-Howell indicated that Paxilline but not Iberiotoxin was able to significantly inhibit depolarization following nsPEF.

If the nsPEF application was depolarizing transmembrane potential via activating the BK channel, as suggested by the inhibition of these effects by BK inhibitors, one would also expect that activation of the BK channel by pharmacological agonists should produce similar changes in PMPI as induced by nsPEF. To confirm this, a specific activator of the BK channel was used without any exposure to pulsed electric fields. When 10 μM Phloretin was added to gate the BK channel, a depolarization was observed that was statistically similar to that observed following nsPEF (Fig. 3.6b).

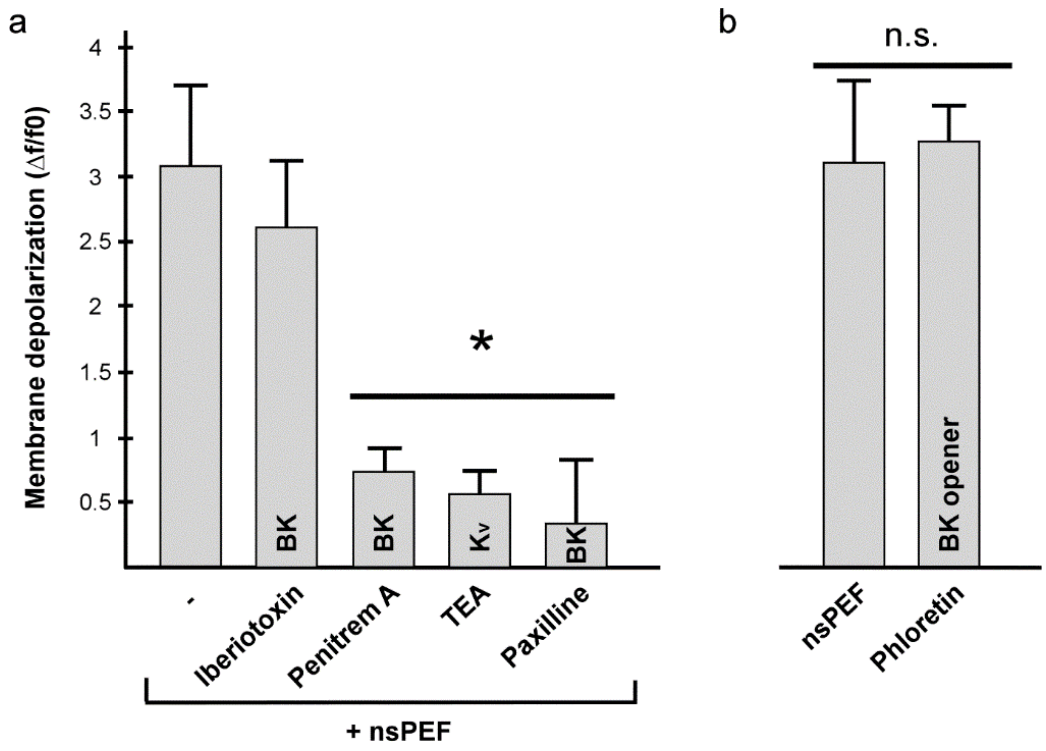

Figure 3.6 - BK channel blockers significantly inhibit membrane depolarization following 34 kV/cm nsPEF. a- An analysis of variance indicated there was a significant difference in mean fluorescence between groups [$F(4, 49) = 27.79$, $p < 0.01$, $\Omega^2 = 0.70$]. *Post hoc analysis followed using the Games-Howell method.* When comparing nsPEF only conditions to those with Paxilline [n = 5, X = 0.35, SE = 0.25, $p < 0.01$, r = 0.94] and Iberiotoxin [n = 15, X = 2.64, SE = 0.26], only the condition with 100 μM Paxilline significantly inhibited the nsPEF-induced depolarization. **b**- A two-tailed t-test comparing relative fluorescence measures indicated there was no significant difference between group means [$t_{(2\ tail)}(11) = 0.32$, $p = 0.75$] when 10 μM of Phloretin [n = 4, X = 3.26, SE = 0.14] was added to the external media, compared to the response observed when cells were exposed to nsPEF [n = 9, X = 3.10, SE = 0.32]. Data for tetraethyl ammonium chloride (TEA) and Penitrem A are included from figure 4. Asterisks * represents statistical significance at alpha = 0.05 compared to nsPEF only condition. Error bars represent +/- 2 SE

3.4.5 Depolarizing response of nsPEF is calcium-sensitive.

Among the potassium channel blockers explored, BK channel blockers were the only ones able to significantly inhibit membrane depolarization following nsPEF application. Its role was confirmed by using specific BK channel activators which mimicked the response observed following pulse application. Given that the BK channel can be gated by voltage-and-calcium, it was expected that modulating calcium should influence the sensitivity of the response to nsPEF. To test whether modulating intracellular and extracellular calcium concentrations could influence the threshold depolarization response following nsPEF, experiments were conducted using the following parameters: calcium-free conditions were performed with cells that were incubated with 10 μM BAPTA–AM and 1.8 mM Ethylene glycol tetraacetic acid (EGTA) substituted for 1.8 mM calcium chloride; and conditions where 10 μM of the calcium ionophore Ionomycin was added.

As represented in Fig. 3.7, altering the concentration of calcium shifted the threshold of the electric field intensity required for depolarization. In the control condition (n = 25), the EF50 (electric field required for 50 % maximal depolarization response) was determined to be 26.15 kV/cm where a maximal response was considered 100 %: A significant shift to the left was observed in the Ionomycin condition (n = 19) where the EF50 was 20.34 kV/cm and the maximal response exceeded the control by 10 %, whereas in the calcium-free condition (n = 21) the EF50 was shifted significantly to the right to a value of 45.43 kV/cm with the maximal response being less than 50 % of that under control conditions. Descriptive statistics for these results can be found in Table 3.3.

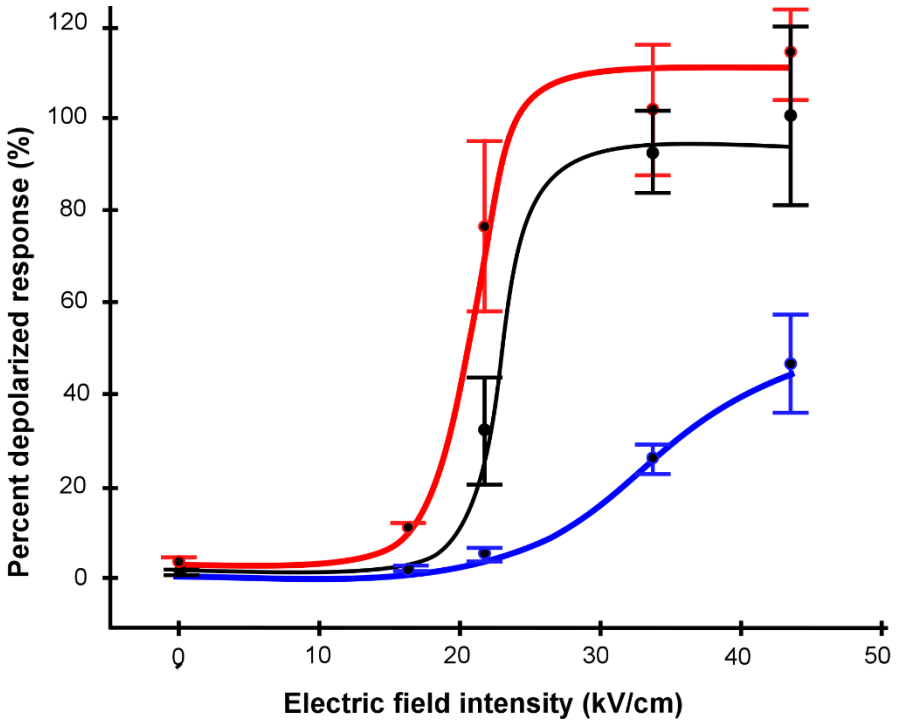

Figure 3.7 - Calcium-dependent threshold response curves in response to nsPEF of varying electric field strengths. Removing extracellular and intracellular calcium resulted in an EF50 (electric field intensity required to produce 50 % of the maximal depolarization) of 45.43 kV/cm (blue trace) and reduced the maximal response to less than 50 % of that observed in control conditions where the EF50 was determined to be 26.15 kV/cm (black trace). An opposite shift in EF50 of 20.34 kV/cm (red trace) was observed using the calcium ionophore Ionomycin, which also resulted in a 10 % increase in maximal response compared to control conditions. The overall fit for these dose-response curves was very good with statistically significant differences between groups [$\chi^2(2) = 0.38$, $p < 0.01$, Adj. $R^2 = 0.99$]. Error bars represent +/- 2 SE

Electric field strength (kV/cm)	Control	Calcium-free	Ionomycin
Baseline	n = 8, X = 1.87, SE = 0.47	n = 3, X = 0.93, SE = 0.40	n = 4, X = 2.58, SE = 0.76
16.5	n = 3, X = 2.47, SE = 1.02	n = 3, X = 1.56, SE = 0.21	n = 3, X = 10.38, SE = 1.70
22	n = 4, X = 30.73, SE = 10.78	n = 5, X = 5.42, SE = 1.22	n = 4, X = 75.30, SE = 19.38
34	n = 5, X = 91.93, SE = 8.56	n = 5, X = 25.40, SE = 3.06	n = 3, X = 100.94, SE = 14.83
44	n = 5, X = 100.00, SE = 8.56	n = 5, X = 46.01, SE = 10.60	n = 5, X = 114.03, SE = 9.42

Table 3.3 - Descriptive statistics from figure 3.7. Sample sizes (n), means (X), and standard errors (SE) are included by calcium condition for each level of electric field strength used.

Knowing that calcium was important for the nsPEF depolarizing effect, subsequent experiments were undertaken to determine whether the source of the calcium; being either extracellular (EC), intracellular (IC) or via release from the endoplasmic reticulum (ER) played a role in the amplitude of the response. These experiments were separated into extracellular calcium-free, intracellular calcium-free, and ER depleted; and these were compared to both the controls and the calcium-free (IC+EC) results above. Cells were incubated with 1.8 mM Ethylene glycol tetraacetic acid (EGTA), which was substituted for the calcium chloride in the media for the EC calcium-free condition; whereas for the IC calcium-free condition cells were incubated with 10 μM BAPTA-AM; and for the ER calcium-depleted procedure cells were incubated with 1 μM Cyclopiazonic acid (Fig. 3.8).

Whereas conditions using 1 μM Cyclopiazonic acid were not significantly different than controls, removing calcium from the extracellular and intracellular environment resulted in significant inhibition that was statistically similar to those observed when removing EC and IC calcium. Although removing EC and IC calcium resulted in significant inhibition of the nsPEF-induced membrane depolarization, the greatest effect was observed when EC calcium was removed.

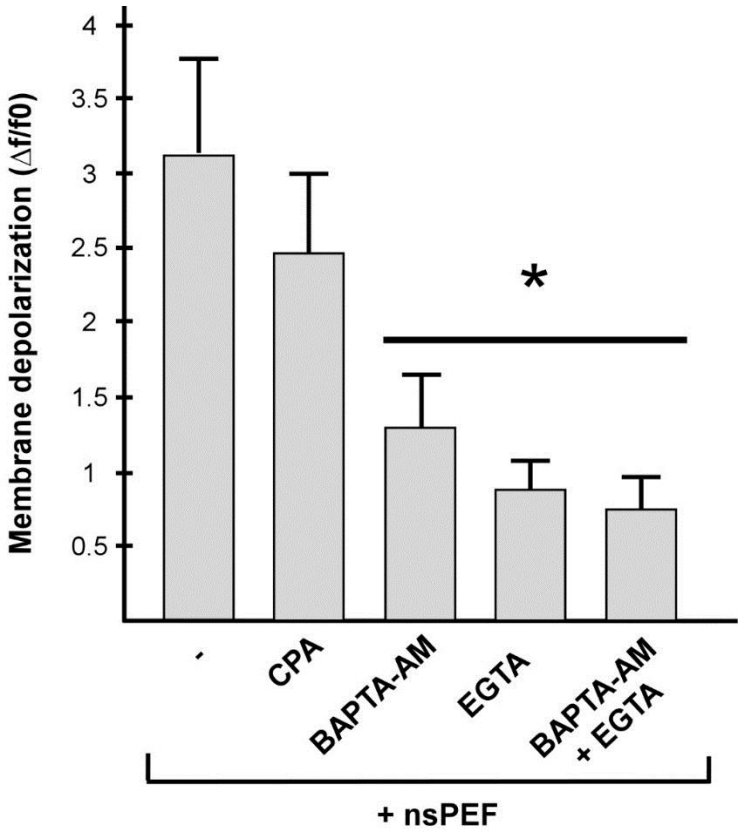

Figure 3.8 - Comparing the role of calcium from intracellular, extracellular and endoplasmic reticulum compartments. An analysis of variance indicated there was a significant difference in average fluorescence between groups [$F(4, 41) = 16.44$, $p < 0.01$, $\Omega^2 = 0.60$]. *Post hoc analysis followed using the Games-Howell method.* Significant differences in depolarization were observed when comparing controls with 1.8 mM calcium in media [n = 9, X = 3.10, SE = 0.32] to conditions where EC calcium was removed by substituting 1.8 mM EGTA for calcium in the media [n = 7, X = 0.88, SE = 0.11, $p < 0.01$, r = 0.95], IC calcium was removed by adding 10 μM BAPTA-AM [n = 10, X = 1.28, SE = 0.18, $p < 0.01$, r = 0.89], or both [n = 5, X = 0.74, SE = 0.09, $p < 0.01$, r = 0.96]; however, no significant effect was observed when calcium from the ER was depleted using 1 μM Cyclopiazonic acid [n = 11, X = 2.44, SE = 0.27]. Asterisks * represents statistical significance at alpha = 0.05 compared to nsPEF only condition. Error bars represent +/- 2 SE

Next, to test whether the influence of calcium on the depolarizing response was solely due to its role in modulating BK channel function or by nsPEF modulation of voltage-gated calcium channels, a series of experiments using several calcium channel blockers were performed (Fig. 3.9). Broad calcium entry channel blockers, Gadolinium, Lanthanum chloride and Ruthenium Red were investigated; as were L-type calcium channel blocker Nifedipine and T-type calcium channel blocker Mibefradil. Calcium can also enter via non-voltage-gated calcium channels such as the family of transient receptor potential (TRP) channels; therefore, selective TRPA1 blocker HC030031, TRPV1 blocker A784168, TRPC blocker 2-APB, and TRPM8 blockers M8-B and AMTB hydrate were tested for the capacity to block the nsPEF depolarization response.

Analysis revealed a statistically significant difference between conditions. Post hoc analyses using Games-Howell method revealed a significant inhibition of membrane depolarization between 10 μM Nifedipine, 20 μM Mibefradil, combined 10 μM Nifedipine and 20 μM Mibefradil, 100 μM Gadolinium, 100 μM Ruthenium Red, 100 μM Lanthanum chloride, 100 μM 2-APB, 50 μM M8-B, and 50 μM AMTB hydrate conditions when compared with controls. Conversely, no significant differences were observed between control conditions and those using 300 μM HC030031 or 10 μM A784168.

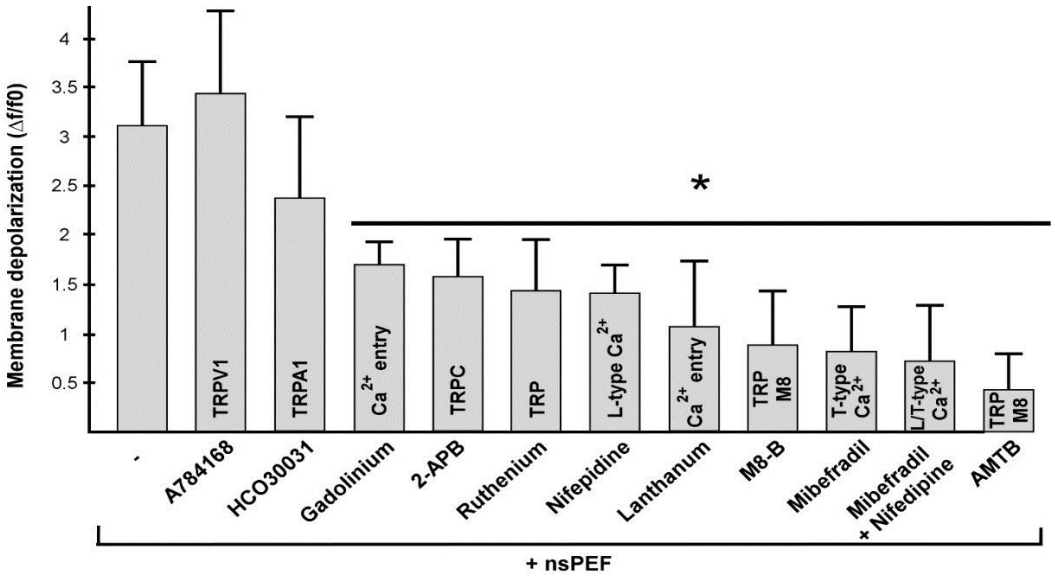

Figure 3.9 - Effects of calcium channel blockers on nsPEF-induced membrane depolarization. An analysis of variance revealed a significant difference in mean fluorescence between groups [$F(11, 91) = 11.71$, $p < 0.01$, $\Omega^2 = 0.56$]. *Post hoc analysis were then performed using the Games-Howell method.* Conditions using 10 μM of TRPV1 blocker A784168 [n = 9, X = 3.43, SE = 0.42], or 300 μM of TRPA1 blocker HC030031 [n = 6, X = 2.38, SE = 0.41] produced no significant differences from control conditions [n = 9, X = 3.10, SE = 0.32]. Significant inhibition of nsPEF-induced membrane depolarization was observed in conditions using broad calcium channel blockers 100 μM Gadolinium [n = 9, X = 1.69, SE = 0.12, p = 0.04, r = 0.70], 100 μM Ruthenium Red [n = 7, X = 1.43, SE = 0.23, p = 0.04, r = 0.71] and 100 μM Lanthanum chloride [n = 7, X = 1.07, SE = 0.33, p = 0.02, r = 0.83]; with the selective L-type calcium channel blocker 10 μM Nifedipine [n = 6, X = 1.41, SE = 0.14, p = 0.02, r = 0.90], T-type calcium channel blocker 20 μM Mibefradil [n = 8, X = 0.81, SE = 0.23, p < 0.01, r = 0.91], or when 10 μM Nifedipine was combined with 20 μM Mibefradil [n = 4, X = 0.71, SE = 0.29, p < 0.01, r = 0.93]; as well as with TRPC blocker 100 μM 2-APB [n = 9, X = 1.57, SE = 0.19, p = 0.03, r = 0.69], or TRPM8 blockers 50 μM M8-B [n = 5, X = 0.88, SE = 0.28, p < 0.01, r = 0.91] and 50 μM AMTB hydrate [n = 9, X = 0.44, SE = 0.18, p < 0.01, r = 0.95]]. Asterisks * represents statistical significance at alpha = 0.05 compared to nsPEF only condition. Error bars represent +/- 2 SE

3.4.6 nsPEF-induced membrane depolarization is not mediated by voltage-gated Na^+ channels; however, Na^+ ions may still be involved.

With evidence that nsPEF depolarization responses were abrogated by inhibitors of voltage-gated K^+ and voltage-gated Ca^{2+} channels, the following section investigated inhibitors of voltage-gated Na^+ and Cl^- channels. For these experiments 1 μM of Tetrodotoxin (TTX) and 200 μM of Amiloride hydrochloride were used to block voltage-dependent Na^+ channels. Further tests were performed by removing extracellular Na^+ and replacing it with equimolar 140 mM N – methyl – D - glucamine (NMDG) or Choline chloride.

The results from this series of investigations revealed (Fig. 3.10) a significant difference in group means. It should be noted that the assumption of homogeneity of variance was not met as determined using Levene's test; therefore, Welch's F test was used as a correction. Post hoc analysis using Games-Howell test showed no significant differences between conditions using TTX or Amiloride HCl when compared with controls. In contrast, removing extracellular sodium using either NMDG or Choline chloride significantly inhibited membrane depolarization caused by nsPEF.

These results, however, are difficult to interpret given that both NMDG and Choline chloride are known to block BK channel activity [122, 123]. Confirmation of this fact is evident in the same analysis where 10 μM Phloretin was applied in the presence of Choline chloride and the depolarizing effect observed above, which was on the same order of magnitude as that observed following nsPEF delivery, was abolished.

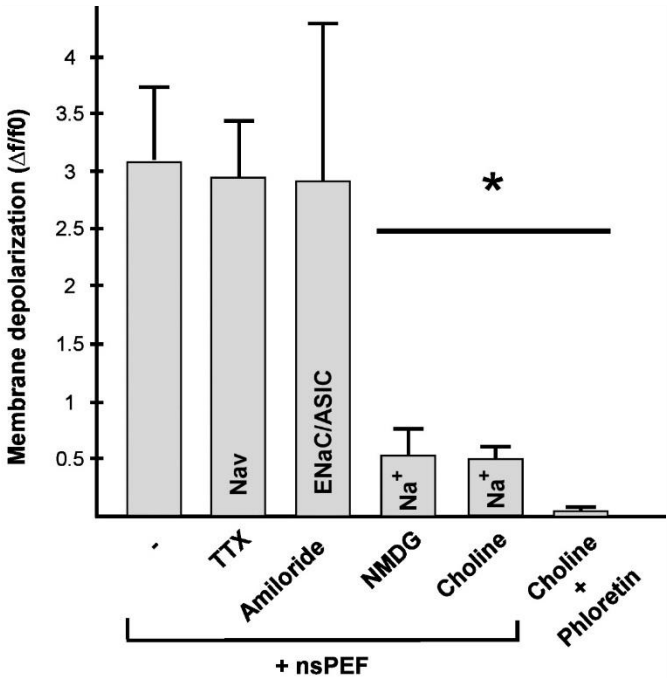

Figure 3.10 - Comparing effects from sodium and chloride channel blockers on nsPEF-induced membrane depolarization. An analysis of variance, reporting Welch's F due to a violation of the assumption of homogeneity of variance, revealed a significant difference in mean depolarization responses between groups [$F(6, 20.3) = 61.69$, $p < 0.01$, $\Omega^2 = 0.70$]. Post hoc analysis using the Games-Howell method found no significant effects on depolarization response following nsPEF delivery when comparing control conditions [n = 9, X = 3.10, SE = 0.32] to those with voltage-gated sodium channel blockers 1 μM TTX [n = 7, X = 2.96, SE = 0.25] and 200 μM Amiloride hydrochloride (HCl) [n = 8, X = 2.93, SE = 0.69]. Conversely, when sodium was replaced in the extracellular media there was significant inhibition of the membrane depolarization using either N – methyl – D - glucamine (NMDG) [n = 9, X = 0.53, SE = 0.11, $p < 0.01$, r = 0.96] or Choline chloride [n = 9, X = 0.51, SE = 0.05, $p < 0.01$, r = 0.97]. Repeating the experiments with Choline chloride in the presence of the BK channel activator Phloretin 10 μM resulted in inhibition of the depolarizing response [n = 10, X = 0.04, SE = 0.02, $p < 0.01$, r = 0.98]. Error bars represent +/- 2 SE

3.4.7 nsPEF-block is reversible.

In order to demonstrate that the inhibitors used were in fact inhibiting the nsPEF-induced membrane depolarization, we first had to rule out the possibility that the inhibitors were depolarizing the cells during the incubation period. If they were indeed depolarizing the cells they would not have the ability to further depolarize in response to nsPEF, which could explain nsPEF depolarization-inhibition. This possibility was ruled by applying multiple pulses at five minute intervals and observing the response over time. After three initial pulses, the imaging solution containing the inhibitor was washed off and replaced with the control solution (Fig. 3.11).

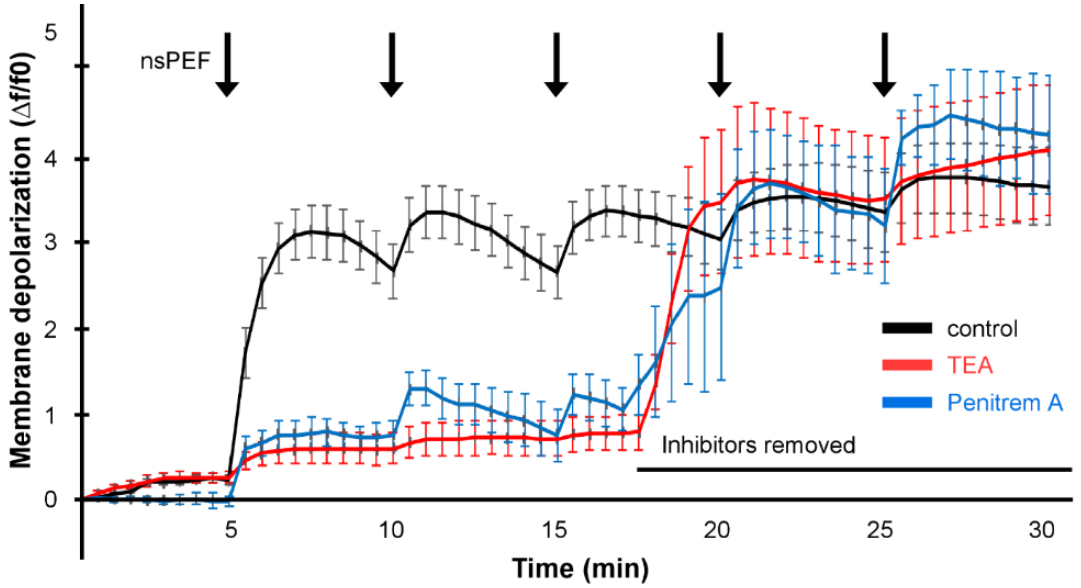

Figure 3.11 - Reversibility of the TEA and Penitrem A inhibition of the nsPEF-induced membrane depolarization. A single 34 kV/cm nsPEF (n = 9) was delivered every 5 minutes (indicated by black arrows in figure) while the TEA (n = 15)/Penitrem A (n = 6) (solution was replaced with control solution after 17.5 minutes (indicated by black bar in figure) demonstrating that the inhibition of the nsPEF-induced depolarizing response was not due to any depolarizing effect of inhibitors during incubation. For the purpose of clarity, only the 10 μM Penitrem A and 100 mM TEA data is displayed. Reversibility of the response was consistent among other inhibitors. Error bars represent +/- 2 SE

Following the removal of the pharmacological inhibitor, subsequent nsPEF delivery produce depolarizing response expected in the control conditions. This reversibility of the nsPEF block demonstrates that the cells were not depolarized during incubation and that the inhibitors used were in fact inhibiting the plasma membrane depolarization following nsPEF application. Another important feature is that repolarization of the resting membrane potential could be prevented by applying a subsequent pulse every five minutes.

3.5 Discussion

The purpose of this investigation was to study the role of voltage-gated ion channels in the depolarization response of the transmembrane potential following delivery of a single 10 nanosecond pulsed electric field. A combination of pharmacological inhibitors and a fluorescent indicator of plasma membrane potential was used with live cell imaging to evaluate the role of the various ion channels expressed in human U87 glioblastoma cells. These intense, short duration pulsed electric fields are known to exert their influence on cell physiology by inducing a transmembrane voltage across the cell leading to the formation of pores in the plasma membrane and intracellular organelles. This study implicated several ion channels in the nsPEF response and pharmacologically discriminated the specific voltage-gated channels involved.

The membrane potential indicator (PMPI) we employed in our investigations has previously been used in several studies and has been shown to be a valuable tool for monitoring membrane potential with higher throughput than patch clamp electrophysiology [77, 124, 125]. Our calibration of PMPI fluorescence with transmembrane potential was consistent with previous studies that compared PMPI fluorescence using electrophysiology [126].

By using a wide range of ion channel blockers and ion substitutions, we have provided strong evidence that the application of a single nsPEF is directly modulating ion channels within the parameters used in this study (10 ns pulse, 34 kV/cm). With that said, these results

may at first appear to be somewhat contrary to what one would expect. It is counterintuitive that the BK channel would gate at a negative resting membrane potential in the absence of Ca^{2+} as we have observed with nsPEF depolarization; however, this has been reported in non-excitable cells and the mechanism is well characterized [127]. The BK channel is primarily a hyperpolarizing channel and blocking the BK channel would be expected to increase the depolarizing effect observed; however, multiple studies have demonstrated that blocking the BK channels could have an inhibitory effect on depolarization and neurotransmitter release [128–130]. Interestingly, the BK channel has been demonstrated in some cells to operate in a biphasic mode [131, 132]. In excitable cells such as neurons, the activation of BK channels induces a hyperpolarizing response leading to a decrease in intracellular calcium and closing of voltage-gated calcium channels creating a negative feedback loop. Conversely, in non-excitable cells activation of BK results in increased intracellular calcium through activation of non-voltage gated calcium channels thereby increasing the driving force of calcium, and creating a positive feedback loop.

It is worth noting that the dimensions of punctate depolarized clusters and "hotspots" observed in PMPI labelling are consistent with previously measured size and distribution of lipid rafts within the cell membrane [133, 134]. From a physiological perspective, it is well established that many ion channels including voltage-gated ion channels are commonly clustered in lipid rafts [117, 134]. Specifically the BK channel has been shown to form complexes with T-type calcium channels [135] and L-type calcium channels [136].

The positive-feedback relationship between calcium channels and BK channels explains the results presented in this work and can be summarized as follows: Activation of T-type and L-type voltage-gated calcium channels by the nsPEF generates an inward calcium current which results in activation of BK channels. Activation of voltage-gated calcium channels has been confirmed previously with 5 ns, 50 kV/cm pulses [64] and shorter 500 ps, 190 kV/cm pulses [63]. Here, BK activation creates an outward potassium current which can activate calcium influx through non-voltage-gated calcium channels [131, 132], in the case of

U87 cell, where TRPM8 channels are known to interact with BK channels in glioblastoma cells [137]. It is also possible that the nsPEF could simultaneously activate BK channels and voltage-gated calcium channels. The fact that using a specific BK channel activator could depolarize the cells to a similar degree as the nsPEF corroborates this possibility (Fig. 3.12).

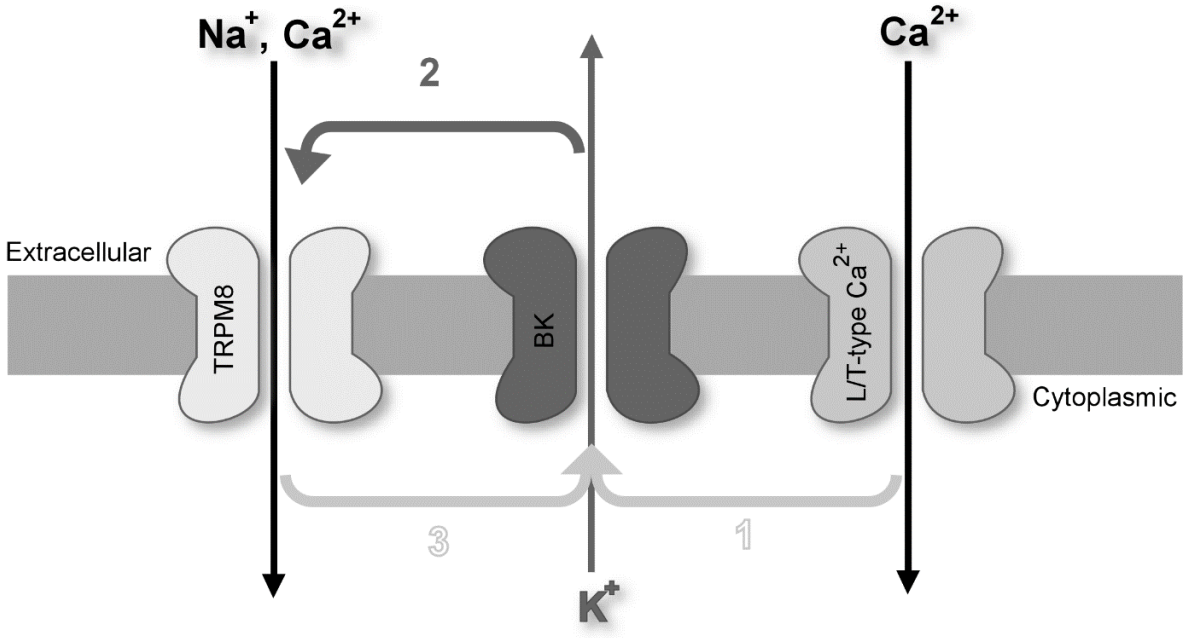

Figure 3.12 - Proposed mechanism of direct interaction between nsPEF and voltage-gated channels along with downstream effects on non-voltage dependent channels. 1. A single 10 ns, 34 kV/cm nsPEF activated voltage-gated calcium channels (L and T-type) along with the voltage- and calcium-dependent BK channels, causing an influx of Ca^{2+} and efflux of K^{+}. 2. The K^{+} efflux then triggers further Ca^{2+} entry through non-voltage-gated cation channels (TRPM8). 3. This action establishes a positive feedback loop and results in further membrane depolarization.

Considered the "gold standard" for studying BK channel activity, the lack of inhibitory action of the selective BK channel blocker, Iberiotoxin, was an unexpected result. However, reviewing the literature shed light on this apparent mystery. Toxin resistant BK channels have

been described since the late 1980's [138]. Originally found to be insensitive to Charybdotoxin, these channels are also insensitive to Iberiotoxin, which is a closely related toxin [139].

As a general overview of the BK channel, it consists of a tetrameric assembly of alpha subunits (BKα), which are responsible for creating the pore forming domain, and also contain the calcium biding domain and voltage sensing domain. Co-expressed with the alpha subunits are auxiliary beta subunits which are known to modulate the channel's activity [132, 140, 141]. The resistance to toxins is due to the presence of a specific isoform of the beta subunit (β4), which is known to be widely expressed in the brain [142–144]. Moreover, glioblastoma cells are known to express a specific subtype of BK channel known as the glioma BK or gBK [117], which incidentally are also known to express the Iberiotoxin-and-Charybdotoxin resistant β4 subunit [145].

It was not possible to definitively rule out Na^+ in the nsPEF transmembrane depolarization response, although it was clear from our results that voltage-gated Na^+ channels were not involved. When Na^+ was removed from the extracellular media and replaced with equimolar $NMDG^+$ or $Choline^+$, the depolarizing effect of Phloretin was eliminated. This result makes sense as both $NMDG^+$ and $Choline^+$ are also known to inhibit BK channel activity [122, 123, 146, 147]. It is of interest that TRPM8 channels were found to have a role in the nsPEF depolarization response as they are permeable to divalent and monovalent cations [148–151]. BK activation with TRPM8 gating would undoubtedly transport Na^+ in addition to Ca^{2+} into the cell and this would be commensurate with recent electrophysiological studies that have identified Na^+ currents in the early stage of nsPEF effects [152].

The involvement of TRP channels in the depolarization response caused by nsPEFs was also an important finding as some of the TRP channels are known to dilate to form pores permeable to small cationic fluorescent molecules such as YO-PRO-1 and ethidium. TRPA1, TRPV1 and TRPM8 are cell sensors for thermal, chemical and mechanical stimuli that are also known to form large, stable and reversible pores [149, 153], intriguingly similar to those caused by nsPEFs. Our investigation showed TRPM8 inhibition partially abrogated the nsPEF

depolarization response. It is still controversial whether TRPM8 form large pore complexes [154], and pore dilation is more confirmed with TRPA1 and TRPV1 [154–156]; so future studies should consider the influence of nsPEFs on pore-dilating TRPs as these are also known to be upregulated in cancer [113, 137].

BK channels (Big Potassium, also called Maxi-K or slo1), are a potentially important target for nsPEF effects as they have currents in order of 100-300 picoSiemens [157] and they are known to be upregulated in glioma and many other types of cancer [158, 159]. BK activators are also known to lead to apoptosis [160]. Mechanistically, it is not clear whether electric pulses in the nanosecond timescale could directly open BK channels as their gating time at physiological voltages requires multiple states with an activation time constant in the order or 150-200 microseconds [161]. Certain isoforms of BK channels are also known to be sensitive to mechanical stimulation and membrane stretch [162]. Further investigations should consider the mechanical properties of both BK and TRP channels in nsPEF effects, given that these stimuli have recently been shown to generate pressure transients [163].

Finally, we have also demonstrated that a single nsPEF delivered at five minute intervals can depolarize and prevent reestablishment of the resting membrane potential of U87 glioblastoma cells. Experiments are underway exploring the long-term manipulation of transmembrane potential to determine if non-electroporating nsPEFs can disrupt cell physiology in a manner that may be therapeutically useful for the treatment of cancer. The repolarization of plasma membrane potential in cancer cells repeatedly depolarized by nsPEF would be expected to occur via the Na^+/K^+-ATPase at great energetic cost, and given that only cancer cells expressing voltage-gated ion channels would be sensitive to this treatment, this may represent a new means to bioelectrically exhaust cancer, while sparing non-malignant cells nearby.

3.6. Conclusion

The primary aim of this section was to investigate the possibility that nsPEF are acting on transmembrane ion channels. A single 10 nsPEF was used at varying electric field

intensities to explore this. We monitored the transmembrane potential using the commercial indicator, PMPI, which proved to be a useful tool for studying long-term effects. Using a variety of pharmacological modulators of ion channel activity, we found that voltage-gated potassium and calcium channels were intimately connected to the observed depolarization following nsPEF exposure, as was the TRPM8 cation channel. Blocking these channels resulted in a significant decrease in membrane depolarization post-nsPEF exposure. We provided a potential theoretical model explaining how the interconnectivity between these channels, that are often found in proximity in lipid rafts, could help explain our results. Because the expression of ion channels varies significantly among cell lines, nsPEF effects would most likely be explained by different ion channels in different cells.

Chapter 4 -
Plasma membrane depolarization and permeabilization due to electric pulses in cell lines of different excitability

4.1 – Introductory remarks

The following chapter has been adapted from a manuscript that is currently under revision. This was a collaborative project between our lab and the University of Ljubljana. Results presented will include only those to which I directly contributed. Three cell lines were used for the following experiments: U87 glioblastoma cells, CHO cells, and HT22 mouse hippocampal neurons. HT22 cells were used in their differentiated and non-differentiated states. Experiments were conducted using pulse durations ranging from 10 ns up to 10 ms, where membrane potential and membrane integrity were the outcome variables measured. For both variables, the goal was to determine the threshold, or the lowest electric field intensity, required to depolarize or permeabilize the cells.

The bigger picture for these experiments was to test the potential for optimizing current treatments using electropermeabilization, such as electrochemotherapy. One common complaint for electrically based therapies is the associated discomfort due to the electrical excitation of the surrounding muscle and nervous tissues, which leads to muscle contractions and pain. We investigated whether it would be possible to find an electric field intensity that could simultaneously permeabilize the target tissues while minimizing the excitation of the surrounding nerves and muscles.

We found a statistically significant difference in excitability between cell types. Although the electric field threshold required to permeabilize the cells did not differ significantly between cell lines, the differentiated neurons required a stronger electric field to depolarize their transmembrane potential compared to the other cell lines. Although this was an *in vitro* study, these results indicate that it may be possible to modulate the electric field intensity in a clinical setting to enhance permeabilization, while limiting the excitation of neighboring nerves and muscles, thus the sensation of pain.

4.2 Introduction

Short, high-voltage pulses have been shown to increase the permeability of cell membranes to different molecules (reversible electroporation) or cause cell death (irreversible electroporation - IRE) [164–166]. Electropermeabilization is used in biotechnology sectors for food-processing [167–169], and in medicine [170] for gene electrotransfer (GET) [37, 48, 171], DNA vaccination [172–175], transdermal drug delivery [176, 177], IRE as a soft tissue ablation technique [42, 45, 46, 178] and electrochemotherapy (ECT) [179–182].

Medical applications of electroporation extend to a variety of tissues and tumours. Some of these tissues are electrically excitable, such as neurons in the central and peripheral nervous systems as well as muscle tissues. These cells are known to undergo sponataneous electrical activity [183] which is how they communicate with other tissues, and these excitable cells may be particularily vulnerable to electrically-based treatments.

In the literature, there are several examples of ECT, IRE and GET targeting excitable tissues using electric pulses. Brain cancer has been treated with IRE, and electric pulses have been shown to transiently disturb the blood-brain-barrier allowing chemotherapeutics to enter the brain [44, 184–188]. Treating prostate cancer [43, 189], bone metastases [179, 190], and tumours in the spine can affect the surrounding nervous tissue [190]. When treating tumours in other parts of the body, electrodes will invariably be in the vicinity of the nerves or muscles where the electric field is high enough for excitation or even permeabilization. Electric pulses are also used for ablation of myocardial tissue to treat atrial fibrillation [191–193]. Muscles are a popular target for gene electrotransfer as they are easily accessible and transfected [194, 195]. Among them, the heart can be electroporated to treat ischemia [196, 197].

Several studies have shown that the effect of electric pulses on the functionality of excitable tissues was only short-term. Following IRE, nerves in different animal models recovered electro-physiologically, histologically and functionally [190, 198–200] or at least showed a

potential for regeneration [201]. After electroporation of neurons within the rat neocortex , *in vitro* and *in vivo*, the membrane potential, the action potential waveform and passive membrane properties remained unchanged [202]. Following pulmonary vein ablation using electroporation, the histology and functionality of phrenic nerve remained unchanged [203]. Finally, no histological damage on nerves in the neurovascular bundle was observed post-IRE treatment of the prostate [199].

Some of the main drawbacks to treating tissues with pulsed electric fields are; the pain associated with repeated electrical stimulation [204–207], the need to administer muscle relaxants and anaesthesia [208] and synchronization with the ECG [209–211]. The neurons responsible for pain sensation are also known as nociceptors and have been shown to be stimulated by electric pulses [212, 213]. An important advancement for PEF treatments would be to determine a point at which maximum permeability of the membrane could be achieved while minimizing excitation of the nearby excitable cells. In ECT, for example, this would translate to maximum drug delivery into tumour cells with minimum tissue damage to surrounding regions, reduced pain experienced by the patient, and minimal use of muscle relaxants.

The following experiments will explore how pulsed electric fields will effect excitable and non-excitable cells. This will be addressed using measures of membrane potential and membrane permeability for pulse durations ranging from 10 ns to 10 ms. Using a range of electric field intensities, the goal will be to determine the lowest intensity required to depolarize the transmembrane potential and to permeabilize the plasma membrane. The results will be compared between cell types to determine whether or not it could be possible to optimize current treatments to reduce the sensation of pain due to repeated electrical stimulation.

4.3 Materials and Methods

Some of the materials and methods are common between thesis chapters. These include cell culture, growth and maintenance; fluorescence microscopy, pulse generators and electrodes used; data extraction from images, as well as statistical methods used to analyze data. In the interest of not repeating information, these have been explained in detail in the general methods section of the introductory chapter.

4.3.1 Cell culture and preparation

Three cell lines were used (Fig. 4.1) for the following experiments. CHO Chinese hamster ovary cells (Fig. 4.1a), U87 human glioblastoma cells (Fig. 4.1b), and HT22 immortalized mouse hippocampal neurons. The HT22 cell line was used in their non-differentiated and differentiated states. Following differentiation, morphological changes were evident and the cells stopped dividing (Fig. 4.1 c vs d).

4.3.2 Potassium calibration of PMPI.

A chemical calibration was performed for all cell types to determine their degree of excitability. This was accomplished by measuring membrane depolarization (PMPI fluorescence) in conditions with increasing [K^+] in the imaging solution (2.5 mM, 25 mM, 50 mM, 75 mM, 100 mM, 140 mM). Osmolarity was maintained by removing NaCl in an equimolar manner as KCl was increased. Each sample was monitored continuously with the buffer being replaced every 5 minutes.

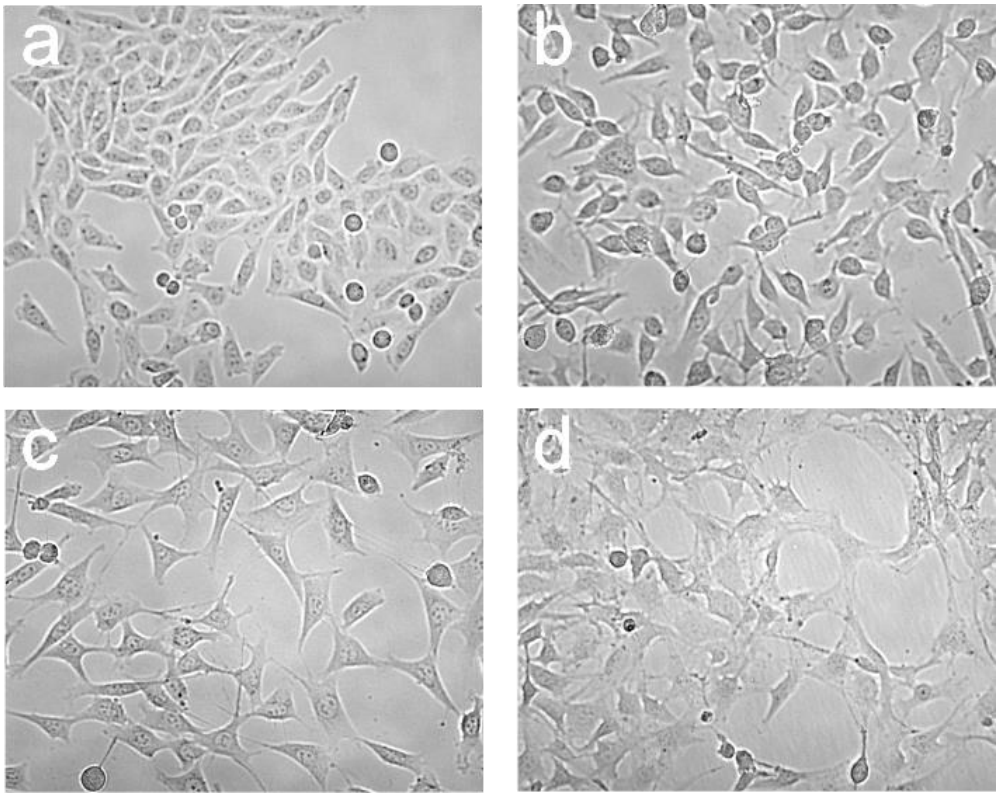

Figure 4.1 - Phase-contrast images of all four cell lines used in experiments. a – CHO; b - U87 MG; c - undifferentiated HT22; and d - differentiated HT22. All images were taken at 200x magnification.

4.4 Results

4.4.1 Cell Excitability

The first experiment compared how each cell line responded to chemical depolarization by increasing the extracellular [K^+] over time (Fig. 4.2). Here we found that the greatest relative change in membrane potential occurred in the CHO cell line. U87 cells and the undifferentiated HT22 cells responded almost identically, whereas the differentiated HT22 cells showed the least amount of relative change. The four cell lines began to show the greatest divergence when the 50 mM [K^+] buffer was added.

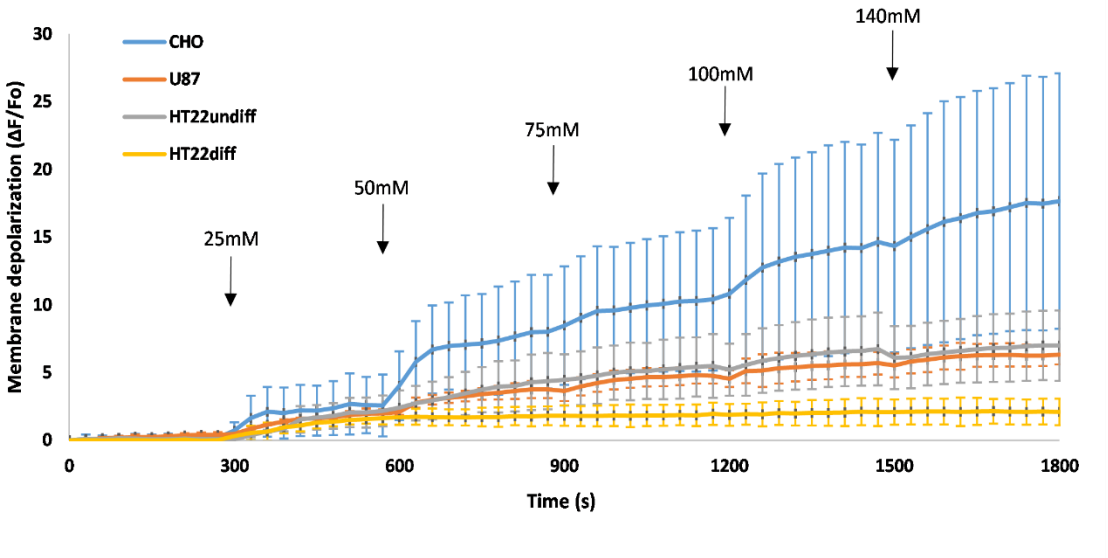

Figure 4.2 – Chemical depolarization of cells using K^+. Fluorescence changes were monitored in all four cell lines. The imaging solution was changed every 5 minutes with increasing [K^+] ranging from 2.5 mM in the original imaging solution up to 140 mM. Error bars represent +/- 2SE.

A representative response to the depolarization dynamics following pulsed electric field exposure can be seen in (Fig. 4.3). A similar trend was observed for all pulse durations, where the U87 cells showed the greatest depolarization and the differentiated HT22 cells showed the least. One exception to this was in the 10 ms condition, where the CHO cells were depolarized more than all other cells. The maximal depolarization was observed within the first 2.5 minutes following pulse exposure, after which the membrane potential gradually returned to near baseline levels. The time for repolarization differed based on the magnitude of depolarization but ranged anywhere from 5 – 25 minutes.

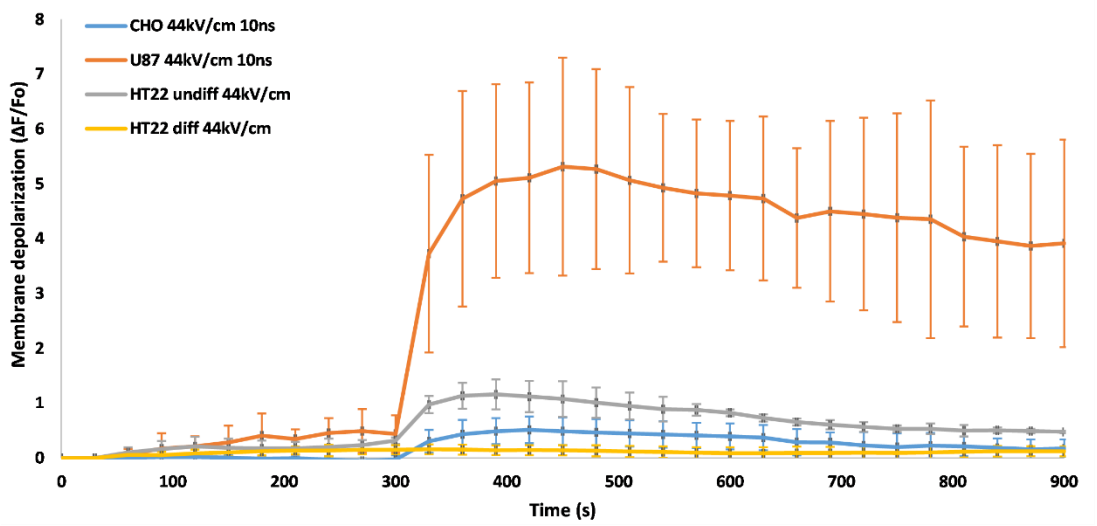

Figure 4.3 – Representative depolarization dynamics following PEF exposure. Membrane depolarization was observed after a single 10 ns PEF of 44 kV/cm, with the exception of the differentiated HT22 cells requiring a minimum of 52 kV/cm to depolarize the transmembrane potential. Error bars represent +/- 2SE.

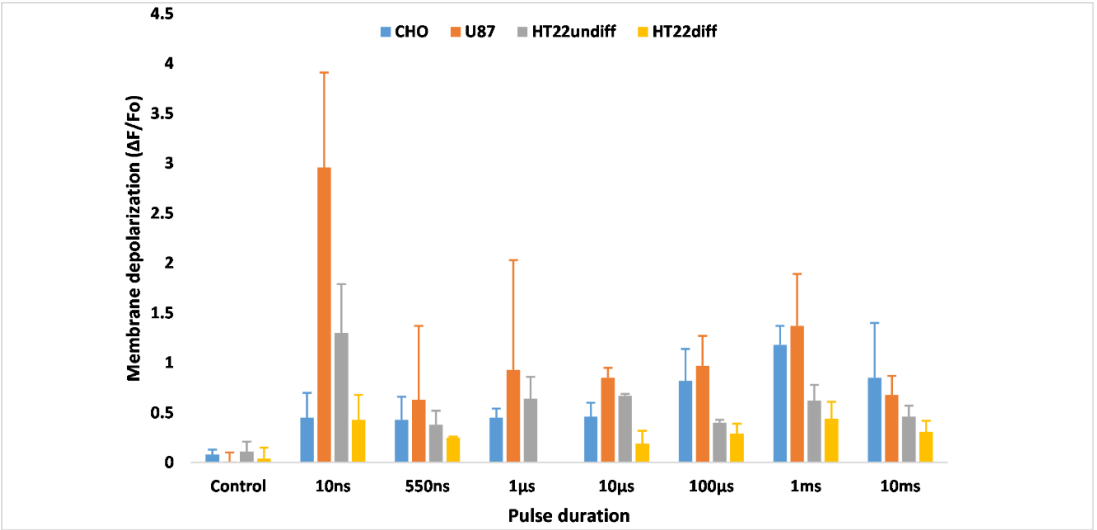

Figure 4.4 – Magnitude of depolarizing response to pulsed fields from 10 ns – 10 ms. U87 cells show a greater response to PEF-induced membrane depolarization compared to all cells, but they also show the greatest variability. Error bars represent +/- 2SE.

Another interesting feature is highlighted in Fig. 4.4, where the U87 cells not only show the largest depolarization response, but they also show the greatest variability in their response. In some cases, such as the 1 μs duration, U87 cells had 5 times more variability than the other cell lines. An ANOVA was performed comparing the variance between cells, which confirmed that the variability in the U87 cell line was statistically greater than the other cells [$F(3, 27) = 4.19$, $p = 0.01$, $\Omega^2 = 0.24$].

Fig. 4.5 shows the strength-duration curve for depolarization of all cell lines. The exact values are listed in Table 4.1. We can see that an inverse relationship between the threshold and pulse duration is evident, such that longer pulses require a much lower electric field to elicit a depolarizing response. The statistical parameters for the analyses of the depolarization threshold are shown in the Supplementary data section (Table S1 and S2).

	Electric field (kV/cm)						
Pulse duration	**10 ns**	**550 ns**	**1 μs**	**10 μs**	**100 μs**	**1 ms**	**10 ms**
CHO	44	2.0	1.2	0.45	0.30	0.15	0.10
U-87 MG	34	2.2	1.4	0.60	0.35	0.20	0.12
Undifferentiated HT22	34	2.0	1.4	0.70	0.50	0.35	0.24
Differentiated HT22	52	2.0	1.7*	0.90	0.60	0.40	0.28

Table 4.1 - The depolarization thresholds for all tested pulse durations and cell lines. The results listed here are a tabular representation of the data in Fig. 4.5. The asterisk (*) denotes that the threshold for this condition had to be estimated due to the large variability of the data. All data is presented in kV/cm.

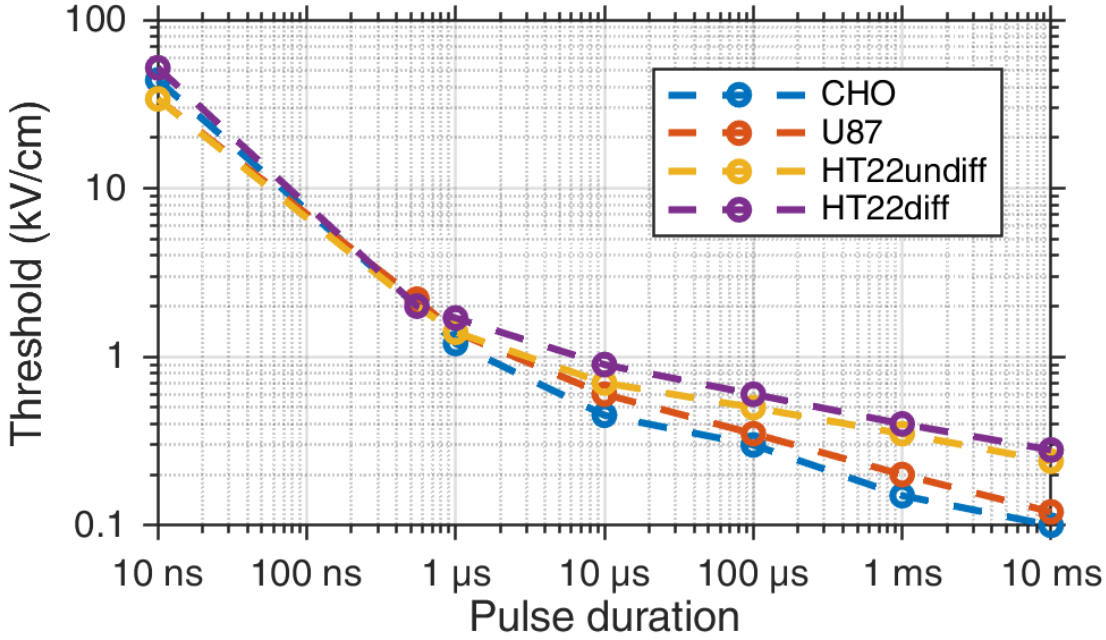

Figure 4.5 - The strength-duration curve for depolarization thresholds of all cell lines. The minimum electric field intensity required to depolarize the transmembrane potential is given for all pulse durations tested in kV/cm. As the pulse duration increases, the electric field required to depolarize the cell decreases.

4.4.2 Plasma Membrane Permeability

The normalized plasma membrane permeabilization curve to YO-PRO is shown for all four cell lines in Fig. 5.6. The threshold for electropermeabilization (Fig. 4.6a) in U87 and CHO cells was 0.4 kV/cm, whereas it was slightly higher (0.6 kV/cm) for the undifferentiated and differentiated HT22 cells. A similar increase in permeabilization was seen for all cell lines as the electric field strength increased. The permeabilization curve could be best described using a symmetric sigmoid (Fig. 4.6b). Table 4.2 summarizes some of the parameters from the curve, which show that all four cell lines reached 50% permeabilization ($E_{50\%}$) between 0.8 and 0.9 kV/cm.

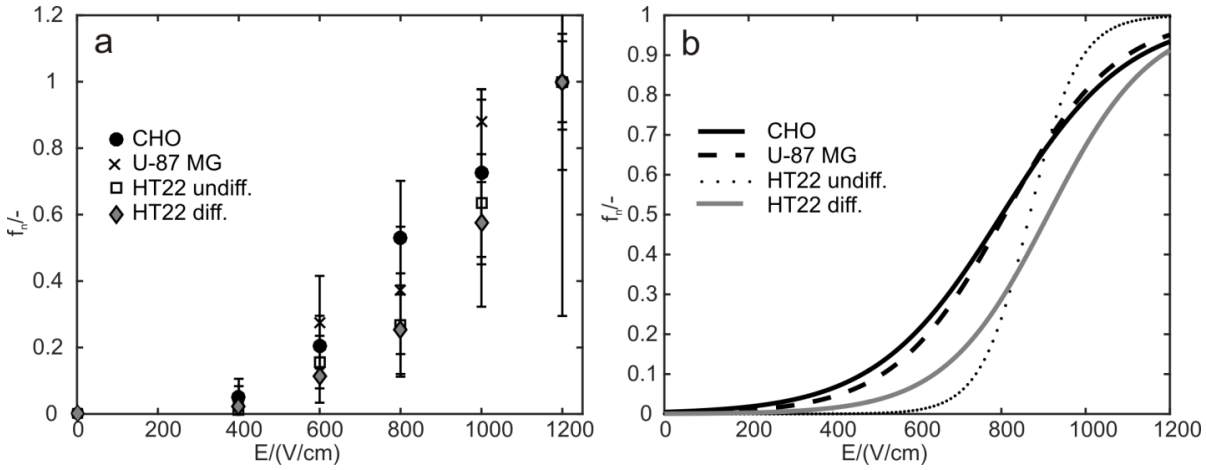

Figure 4.6 - Normalized permeabilization curve of all four cell lines to YO-PRO, 5 min after the pulse application. The threshold for electroporation was reached at 0.4 kV/cm (U-87 MG and CHO) or 0.6 kV/cm (undifferentiated and differentiated HT22 cells). a) Normalized values, the error bars represent one standard deviation and b) the fitted symmetric sigmoid. Normalized fluorescence f_n/- is presented as a function of applied electric field E/(kV/cm).

An example of the time dynamics for YO-PRO uptake following 8 x 100 μs pulses at 1.2 kV/cm is shown in Fig. 4.7a. The maximal fluorescence and the resealing dynamics (τ) were extracted by fitting a first-order uptake model. The maximal fluorescence (Fig. 4.7b) was the highest for the U-87 MG cells and the lowest for the CHO cells. There were no significant differences in maximal fluorescence between the differentiated and undifferentiated HT22s, while all other pairwise comparisons using a t-test yielded statistically significant differences. The value of time constant τ (Fig. 4.7c) corresponds to the time when 63% of the pores in the membrane resealed. The resealing was the fastest for the U-87 MG cells, similar for the undifferentiated HT22s and CHO cells, and slowest for the differentiated HT22 cells.

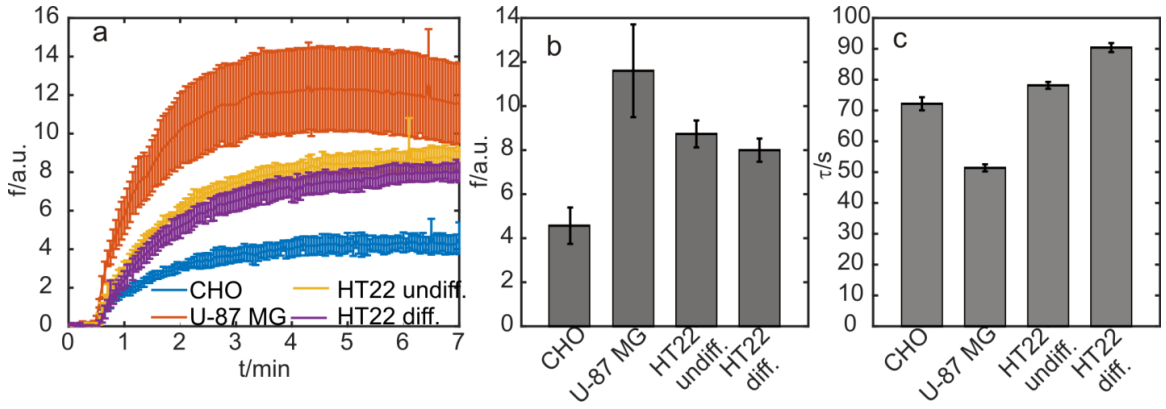

Figure 4.7 - Time dynamics of YO-PRO uptake and analyses. a - Time dynamics of the YP uptake for all four cell lines following 8 x 100 μs pulses at 1.2 kV/cm and 1 Hz repetition frequency. Error bars represent one standard deviation. Fluorescence (arbitrary units) is presented as a function of time (min). b - The maximal value of YP fluorescence (arbitrary units) for all four cell lines. c - The resealing constant (τ/s) is presented for each cell line. Error bars for b and c represent the 95% confidence interval.

Cell line	$E_{50\%}$ (kV/cm)	b (kV/cm)	R-squared
CHO	0.80 ± 0.06	0.15 ± 0.11	0.98
U-87 MG	0.81 ± 0.10	0.13 ± 0.09	0.99
HT22 undifferentiated	0.94 ± 0.07	0.12 ± 0.06	0.99
HT22 differentiated	0.91 ± 0.07	0.12 ± 0.06	0.99

Table 4.2 - Parameters of the fitted symmetric sigmoid to the normalized data of YO-PRO uptake. The numbers listed denote the optimal value and the corresponding 95% confidence intervals.

4.5 Discussion

The goal of this study aimed to compare the depolarization thresholds between excitable and non-excitable cells. For each cell, the strength-duration curve was determined, using the obtained threshold values, following exposure to a single pulse ranging in duration from 10 ns

to 10 ms. The permeability curve was also determined for each cell line following application of 8 x 100 μs pulses, delivered at 1 Hz. For the assessment of cell depolarization we used the PMPI dye. For the assessment of the plasma membrane permeabilization we used YO-PRO (YP) dye.

PMPI is a valuable tool for the measurement of membrane potential [125] and ion channel pharmacology [214, 215]. Although electrophysiology is considered the gold standard for measurement of membrane potential, PMPI has several advantages, namely the ease of use, the ability to monitor long-term changes, and the ability to monitor multiple cells simultaneously. Furthermore, PMPI has been compared directly to electrophysiology data with a good agreement [126]. It consists of a two-part system which includes a fluorescent anionic voltage-sensor and a quencher. When a cell is depolarized, the sensor translocates across the plasma membrane resulting in an increase in fluorescence. Conversly, the quenching molecule is excluded from the cell. With that said, when the plasma membrane is permeabilized, it could be possible for the quenching molecule to enter the cell through pores formed in the membrane and decrease the fluorescence in the cell. Interestingly, when pulses were applied well above the depolarization threshold, we observed a decrease in the fluorescent signal which could be indicative of cell electroporation. In the future, it should be established to what extent the PMPI dye could also serve as cell membrane permeabilization indicator.

The results following electrochemical depolarization show that with increasing K^+ concentration, the fluorescence and thus the transmembrane voltage are increasing which is in agreement with theory. It was unexpected, however, that the highest fluorescence was achieved in CHO cells and not with the differentiated HT22 cells. Excitable cells typically have a higher density of voltage-gated channels, thus more ions should enter the cell when these channels are open. CHO cells are non-excitable cells and would be expected to have a low expression of voltage-gated ion channels; however, some reports indicate that these cells express voltage-gated Na^+ channels [216] and voltage-gated Ca^{2+} channels [217].

CHO cells have a resting membrane potential around - 10 mV [218], which is similar to that of U87 cells [116]. Although electrophysiology studies on HT22 cells were not found, a typical neuron has a resting potential around – 70 mV [219]. If we recall from the previous chapter, the depolarizing response measured here would be associated with a change in magnitude less than 30 mV. One possibility could be that the resting potential of the neurons did not reach the threshold required to activate voltage-gated channels.

The relatively low resting potential of the U87 cells combined with the large complement of voltage-gated channels [116] could explain why the U87 cells experienced the greatest depolarizing effect to one pulse. It is also worth noting that cancerous tissues have been shown to be more affected by PEFs than non-cancerous tissues [220, 221].

The repolarization time for all four cell lines was in the range of minutes. Certainly this was most surprising when considering the differentiated neurons which normally would be expected to have repolarization times in the millisecond range [219]. There are several possible explanations for the longer-than-expected repolarization time. First, as the assessment method, we used PMPI dye, which has a time constant of several seconds [222]. Second, our experiments were performed at room temperature which would be expected to slow down the kinetics of the Na^+/K^+ pump. Third, it is possible that cells were depolarized as well as electroporated. If true, electroporation has been reported to cause leakage of ATP [223] which is necessary for repolarizing the membrane. Fourth, due to such a high induced transmembrane voltage (several volts), it is possible that ion channels could be damaged [224].

The time required for reaching the peak fluorescence in depolarization experiments coincided with the resealing time observed in the permeabilization experiments. It is possible that during depolarization and permeabilization experiments, PMPI and YP were entering through voltage-gated channels [154] as well as through pores formed in the plasma

membrane. Even when using channel inhibitors, a total inhibition of depolarization could not be achieved which indicates that during depolarization ions also enter through pores [100].

In the next part of our study, we exposed cells to 8 x 100 μs pulses, which are typically used in electrochemotherapy treatments. All four cell lines reached the threshold of electroporation at approximately the same value - between 0.4 and 0.6 kV/cm. The permeabilization curve of all four lines could be described using a symmetric sigmoid. Although differentiation of HT22 cells causes a drop in the resting membrane potential [225], the more negative resting membrane potential did not affect the threshold for electroporation. The permeabilization curves followed similar dependency and reached 50% of the maximal fluorescence around 0.9 kV/cm. We can conclude that irrespective of the cell's excitability, all four cell lines responded similarly to electroporation pulses.

The YO-PRO uptake was the greatest in the U87 cell line and least in CHO cells. As mentioned previously, cancerous cell have been shown to be more susceptible to PEFs when compared to non-cancerous cells which could explain why they were the most permeabilized. Since the cells were grown attached in a monolayer, the reason CHO cells showed the least YO-PRO uptake could be due to the tendency of CHO cells to grow in colonies in close proximity which decreases the area of the plasma membrane available for dye uptake. The close proximity of cells could have also decreased the induced transmembrane potential due to shielding [226–228].

4.6 Conclusion

In summary, the depolarization threshold was higher for the excitable cells than for the non-excitable cells. All four cell lines responded similarly to pulses of standard electrochemotherapy parameters. The shape of the permeability curve was similar to curves already published in the literature [229]. Thus, electroporation is a feasible means of treating excitable and non-excitable cells with pulses of similar parameters. Furthermore, our results show the potential of achieving permeabilization and minimizing or avoiding excitation/pain

sensation which needs to be explored in more detail. In future studies, it should be established, however, to what extent *in vitro* depolarization and excitability correlate to the actual excitation and pain sensation *in vivo*.

Supplementary Data

Table S1 - Statistical parameters for the strength-duration curve by cell line. F(x, y) = ANOVA score with degrees of freedom in parentheses. F_w = Welch's F adjustment when the assumtion of homogeneity of variance was not met. The statistical significance provides the p-values which are compared to our alpha criterion of $\alpha = 0.05$. The effect size column provides the proportion of variation in response attributed to the PEF.

CHO			
	ANOVA	**Significance**	**Effect size (Ω^2)**
10 ns	$F(2, 17) = 9.00$	$p < 0.01$	0.47
550 ns	$F(3, 15) = 4.56$	$p = 0.02$	0.36
1 µs	$F(3, 16) = 91.52$	$p < 0.01$	0.93
10 µs	$F_W(3, 6.08) = 14.12$	$p < 0.01$	0.67
100 µs	$F(4, 19) = 10.35$	$p < 0.01$	0.61
1 ms	$F_W(3, 5.55) = 53.76$	$p < 0.01$	0.89
10 ms	$F(3, 13) = 10.80$	$p < 0.01$	0.63
U87			
	ANOVA	**Significance**	**Effect size (Ω^2)**
10 ns	$F(4, 19) = 2.90$	$p < 0.01$	0.80
550 ns	$F(3, 15) = 3.60$	$p = 0.04$	0.29
1 µs	$F(3, 16) = 4.32$	$p = 0.02$	0.33
10 µs	$F_W(4, 9.27) = 43.54$,	$p < 0.01$	0.63
100 µs	$F(3, 21) = 47.64$	$p < 0.01$	0.85
1 ms	$F_W(4, 6.62) = 13.96$	$p < 0.01$	0.71
10 ms	$F(3, 19) = 10.66$	$p < 0.01$	0.56
Undifferentiated HT22			
	ANOVA	**Significance**	**Effect size (Ω^2)**
10 ns	$F_W(3, 3.06) = 21.88$	$p = 0.01$	0.81
550 ns	$F(2, 9) = 12.96$	$p < 0.01$	0.67
1 µs	$F(3, 9) = 11.14$	$p < 0.01$	0.70
10 µs	$F(4, 10) = 5.24$	$p = 0.02$	0.53
100 µs	$F(2, 12) = 3.79$	$p = 0.05$	0.27
1 ms	$F(3, 10) = 9.06$	$p < 0.01$	0.63
10 ms	$F(4, 13) = 4.15$	$p = 0.02$	0.41
Differentiated HT22			
	ANOVA	**Significance**	**Effect size (Ω^2)**
10 ns	$F_W(3, 11.76) = 13.41$	$p < 0.01$	0.60
550 ns	$F(2, 10) = 5.20$	$p = 0.03$	0.39
1 µs	$F(2, 16) = 4.56$	$p = 0.03$	0.29
10 µs	$F(6, 21) = 3.97$	$p < 0.01$	0.39
100 µs	$F(4, 16) = 6.13$	$p < 0.01$	0.49
1 ms	$F(3, 19) = 8.80$	$p < 0.01$	0.50
10 ms	$F(4, 20) = 6.02$	$p < 0.01$	0.45

Table S2 - Additional statistical parameters from the strength-duration curve.

All electric fields that were tested for threshold determination are provided by cell line, including the sample size for each.

Cell type	CHO		U-87		HT22 undiff		HT22 diff	
Control		7		11		7		8
10 ns	22 kV/m	5	16.5 kV/m	4	22 kV/m	6	44 kV/m	8
	34 kV/m	3	22.0 kV/m	4	34 kV/m	4	52 kV/m	6
	44 kV/m	6	34.0 kV/m	4	44 kV/m	2	76 kV/m	5
			44.0 kV/m	4				
550 ns	1.6 kV/cm	4	1.2 kV/cm	3	1.6 kV/cm	4	2.0 kV/cm	3
	2.0 kV/cm	4	1.6 kV/cm	2	2.0 kV/cm	5	4.5 kV/cm	2
	2.4 kV/cm	4	2.0 kV/cm	3				
1 µs	1.0 kV/cm	4	1.0 kV/cm	3	1.0 kV/cm	4	4.5 kV/cm	2
	1.2 kV/cm	4	1.2 kV/cm	3	1.2 kV/cm	3	10. kV/cm	4
	1.4 kV/cm	4	1.4 kV/cm	3	1.4 kV/cm	3		
10 µs	0.30 kV/cm	3	0.35 kV/m	5	0.35 kV/m	3	0.60 kV/m	3
	0.45 kV/cm	4	0.45 kV/m	6	0.45 kV/m	3	0.80 kV/m	3
	0.60 kV/cm	4	0.60 kV/m	4	0.60 kV/m	3	1.20 kV/m	3
			0.75 kV/m	5	0.75 kV/m	3	1.60 kV/m	4
							1.80 kV/m	4
							2.00 kV/m	3
100 µs	0.10 kV/cm	4	0.25 kV/m	3	0.50 kV/m	3	0.35 kV/cm	3
	0.20 kV/cm	4	0.35 kV/m	6	0.75 kV/m	5	0.45 kV/cm	3
	0.30 kV/cm	4	0.45 kV/m	5			0.75 kV/cm	3
	0.40 kV/cm	4					1.00 kV/cm	6
1 ms	0.10 kV/cm	4	0.10 kV/cm	3	0.25 kV/cm	4	0.40 kV/cm	4
	0.15 kV/cm	4	0.20 kV/cm	4	0.30 kV/cm	4	0.50 kV/cm	5
	0.20 kV/cm	4	0.30 kV/cm	4	0.35 kV/cm	3	0.60 kV/cm	6
			0.60 kV/cm	4				
10 ms	0.02 kV/cm	3	0.04 kV/cm	4	0.24 kV/cm	3	0.20 kV/cm	4
	0.06 kV/cm	3	0.08 kV/cm	4	0.28 kV/cm	3	0.24 kV/cm	3
	0.10 kV/cm	3	0.12 kV/cm	4	0.32 kV/cm	3	0.28 kV/cm	6
					0.40 kV/cm	2	0.36 kV/cm	4

Chapter 5 –
Discussion and Conclusion

5.1 Summary

This thesis investigated the effects of pulsed electric fields on multiple cell lines. Three chapters evaluated important questions regarding cell membrane – electric field interactions. The first experimental chapter compared the traditional view of this interaction with experimental results using a statistical approach. The next chapter studied the role of transmembrane proteins in PEF effects. These proteins, or ion channels, are often overlooked in PEF research and are critically important to a cells response to environmental stimuli. Finally, the last chapter investigated the electric field thresholds required to depolarize the transmembrane potential and permeabilize the plasma membrane in multiple cell lines. Several pulse durations, ranging from 10 ns to 10 ms were used. The results from each chapter will be discussed as they pertain to the literature.

5.2 A comparative analysis of the theoretical and experimental interactions of PEF with cells *in vitro*

The effects of pulsed electric fields on biological systems has been studied for more than a half of a century. As with any scientific inquiry, a model was required to help understand how these fields interact with cells. But what happens when the model fails to provide a true representation of the effects we are interested in measuring?

The results from this section indicate that the fundamental mathematical models that were intended to help guide us in designing and interpreting experiments have very low predictive power. Specifically, when considering size, shape, orientation to the electric field, and density of cells exposed, the currently accepted models account for less than 5 % of the changes observed. It is important to mention that this chapter looked at the induced transmembrane potential as the outcome variable.

Transmembrane potential was selected because the literature states that this is the gateway to modulating cellular activity with applied electric fields. Both older and newer

literature have stated that an induced transmembrane voltage of ~ 1V is required to cause breakdown of the cell membrane [17, 18, 34, 84, 230–234]

Cell have mechanisms by which they cope with induced transmembrane voltage under physiological conditions. Transmembrane proteins, or ion channels, control the induced voltage through opening and closing of these proteins. These channels, although studied mostly in excitable cells, are present to a certain degree in all cells. They are responsible for many cell processes from cell volume regulation, DNA replication and cell division [96, 235].

5.3 Nanosecond pulsed electric fields depolarize transmembrane potential via voltage-gated K^+, Ca^{2+} and TRPM8 channels in U87 glioblastoma cells

The purpose of this section was to look at electric field - cell interactions with the following question in mind: What if the changes in transmembrane potential following a single 10 nanosecond pulsed electric field were not due to electroporation of the plasma membrane? As we saw in the previous section, there appears to be a fundamental flaw with the description provided by the traditional theoretical model. This is most likely due to an oversimplification of a cell, which is not merely a leaky dielectric membrane separating two conductive solutions. A cell is a complex, living organism that is always adapting to its environment. As a result, modelling the cell in the traditional way has very little predictive power when analyzing experimental results.

Since we were working with applied voltage, it seemed most logical to study cellular mechanisms which were responsible for regulating transmembrane potential. To accomplish this task a series of pharmacological ion channel modulators were employed to monitor their effects on membrane depolarization following nsPEF exposure. The underlying hypothesis supposed that if the observed change in membrane potential was due to simple diffusion of

ions across the electroporated plasma membrane, then we should expect no significant effect from chemical blockers or activators of ion channels.

Although few articles have explored the possibility of PEF influencing ion channel behavior, our results appear to be consistent with the literature. Specifically, calcium influx was abolished following PEF exposure of bovine chromaffin cells [64], as well as GH3 and NG108 cells [63] when specific voltage-gated calcium channel blockers were used. In the latter study, CHO cells were used as a negative control due to the lack of voltage-gated calcium channels. When PEF was combined with or without calcium channel blockers, no increase in intracellular calcium was observed.

In our study we have implicated additional channels, such as voltage-gated K^+ channels and TRPM8 channels, in the depolarization response following nsPEF exposure. Although TRPM8 channels were originally described as cold-receptors, more recently they have been shown to display voltage sensitivity [236–238]. We had to explore the possibility that TRPM8 involvement may have been an artefact because experimentation took place at ambient temperature. To rule this out, experiments were replicated at 37°C and similar results were observed.

Of course the presence of voltage-gated channels will differ significantly between cell types and possibly within the same cell type. These differences could prove to be important when designing in vivo experiments. As an example, in certain cases electrochemotherapy could be refined to maximize effects on a given target cell type while minimizing effects on surrounding tissues by exploiting these differences. The following chapter has been dedicated to investigating these effects among various cell types and pulse durations.

5.4 Plasma membrane depolarization and permeabilization due to electric pulses in cell lines of different excitability

More than 20 years ago the first clinical trial used electroporation as a means to significantly enhance chemotherapeutic uptake into tumors [239]. Since then, the study of electrochemotherapy has continued to gain traction in the scientific and medical community. Whether studies have utilized chemotherapeutics, high concentrations of extracellular calcium or electric fields alone, PEF have shown to be an effective alternative to traditional chemotherapy [40, 52, 66, 102, 182, 240, 241].

Treatment of malignant tissues with PEF has shown several significant advantages over conventional treatments. One such advantage consists of chemical delivery directly into the tumor. Chemotherapy is generally delivered intravenously in significant concentrations which ultimately circulate through the entire body. Since these are highly toxic compounds, serious secondary effects can often be expected. With electrochemotherapy, chemotherapeutics can be injected locally to into the target tissues, and subsequent application of PEF protocol permeabilizes the target and leads to enhanced uptake of the drug [50, 51] while minimizing secondary effects associated with systemic administration.

Another advantage comes in the selectivity of the treatment. Whereas chemotherapy is toxic to all cells, PEFs appear to have a greater effect on malignant cells than normal cells [220]. Although not very well understood, this difference in sensitivity may be linked to membrane repair. When comparing dye uptake following the standard ECT protocol and viability 24 hours later, cancerous cell lines have been shown to be significantly more vulnerable than normal primary cell lines [221].

Despite the advantages, one of the primary drawbacks with PEF treatment is the potential for pain. This is due to nervous and muscular tissues in areas adjacent to the treatment site which have become electrically excited from the applied electric field [212, 213]. The purpose of this section was to investigate PEF-induced permeability and excitation of

various cell lines. An important advance in PEF treatment would involve finding the appropriate electric field duration and intensity that would minimize the excitation of surrounding nervous tissue yet remain effective at permeabilizing the target cells.

Four cells lines were used for these experiments, three of which were non-excitable under physiologic conditions, the other being terminally differentiated neurons. For each cell line, PMPI was used to measure changes in membrane potential, and YO-PRO was used as a measure of membrane permeability.

Consistent with the literature, we found that the electric field intensity required to depolarize the transmembrane potential decreased as the pulse durations increased [25, 242, 243]. We also found that the electric field required to depolarize cells was significantly greater in the differentiated neurons than the non-excitable cells. When we combine these results with the fact that no difference in thresholds were observed for membrane permeability, we find that by carefully selecting a treatment protocol with the appropriate intensity, it is possible to achieve clinically relevant enhancement of chemical uptake while minimizing or preventing the pain associated with excitation of the surrounding nervous tissues.

5.5 Conclusion

This thesis focused heavily on understanding the role of transmembrane ion channels in pulsed electric field effects. These have been shown to be directly influenced in several studies [63–65, 93]. In the first section we compared theoretical parameters influencing membrane-electric field interactions with experimental results. We found that less than 5 % of the experimental results could be attributed to factors included in current electro-physical model, such as size, shape, orientation with respect to the electric field and the density of cells. These results suggested, at least for long-lasting changes that were measured here, were mediated to a large extent by other parameters.

One of those parameters are voltage-gated ion channels, which was the focus of the second chapter. These are channels that are integral for many physiological processes and are present, to varying degrees, in every type of cell. Although it is important that future experiments look to understand the precise mechanism, it is no surprise that applying an electric field would somehow influence the activity of electric field sensors in a cell. In addition to directly acting on these channels, other research has suggested they may be damaged by PEF exposure [224, 244, 245].

It was interesting that no ion channel blocker was able to completely abolish the depolarizing response. It is important to consider the possibility that pores were formed in the plasma membrane which allowed the diffusion of ions, and it was this diffusion that resulted in the transmembrane potential being sufficiently depolarized to allow voltage-gated channels to open. Whether or not the PEF acted directly or indirectly on the ion channels is something that needs to be explored in the future; however, it is clear that they play a significant role in the change in transmembrane potential following PEF exposure.

In the final experimental chapter we extended these results to include multiple cell lines. A series of experiments looking at pulse durations from 10 ns to 10 ms were conducted with membrane potential and membrane permeability as outcome variables. Multiple electric field intensities were used for each duration in order to find the minimum fields strength required to either depolarize, or permeabilize the plasma membrane. One of the most common complaint reported from patients treated with PEF treatments is the pain associated with repeated electrical stimulation. It would be beneficial to find a protocol which could limit or prevent the pain associated with treatment.

Since the experienced pain is due to electrically exciting nervous tissue surrounding the treatment site, we aimed to explore the possibility of preventing excitation without interfering with the permeability required for enhanced drug uptake in electrochemotherapy. Our results demonstrated that the threshold required for membrane depolarization was

different between cell lines. Specifically, the differentiated neurons required a significantly greater field strength than the non-excitable cell.

In the second series of experiments investigating the threshold for electropermeabilization in the same cells, we found that there were no significant difference between field strengths required. This effect was consistent at every pulse duration tested. These results are promising as they suggest it may be possible to find an electric field intensity that would be able to enhance drug uptake, all the while avoiding excitation of the surrounding nervous tissue associated with the sensation of pain. Most likely this effect would differ based on several factors such as cell type, treatment site, or density of nervous tissue in the area.

Future research should focus on testing how well *in vitro* excitability correlates with *in vivo* perception of pain. Potentially, this could reduce or eliminate the requirement for sedatives and muscle relaxants in PEF treatments.

5.6 Perspectives

In the first experimental chapter we uncovered two significantly different populations of U87 cells. This came in spite of the care taken to keep as many variables constant as possible, including temperature, imaging medium, electric field intensity etc. Although there was not enough time to experimentally pursue these differences further, these results require more investigation. There were many interesting coincidences which may implicate cell cycle as a target for future experimentation.

This is not something that has received a lot of attention in this field of study; however, one study did report significant differences in PEF effects depending on the phase of cell cycle [89]. Of course, during my last month as a Ph.D. student, an incredible tool arrived in our lab. A Digital holographic microscope capable of monitoring cells long-term in 3D without the need for fluorescent molecules. I truly hope future researchers will use this tool to investigate the role of cell cycle.

In the second experimental chapter, we showed that by delivering a single 10 nsPEF every 2.5 minutes, the membrane potential could not be recovered. This could be important since cells oscillate between periods of depolarization and hyperpolarization that are associated with DNA replication and division. If cells need to hyperpolarize to replicate their DNA, maintaining a depolarized transmembrane potential over time could prove to be a novel treatment for cancer that would require no chemotherapeutics and would not damage surrounding tissues. Whether or not this is the case, I look forward to reading future results investigating this question.

References

1. Barba FJ, Parniakov O, Pereira SA, et al (2015) Current applications and new opportunities for the use of pulsed electric fields in food science and industry. Food Res Int 77:773–798. doi: 10.1016/j.foodres.2015.09.015

2. Xue D, Farid MM (2015) Pulsed electric field extraction of valuable compounds from white button mushroom (Agaricus bisporus). Innov Food Sci Emerg Technol 29:178–186. doi: 10.1016/j.ifset.2015.03.012

3. Yang N, Huang K, Lyu C, Wang J (2016) Pulsed electric field technology in the manufacturing processes of wine, beer, and rice wine: A review. Food Control 61:28–38. doi: 10.1016/j.foodcont.2015.09.022

4. Lin L, Yahong M, Jinghui G, et al (2013) Effects of AC electric fields on the cryopreservation of SD rat liver tissues. Annu Rep - Conf Electr Insul Dielectr Phenomena, CEIDP 555–558. doi: 10.1109/CEIDP.2013.6748328

5. Dovgan B, Barlič A, Knežević M, Miklavčič D (2016) Cryopreservation of Human Adipose-Derived Stem Cells in Combination with Trehalose and Reversible Electroporation. J Membr Biol. doi: 10.1007/978-981-287-817-5

6. Dovgan B, Dermol J, Barlič A, et al (2016) Cryopreservation of Human Umbilical Stem Cells in Combination with Trehalose and Reversible Electroporation. In: Jarm T, Kramar P (eds) 1st World Congr. Electroporation Pulsed Electr. Fields Biol. Med. Food {&} Environ. Technol. Portoro{ž}, Slov. Sept. 6 --10, 2015. Springer Singapore, Singapore, pp 307–310

7. Cemazar M, Sersa G (2007) Electrotransfer of therapeutic molecules into tissues. Curr Opin Mol Ther 9:554–562.

8. Pucihar G, Kotnik T, Miklavcic D, Teissie J (2008) Kinetics of transmembrane transport of small molecules into electropermeabilized cells. Biophys J 95:2837–2848. doi: 10.1529/biophysj.108.135541

9. Calvet CY, Thalmensi J, Liard C, et al (2014) Optimization of a gene electrotransfer procedure for efficient intradermal immunization with an hTERT-based DNA vaccine in mice. Mol Ther Methods Clin Dev 1:14045. doi: 10.1038/mtm.2014.45

10. Chopinet L, Batista-Napotnik T, Montigny A, et al (2013) Nanosecond electric pulse effects on gene expression. J Membr Biol 246:851–859. doi: 10.1007/s00232-013-9579-y

11. Pakhomova ON, Gregory BW, Semenov I, Pakhomov AG (2013) Two Modes of Cell Death Caused by Exposure to Nanosecond Pulsed Electric Field. PLoS One. doi: 10.1371/journal.pone.0070278

12. Beebe SJ, Sain NM, Ren W (2013) Induction of Cell Death Mechanisms and Apoptosis by Nanosecond Pulsed Electric Fields (nsPEFs). Cells 2:136–62. doi: 10.3390/cells2010136

13. Rubinsky B, Onik G, Mikus P (2007) Irreversible electroporation: A new ablation modality - Clinical implications. Technol Cancer Res Treat 6:37–48. doi: 10.1177/153303460700600106

14. Meer G Van, Voelker DR, Feigenson GW (2008) Membrane lipids : where they are and how they behave. Nat Rev Mol cell Biol 9:112–124. doi: 10.1038/nrm2330

15. Alberts B, Johnson A, Lewis J, et al (2002) Molecular biology of the cell, 4th ed. Garland Science

16. Tortora G, Derrickson B (2008) Principles of anatomy and physiology, 12th ed. Wiley

17. Teissie J, Golzio M, Rols MP (2005) Mechanisms of cell membrane electropermeabilization: A minireview of our present (lack of ?) knowledge. Biochim Biophys Acta - Gen Subj 1724:270–280. doi: 10.1016/j.bbagen.2005.05.006

18. Rems L, Miklavcic D (2016) Tutorial: Electroporation of cells in complex materials and tissue. J Appl Phys. doi: 10.1063/1.4949264

19. Gurtovenko AA, Vattulainen I (2005) Pore Formation Coupled to Ion Transport through Lipid Membranes as Induced by Transmembrane Ionic Charge Imbalance : Atomistic Molecular Dynamics Study. J Am Chem Soc 127:17570–17571.

20. Tarek M (2005) Membrane Electroporation: A Molecular Dynamics Simulation. Biophys J 88:4045–4053. doi: 10.1529/biophysj.104.050617

21. Tieleman DP (2004) The molecular basis of electroporation. BMC Biochem 5:10. doi: 10.1186/1471-2091-5-10

22. Jianfei WJW, Yan MYM, Chenguo YCY, Chengxiang LCL (2008) A Review on Molecular Dynamics Simulation for Biological Effects of Pulsed Electric Field. 2008 Int Conf High Volt Eng Appl 763–766. doi: 10.1109/ICHVE.2008.4774046

23. Vernier PT, Ziegler MJ (2007) Nanosecond Field Alignment of Head Group and Water Dipoles in Electroporating Phospholipid Bilayers. J Phys Chem 111:12993–12996.

24. Sözer EB, Levine ZA, Vernier PT (2017) Quantitative Limits on Small Molecule Transport via the Electropermeome — Measuring and Modeling Single Nanosecond Perturbations. Sci Rep 7:57. doi: 10.1038/s41598-017-00092-0

25. Rogers WR, Merritt JH, Comeaux JA, et al (2004) Strength-duration curve an electrically excitable tissue extended down to near 1 nanosecond. IEEE Trans Plasma Sci 32:1587–1599. doi: 10.1109/TPS.2004.831758

26. Romeo S, Wu YH, Levine Z a., et al (2013) Water influx and cell swelling after nanosecond electropermeabilization. Biochim Biophys Acta - Biomembr 1828:1715–1722. doi: 10.1016/j.bbamem.2013.03.007

27. Carr L, Bardet SM, Burke RC, et al (2017) Calcium-independent disruption of microtubule dynamics by nanosecond pulsed electric fields in U87 human glioblastoma cells. Sci Rep. doi: 10.1038/srep41267

28. Kotnik T, Mir LM, Flisar K, et al (2001) Cell membrane electropermeabilization by

symmetrical bipolar rectangular pulses: Part I. Increased efficiency of permeabilization. Bioelectrochemistry 54:83–90.

29. Pakhomov AG, Semenov I, Xiao S, et al (2014) Cancellation of cellular responses to nanoelectroporation by reversing the stimulus polarity. Cell Mol Life Sci 71:4431–4441. doi: 10.1007/s00018-014-1626-z

30. Schoenbach KH, Pakhomov AG, Semenov I, et al (2014) Ion transport into cells exposed to monopolar and bipolar nanosecond pulses. Bioelectrochemistry. doi: 10.1016/j.bioelechem.2014.08.015

31. Ibey BL, Ullery J, Pakhomova ON, et al (2014) Bipolar nanosecond electric pulses are less efficient at electropermeabilization and killing cells than monopolar pulses. Biochem Biophys Res Commun 443:568–573. doi: 10.1016/j.bbrc.2013.12.004.Bipolar

32. Gowrishankar TR, Weaver JC (2006) Electrical behavior and pore accumulation in a multicellular model for conventional and supra-electroporation. Biochem Biophys Res Commun 349:643–653. doi: 10.1016/j.bbrc.2006.08.097

33. Tekle E, Oubrahim H, Dzekunov SM, et al (2005) Selective Field Effects on Intracellular Vacuoles and Vesicle Membranes with Nanosecond Electric Pulses. Biophys J 89:274–284. doi: 10.1529/biophysj.104.054494

34. Schwan HP (1988) Biological effects of non-ionizing radiations: Cellular properties and interactions. Ann Biomed Eng 16:245–263. doi: 10.1007/BF02368002

35. Dev SB, Rabussay DP, Widera G, Hofmann GA (2000) Medical Applications of Electroporation. IEEE Trans plasma Sci 28:206–223.

36. Vandermeulen G, Richiardi H, Escriou V, et al (2009) Skin-specific promoters for genetic immunisation by DNA electroporation. Vaccine 27:4272–4277. doi: 10.1016/j.vaccine.2009.05.022

37. Heller R, Cruz Y, Heller LC, et al (2010) Electrically Mediated Delivery of Plasmid DNA to the Skin, Using a Multielectrode Array. Hum Gene Ther 21:357–362. doi: 10.1089/hum.2009.065

38. Teissié J (2013) Electrically Mediated Gene Delivery: Basic and Translational Concepts. Nov Gene Ther Approaches. doi: 10.5772/54780

39. Gothelf A, Gehl J (2010) Gene electrotransfer to skin; review of existing literature and clinical perspectives. Curr Gene Ther 10:287–299. doi: 10.2174/156652310791823443

40. Gothelf A, Mir LM, Gehl J (2003) Electrochemotherapy : results of cancer treatment using enhanced delivery of bleomycin by electroporation. Cancer Treat Rev 29:371–387. doi: 10.1016/S0305-7372(03)00073-2

41. Breton M, Mir LM (2012) Microsecond and nanosecond electric pulses in cancer treatments. Bioelectromagnetics 33:106–123. doi: 10.1002/bem.20692

42. Davalos R V., Mir LM, Rubinsky B (2005) Tissue Ablation with Irreversible Electroporation. Ann Biomed Eng 33:223–231. doi: 10.1007/s10439-005-8981-8

43. Ting F, Tran M, Böhm M, et al (2016) Focal irreversible electroporation for prostate cancer: functional outcomes and short-term oncological control. Prostate Cancer Prostatic Dis 19:46–52. doi: 10.1038/pcan.2015.47

44. Rossmeisl JH, Garcia PA, Pancotto TE, et al (2015) Safety and feasibility of the NanoKnife system for irreversible electroporation ablative treatment of canine spontaneous intracranial gliomas. J Neurosurg 123:1008–1025. doi: 10.3171/2014.12.JNS141768

45. Jiang C, Davalos R V., Bischof JC (2015) A Review of Basic to Clinical Studies of Irreversible Electroporation Therapy. IEEE Trans Biomed Eng 62:4–20. doi: 10.1109/TBME.2014.2367543

46. Scheffer HJ, Nielsen K, de Jong MC, et al (2014) Irreversible Electroporation for

Nonthermal Tumor Ablation in the Clinical Setting: A Systematic Review of Safety and Efficacy. J Vasc Interv Radiol 1–15. doi: 10.1016/j.jvir.2014.01.028

47. Fruhling P, Nilsson A, Duraj F, et al (2017) Single-center nonrandomized clinical trial to assess the safety and efficacy of irreversible electroporation (IRE) ablation of liver tumors in humans : Short to mid-term results. Eur J Surg Oncol 1–7. doi: 10.1016/j.ejso.2016.12.004

48. Heller R, Heller LC (2015) Gene Electrotransfer Clinical Trials. In: Adv. Genet. Elsevier, pp 235–262

49. Orlowski S, Belehradek JJ, Paoletti C, Mir L (1988) Transient electropermeabilization of cells in culture. Increase of the cytotoxicity of anticancer drugs. Biochem Pharmacol 37:4727–4733.

50. Horiuchi A, Nikaido T, Mitsushita J, et al (2000) Enhancement of antitumor effect of bleomycin by low-voltage in vivo electroporation- a study of human uterine leiomyosarcomas in nude mice. Int J cancer J 88:640–644.

51. Gehl J, Skovsgaard T, Mir LM (1998) Enhancement of cytotoxicity by electropermeabilization: an improved method for screening drugs. Anticancer drugs 9:319–325.

52. Falk H, Lambaa S, Johannesen HH, et al (2017) Electrochemotherapy and calcium electroporation inducing a systemic immune response with local and distant remission of tumors in a patient with malignant melanoma – a case report. Acta Oncol (Madr). doi: 10.1080/0284186X.2017.1290274

53. Beebe SJ, Chen YJ, Sain NM, et al (2012) Transient Features in Nanosecond Pulsed Electric Fields Differentially Modulate Mitochondria and Viability. PLoS One. doi: 10.1371/journal.pone.0051349

54. Ren W, Beebe SJ (2011) An apoptosis targeted stimulus with nanosecond pulsed

electric fields (nsPEFs) in E4 squamous cell carcinoma. Apoptosis 16:382–393. doi: 10.1007/s10495-010-0572-y

55. Beebe SJ, Fox PM, Rec LJ, et al (2002) Nanosecond Pulsed Electric Field (nsPEF) Effects on Cells and Tissues : Apoptosis Induction and Tumor Growth Inhibition. IEEE Trans plasma Sci 30:286–292.

56. Vernier PT, Li A, Marcu L, et al (2003) Ultrashort Pulsed Electric Fields Induce Membrane Phospholipid Translocation and Caspase Activation : Differential Sensitivities of Jurkat T Lymphoblasts and Rat Glioma C6 Cells. IEEE Trans Dielectr Electr Insul 10:795–809.

57. Chen N, Schoenbach KH, Kolb JF, et al (2004) Leukemic cell intracellular responses to nanosecond electric fields. Biochem Biophys Res Commun 317:421–427. doi: 10.1016/j.bbrc.2004.03.063

58. Yin S, Chen X, Hu C, et al (2014) Nanosecond pulsed electric field (nsPEF) treatment for hepatocellular carcinoma : A novel locoregional ablation decreasing lung metastasis. Cancer Lett 346:285–291. doi: 10.1016/j.canlet.2014.01.009

59. Stacey M, Fox P, Buescher S, Kolb J (2011) Nanosecond pulsed electric field induced cytoskeleton, nuclear membrane and telomere damage adversely impact cell survival. Bioelectrochemistry 82:131–134. doi: 10.1016/j.bioelechem.2011.06.002

60. Silve A, Leray I, Mir LM (2012) Demonstration of cell membrane permeabilization to medium-sized molecules caused by a single 10 ns electric pulse. Bioelectrochemistry 87:260–264. doi: 10.1016/j.bioelechem.2011.10.002

61. Breton M, Delemotte L, Silve A, et al (2012) Transport of siRNA through Lipid Membranes Driven by Nanosecond Electric Pulses: An Experimental and Computational Study. J Am Chem Soc 134:13938–13941.

62. Gowrishankar, Thiruvallur, R Esser AT, Vasilkoski Z, Smith KC, Weaver JC (2006)

Microdosimetry for conventional and supra-electroporation in cells with organelles. Biochem Biophys Res Commun 341:1266–1276. doi: 10.1016/j.bbrc.2006.01.094

63. Semenov I, Xiao S, Kang D, et al (2015) Cell stimulation and calcium mobilization by picosecond electric pulses. Bioelectrochemistry 105:65–71. doi: 10.1016/j.bioelechem.2015.05.013

64. Craviso GL, Choe S, Chatterjee P, et al (2010) Nanosecond electric pulses: A novel stimulus for triggering Ca2+ influx into chromaffin cells via voltage-gated Ca2+ channels. Cell Mol Neurobiol 30:1259–1265. doi: 10.1007/s10571-010-9573-1

65. Pakhomov AG, Semenov I, Casciola M, Xiao S (2017) Neuronal excitation and permeabilization by 200-ns pulsed electric field: An optical membrane potential study with FluoVolt dye. BBA - Biomembr. doi: 10.1016/j.bbamem.2017.04.016

66. Nuccitelli R, Wood R, Kreis M, et al (2014) First-in-human trial of nanoelectroablation therapy for basal cell carcinoma : proof of method. Exp Dermatol 23:130–142. doi: 10.1111/exd.12303

67. Miklavčič D (2017) Handbook of electroporation. Springer International Publishing

68. Mazères S, Sel D, Golzio M, et al (2009) Non invasive contact electrodes for in vivo localized cutaneous electropulsation and associated drug and nucleic acid delivery. J Control Release 134:125–131. doi: 10.1016/j.jconrel.2008.11.003

69. Vernier PT, Sun Y, Gundersen MA (2006) Nanoelectropulse-driven membrane perturbation and small molecule permeabilization. BMC Cell Biol 7:1–16. doi: 10.1186/1471-2121-7-37

70. Jin L, Platisa J, Wooltorton JRA, et al (2012) Single action potentials and subthreshold electrical events imaged in neurons with a novel fluorescent protein voltage probe. Neuron 75:779–785. doi: 10.1016/j.neuron.2012.06.040.Single

71. Boyce FM, Bucher NLR (1996) Baculovirus-mediated transfer into mammalian cells.

Proc Natl Acad Sci 93:2348–2352.

72. Ghosh S, Parvez K, Banerjee K, et al (2002) Baculovirus as Mammalian Cell Expression Vector for Gene Therapy : An Emerging Strategy. Mol Ther 6:5–11. doi: 10.1006/mthe.2000.0643

73. Kost TA, Condreat JP, Jarvis DL (2005) Baculovirus as versatile vectors for protein expression in insect and mammalian cells. Nat Biotechnol 23:567–575. doi: 10.1038/nbt1095.Baculovirus

74. Scaduto RC, Grotyohann LW (1999) Measurement of mitochondrial membrane potential using fluorescent rhodamine derivatives. Biophys J 76:469–477. doi: 10.1016/S0006-3495(99)77214-0

75. Solaini G, Sgarbi G, Lenaz G, Baracca A (2007) Evaluating Mitochondrial Membrane Potential in Cells. Biosci Rep 27:11–21. doi: 10.1007/s10540-007-9033-4

76. Plfigek J, Sigler K (1996) Slow fluorescent indicators of membrane potential : a survey of different approaches to probe response analysis. J Photochem Photobiol B Biol 33:101–124.

77. Nicholls DG (2006) Simultaneous monitoring of ionophore- and inhibitor-mediated plasma and mitochondrial membrane potential changes in cultured neurons. J Biol Chem 281:14864–74. doi: 10.1074/jbc.M510916200

78. Spitzner M, Ousingsawat J, Scheidt K, et al (2007) Voltage-gated K+ channels support proliferation of colonic carcinoma cells. FASEB J 21:35–44. doi: 10.1096/fj.06-6200com

79. Whiteaker KL, Gopalakrishnan SM, Groebe D, et al (2001) Validation of FLIPR membrane potential dye for high throughput screening of potassium channel modulators. J Biomol Screen 6:305–312. doi: 0803973233

80. Dorn A, Hermann F, Ebneth A, et al (2005) Evaluation of a High-Throughput

Fluorescence Assay Method for hERG Potassium Channel Inhibition. J Biomol Screen 10:339–347. doi: 10.1177/1087057104272045

81. Field A (2009) Discovering statistics using SPSS, 3rd ed. SAGE publications Ltd

82. Schwan HP (1957) Electrical properties of tissue and cell suspensions. Adv Biol Med Phys 5:147–209.

83. Gabriel B, Teissie J (1999) Time Courses of Mammalian Cell Electropermeabilization Observed by Millisecond Imaging of Membrane Property Changes during the Pulse. Biophys J 76:2158–2165.

84. Frey W, White J a, Price RO, et al (2006) Plasma membrane voltage changes during nanosecond pulsed electric field exposure. Biophys J 90:3608–3615. doi: 10.1529/biophysj.105.072777

85. Valic B, Golzio M, Pavlin M, et al (2003) Electric field induced trans-membrane potential on spheroidal cell : theory and experiment. Eur Biophys J 32:519–528. doi: 10.1007/s00249-003-0296-9

86. Kotnik T, Pucihar G, Miklavcic D (2010) Induced Transmembrane Voltage and Its Correlation with Electroporation-Mediated Molecular Transport. J Membr Biol 236:3–13. doi: 10.1007/s00232-010-9279-9

87. Carr L, Bardet SM, Arnaud-cormos D, et al (2018) Visualisation of an nsPEF induced calcium wave using the genetically encoded calcium indicator GCaMP in U87 human glioblastoma cells. Bioelectrochemistry 119:68–75. doi: 10.1016/j.bioelechem.2017.09.003

88. Puc M, Kotnik T, Mir LM, Miklavc D (2003) Quantitative model of small molecules uptake after in vitro cell electropermeabilization. Bioelectrochemistry 60:1–10. doi: 10.1016/S1567-5394(03)00021-5

89. Hojo S, Shimizu K, Yositake H, et al (2003) The Relationship Between

Electropermeabilization and Cell Cycle and Cell Size of Saccharomyces Cerevisiae. IEEE Trans Nanobioscience 2:35–39.

90. Sukhorukov VL, Djuzenova CS, Frank H, et al (1995) Electropermeabilization and Fluorescent Tracer Exchange : The Role of Whole-Cell Capacitance. Cytometry 21:230–240.

91. Henslee BE, Morss A, Hu X, et al (2011) Electroporation Dependence on Cell Size : Optical Tweezers Study. Anal Chem 83:3998–4003.

92. Denzi A, Camera F, Merla C, et al (2016) A Microdosimeric Study of Electropulsation on Multiple Realistically Shaped Cells : Effect of Neighbours. J Membr Biol. doi: 10.1007/s00232-016-9912-3

93. Teissie J, Tsong TY (1980) Evidence of voltage-induced channel opening in Na/K ATPase of human erythrocyte membrane. J Membr Biol 55:133–140. doi: 10.1007/BF01871155

94. Chen W, Lee RC (1994) Altered ion channel conductance and ionic selectivity induced by large imposed membrane potential pulse. Biophys J 67:603–612. doi: 10.1016/S0006-3495(94)80520-X

95. Levin M (2007) Large-scale biophysics: ion flows and regeneration. Trends Cell Biol 17:261–270. doi: 10.1016/j.tcb.2007.04.007

96. Blackiston DJ, McLaughlin KA, Levin M (2009) Bioelectric controls of cell proliferation: Ion channels, membrane voltage and the cell cycle. Cell Cycle 8:3519–3528. doi: 10.1115/1.3071969.Automating

97. Rao VR, Perez-Neut M, Kaja S, Gentile S (2015) Voltage-gated ion channels in cancer cell proliferation. Cancers (Basel) 7:849–875. doi: 10.3390/cancers7020813

98. Tay D, Bhathal P, Fox R (1991) Quantitation of Go and G1 Phase Cells in Primary Carcinomas. J Clin Invest 87:519–527.

99. Motaln H, Koren A, Gruden K, et al (2015) Heterogeneous glioblastoma cell cross-talk promotes phenotype alterations and enhanced drug resistance. Oncotarget 6:40998–41017.

100. Burke RC, Bardet SM, Carr L, et al (2017) Nanosecond pulsed electric fields depolarize transmembrane potential via voltage-gated K+, Ca2+ and TRPM8 channels in U87 glioblastoma cells. BBA - Biomembr 1859:2040–2050. doi: 10.1016/j.bbamem.2017.07.004

101. Esser AT, Smith KC, Gowrishankar TR, Weaver JC (2009) Towards Solid Tumor Treatment by Nanosecond Pulsed Electric Fields. Technol cancer Res Treat 8:289–306.

102. Nuccitelli R, Pliquett U, Chen X, et al (2006) Nanosecond pulsed electric fields cause melanomas to self-destruct. Biochem Biophys Res Commun 343:351–360. doi: 10.1016/j.bbrc.2006.02.181

103. Guo S, Jackson DL, Burcus NI, et al (2014) Gene electrotransfer enhanced by nanosecond pulsed electric fields. Mol Ther Methods Clin Dev 1:14043. doi: 10.1038/mtm.2014.43

104. SJ B, J W, PF B, et al (2003) Diverse effects of nanosecond pulsed electric fields on cells and tissues. DNA Cell Biol 22:785–796.

105. Pakhomov AG, Kolb JF, White J a., et al (2007) Long-lasting plasma membrane permeabilization in mammalian cells by nanosecond Pulsed Electric Field (nsPEF). Bioelectromagnetics 28:655–663. doi: 10.1002/bem.20354

106. Cantu JC, Tarango M, Beier HT, Ibey BL (2016) The Biological Response Of Cells To Nanosecond Pulsed Electric Fields Is Dependent On Plasma Membrane Cholesterol. Biochim Biophys Acta - Biomembr 1858:2636–2646. doi: 10.1016/j.bbamem.2016.07.006

107. Semenov I, Xiao S, Pakhomov AG (2013) Primary pathways of intracellular Ca(2+) mobilization by nanosecond pulsed electric field. Biochim Biophys Acta 1828:981–9. doi: 10.1016/j.bbamem.2012.11.032

108. Son RS, Smith KC, Gowrishankar TR, et al (2014) Basic Features of a Cell Electroporation Model : Illustrative Behavior for Two Very Different Pulses. J Membr Biol 247:1209–1228. doi: 10.1007/s00232-014-9699-z

109. Bardet SM, Carr L, Soueid M, et al (2016) Multiphoton imaging reveals that nanosecond pulsed electric fields collapse tumor and normal vascular perfusion in human glioblastoma xenografts. Sci Rep 6:1–11. doi: 10.1038/srep34443

110. Tokman M, Lee JH, Levine ZA, et al (2013) Electric Field-Driven Water Dipoles: Nanoscale Architecture of Electroporation. PLoS One. doi: 10.1371/journal.pone.0061111

111. Bowman AM, Nesin OM, Pakhomova ON, Pakhomov AG (2010) Analysis of plasma membrane integrity by fluorescent detection of Tl + uptake. J Membr Biol 236:15–26. doi: 10.1007/s00232-010-9269-y

112. Pakhomov AG, Bowman AM, Ibey BL, et al (2009) Lipid Nanopores Can Form a Stable, Ion Channel-Like Conduction Pathway in Cell Membrane. Biochem Biophys Res Commun 385:181–186. doi: 10.1016/j.bbrc.2009.05.035.Lipid

113. Li M, Xiong ZG (2011) Ion channels as targets for cancer therapy. Int J Physiol Pathophysiol Pharmacol 3:156–166. doi: 10.1115/1.4026364

114. Prevarskaya N, Skryma R, Shuba Y (2010) Ion channels and the hallmarks of cancer. Trends Mol Med 16:107–121. doi: 10.1016/j.molmed.2010.01.005

115. Clark MJ, Homer N, O'Connor BD, et al (2010) U87MG decoded: The genomic sequence of a cytogenetically aberrant human cancer cell line. PLoS Genet. doi: 10.1371/journal.pgen.1000832

116. Ducret T, Vacher A-M, Vacher P (2003) Voltage-dependent ionic conductances in the human malignant astrocytoma cell line U87-MG. Mol Membr Biol 20:329–343. doi: 10.1080/0968763031000138037

117. Molenaar RJ (2011) Ion Channels in Glioblastoma. ISRN Neurol 2011:1–7. doi: 10.5402/2011/590249

118. Chin LS, Park CC, Zitnay KM, et al (1997) 4-Aminopyridine Causes Apoptosis and Blocks an Outward Rectifier K + Channel in Malignant Astrocytoma Cell Lines. J Neurosci Res 48:122–127.

119. Chattopadhyay N, Ye C-P, Yamaguchi T, et al (1999) Evidence for Extracellular Calcium-Sensing Receptor Mediated Opening of an Outward K ⁒ Channel in a Human Astrocytoma Cell Line (U87). Glia 26:64–72.

120. McFerrin MB, Sontheimer H (2006) A role for ion channels in glioma cell invasion. Neuron Glia Biol 2:39–49. doi: 10.1017/S17440925X06000044

121. Arcangeli A, Crociani O, Lastraioli E, et al (2009) Targeting Ion Channels in Cancer : A Novel Frontier in Antineoplastic Therapy. Curr Med Chem 16:66–93.

122. Delmas P, Gola M (1995) Choline blocks large conductance Kca channels in mammalian sympathetic neurones. Neurosci Lett 189:109–112.

123. Lippiat JD, Standen NB, Davies NW (1998) Block of cloned BK(Ca) channels (rSlo) expressed in HEK 293 cells by N-methyl D-glucamine. Pflugers Arch Eur J Physiol 436:810–812. doi: 10.1007/s004240050708

124. Wolff C, Fuks B, Chatelain P (2003) Comparative Study of Membrane Potential-Sensitive Fluorescent Probes and their Use in Ion Channel Screening Assays. J Biomol Screen 8:533–543. doi: 10.1177/1087057103257806

125. Goehring I, Gerencser AA, Schmidt S, et al (2012) Plasma membrane potential oscillations in insulin secreting Ins-1 832/13 cells do not require glycolysis and are not

initiated by fluctuations in mitochondrial bioenergetics. J Biol Chem 287:15706–15717. doi: 10.1074/jbc.M111.314567

126. Baxter DF, Kirk M, Garcia AF, et al (2002) A novel membrane potential-sensitive fluorescent dye improves cell-based assays for ion channels. J Biomol Screen Off J Soc Biomol Screen 7:79–85. doi: 10.1177/108705710200700110

127. Yan J, Aldrich RW (2010) LRRC26 auxiliary protein allows BK channel activation at resting voltage without calcium. Nature 466:513–516. doi: 10.1038/nature09162

128. Warbington L, Hillman T, Adams C, Stern M (1996) Reduced transmitter release conferred by mutations in the slowpoke-encoded Ca2+-activated K+ channel gene of Drosophila. Invertebr Neurosci 2:51–60.

129. Pattillo JM, Yazejian B, Digregorio DA, et al (2001) Contribution of presynaptic calcium-activated potassium currents to transmitter release regulation in cultured xenopus nerve-muscle synapses. Neuroscience 102:229–240.

130. Skinner LJ, Enée V, Beurg M, et al (2003) Contribution of BK Ca2+ -Activated K+ Channels to Auditory Neurotransmission in the Guinea Pig Cochlea. J Neurophysiol 90:320–332.

131. Xu JW, Slaughter MM (2005) Large-Conductance Calcium-Activated Potassium Channels Facilitate Transmitter Release in Salamander Rod Synapse. J Neurosci 25:7660–7668. doi: 10.1523/JNEUROSCI.1572-05.2005

132. Guéguinou M, Chantôme A, Fromont G, et al (2014) KCa and Ca2+ channels: The complex thought. Biochim Biophys Acta 1843:2322–2333. doi: 10.1016/j.bbamcr.2014.02.019

133. Schütz GJ, Kada G, Pastushenko VP, Schindler H (2000) Properties of lipid microdomains in a muscle cell membrane visualized by single molecule microscopy. EMBO J 19:892–901. doi: 10.1093/emboj/19.5.892

134. Dart C (2010) Lipid microdomains and the regulation of ion channel function. J Physiol 588:3169–78. doi: 10.1113/jphysiol.2010.191585

135. Gackière F, Warnier M, Katsogiannou M, et al (2013) Functional coupling between large-conductance potassium channels and Cav3.2 voltage-dependent calcium channels participates in prostate cancer cell growth. Biol Open 2:941–51. doi: 10.1242/bio.20135215

136. Grunnet M, Kaufmann WA (2004) Coassembly of big conductance Ca2+-activated K+ channels and L-type voltage-gated Ca2+ channels in rat brain. J Biol Chem 279:36445–36453. doi: 10.1074/jbc.M402254200

137. Wondergem R, Bartley JW (2009) Menthol increases human glioblastoma intracellular Ca2+, BK channel activity and cell migration. J Biomed Sci 16:1–7. doi: 10.1186/1423-0127-16-90

138. Reinhart PH, Chung S, Levitan IB (1989) A family of calcium-dependent potassium channels from rat brain. Neuron 2:1031–1041. doi: 0896-6273(89)90227-4 [pii]

139. Benton MD, Lewis AH, Bant JS, Raman IM (2013) Iberiotoxin-sensitive and -insensitive BK currents in Purkinje neuron somata. J Neurophysiol 109:2528–41. doi: 10.1152/jn.00127.2012

140. Yu M, Liu S, Sun P, et al (2016) Peptide toxins and small-molecule blockers of BK channels. Acta Pharmacol Sin 37:56–66. doi: 10.1038/aps.2015.139

141. Berkefeld H, Fakler B, Schulte UWE (2010) Ca 2+-Activated K+ Channels : From Protein Complexes to Function. Physiol Rev 90:1437–1459. doi: 10.1152/physrev.00049.2009.

142. Wang B, Jaffe DB, Brenner R (2014) Current understanding of iberiotoxin-resistant BK channels in the nervous system. Front Physiol 5:1–11. doi: 10.3389/fphys.2014.00382

143. Shruti S, Urban-Ciecko J, Fitzpatrick JA, et al (2012) The brain-specific beta4 subunit downregulates BK channel cell surface expression. PLoS One. doi: 10.1371/journal.pone.0033429

144. Meera P, Wallner M, Toro L (2000) A neuronal beta subunit (KCNMB4) makes the large conductance, voltage- and Ca2+-activated K+ channel resistant to charybdotoxin and iberiotoxin. Proc Natl Acad Sci U S A 97:5562–7. doi: 10.1073/pnas.100118597

145. Liu X, Chang Y, Reinhart PH, et al (2002) Cloning and characterization of glioma BK, a novel BK channel isoform highly expressed in human glioma cells. J Neurosci 22:1840–9. doi: 22/5/1840 [pii]

146. Marie C, Verkerke HP, Theodorescu D, Petri WA (2015) A whole-genome RNAi screen uncovers a novel role for human potassium channels in cell killing by the parasite Entamoeba histolytica. Sci Rep 5:1–18. doi: 10.1038/srep13613\rsrep13613 [pii]

147. Brelidze TI, Magleby KL (2004) Protons block BK channels by competitive inhibition with K+ and contribute to the limits of unitary currents at high voltages. J Gen Physiol 123:305–19. doi: 10.1085/jgp.200308951

148. Peier AM, Moqrich A, Hergarden AC, et al (2002) A TRP Channel that Senses Cold Stimuli and Menthol. Cell 108:705–715. doi: 10.1016/S0092-8674(02)00652-9

149. Chen J, Kim D, Bianchi BR, et al (2009) Pore dilation occurs in TRPA1 but not in TRPM8 channels. Mol Pain 5:1–6. doi: 10.1186/1744-8069-5-3

150. Harteneck C (2005) Function and pharmacology of TRPM cation channels. Naunyn Schmiedebergs Arch Pharmacol 371:307–314. doi: 10.1007/s00210-005-1034-x

151. Tominaga M, Caterina MJ (2004) Thermosensation and pain. J Neurobiol 61:3–12. doi: 10.1002/neu.20079

152. Yoon J, Leblanc N, Zaklit J, et al (2016) Enhanced Monitoring of Nanosecond Electric Pulse-Evoked Membrane Conductance Changes in Whole-Cell Patch Clamp

Experiments. J Membr Biol 249:1–12. doi: 10.1007/s00232-016-9902-5

153. Binshtok AM, Bean BP, Woolf CJ (2007) Inhibition of nociceptors by TRPV1-mediated entry of impermeant sodium channel blockers. Nature 449:607–10. doi: 10.1038/nature06191

154. Banke TG, Chaplan SR, Wickenden a D (2010) Dynamic changes in the TRPA1 selectivity filter lead to progressive but reversible pore dilation. Am J Physiol Cell Physiol 298:C1457-68. doi: 10.1152/ajpcell.00489.2009

155. Cao E, Liao M, Cheng Y, Julius D (2013) TRPV1 structures in distinct conformations reveal mechanisms of activation. Nature 504:113–118. doi: 10.1038/nbt.3121.ChIP-nexus

156. Chung M-K, Güler AD, Caterina MJ (2008) TRPV1 shows dynamic ionic selectivity during agonist stimulation. Nat Neurosci 11:555–564. doi: 10.1038/nn.2102

157. Cui J, Yang H, Lee US (2009) Molecular Mechanisms of BK Channel Activation. Cell Mol life Sci 66:852–875. doi: 10.1007/s00018-008-8609-x.Molecular

158. Ge L, Hoa NT, Wilson Z, et al (2014) Big Potassium (BK) ion channels in biology, disease and possible targets for cancer immunotherapy. Int Immunopharmacol 22:427–443. doi: 10.1016/j.intimp.2014.06.040

159. Ge L, Hoa NT, Cornforth AN, et al (2012) Glioma big potassium channel expression in human cancers and possible T cell epitopes for their immunotherapy. J Immunol 189:2625–2634. doi: 10.4049/jimmunol.1102965

160. Han X, Xi L, Wang H, et al (2008) The potassium ion channel opener NS1619 inhibits proliferation and induces apoptosis in A2780 ovarian cancer cells. Biochem Biophys Res Commun 375:205–209. doi: 10.1016/j.bbrc.2008.07.161

161. Cox DH, Cui J, Aldrich RW (1997) Allosteric gating of a large conductance Ca-activated K+ channel. J Gen Physiol 110:257–281. doi: 10.1085/jgp.110.3.257

162. Zhao H, Sokabe M (2008) Tuning the mechanosensitivity of a BK channel by changing the linker length. Cell Res 18:871–8. doi: 10.1038/cr.2008.88

163. Roth CC, Barnes R a, Ibey BL, et al (2015) Characterization of Pressure Transients Generated by Nanosecond Electrical Pulse (nsEP) Exposure. Sci Rep 5:15063. doi: 10.1038/srep15063

164. Kotnik T, Kramar P, Pucihar G, et al (2012) Cell membrane electroporation- Part 1: The phenomenon. IEEE Electr Insul Mag 28:14–23. doi: 10.1109/MEI.2012.6268438

165. Tsong TY (1991) Electroporation of cell membranes. Biophys J 60:297–306. doi: 10.1016/S0006-3495(91)82054-9

166. Weaver JC (1993) Electroporation: a general phenomenon for manipulating cells and tissues. J Cell Biochem 51:426–435.

167. Kotnik T, Frey W, Sack M, et al (2015) Electroporation-based applications in biotechnology. Trends Biotechnol. doi: 10.1016/j.tibtech.2015.06.002

168. Mahnič-Kalamiza S, Vorobiev E, Miklavčič D (2014) Electroporation in food processing and biorefinery. J Membr Biol 247:1279–1304.

169. Toepfl S, Siemer C, Saldaña-Navarro G, Heinz V (2014) Overview of Pulsed Electric Fields Processing for Food. In: Emerg. Technol. Food Process. Elsevier, pp 93–114

170. Yarmush ML, Golberg A, Serša G, et al (2014) Electroporation-Based Technologies for Medicine: Principles, Applications, and Challenges. Annu Rev Biomed Eng 16:295–320. doi: 10.1146/annurev-bioeng-071813-104622

171. Daud AI, DeConti RC, Andrews S, et al (2008) Phase I trial of interleukin-12 plasmid electroporation in patients with metastatic melanoma. J Clin Oncol 26:5896–5903.

172. Calvet CY, André FM, Mir LM (2014) Dual therapeutic benefit of electroporation-mediated DNA vaccination in vivo: Enhanced gene transfer and adjuvant activity. Oncoimmunology 3:e28540. doi: 10.4161/onci.28540

173. Trimble CL, Morrow MP, Kraynyak KA, et al (2015) Safety, efficacy, and immunogenicity of VGX-3100, a therapeutic synthetic DNA vaccine targeting human papillomavirus 16 and 18 E6 and E7 proteins for cervical intraepithelial neoplasia 2/3: a randomised, double-blind, placebo-controlled phase 2b trial. Lancet 386:2078–2088. doi: 10.1016/S0140-6736(15)00239-1

174. Vasan S, Hurley A, Schlesinger SJ, et al (2011) In Vivo Electroporation Enhances the Immunogenicity of an HIV-1 DNA Vaccine Candidate in Healthy Volunteers. PLoS One 6:e19252. doi: 10.1371/journal.pone.0019252

175. Serša G, Teissié J, Čemažar M, et al (2015) Electrochemotherapy of tumors as in situ vaccination boosted by immunogene electrotransfer. Cancer Immunol Immunother 64:1315–1327. doi: 10.1007/s00262-015-1724-2

176. Denet A-R, Vanbever R, Préat V (2004) Skin electroporation for transdermal and topical delivery. Adv Drug Deliv Rev 56:659–674. doi: 10.1016/j.addr.2003.10.027

177. Zorec B, Préat V, Miklavčič D, Pavšelj N (2013) Active enhancement methods for intra- and transdermal drug delivery: a review. Zdr Vestn 82:339–56.

178. Al-Sakere B, André F, Bernat C, et al (2007) Tumor Ablation with Irreversible Electroporation. PLoS One 2:e1135. doi: 10.1371/journal.pone.0001135

179. Gasbarrini A, Campos WK, Campanacci L, Boriani S (2015) Electrochemotherapy to Metastatic Spinal Melanoma: A Novel Treatment of Spinal Metastasis? Spine (Phila Pa 1976) 40:E1340–E1346. doi: 10.1097/BRS.0000000000001125

180. Mali B, Jarm T, Snoj M, et al (2013) Antitumor effectiveness of electrochemo-therapy: A systematic review and meta-analysis. Eur J Surg Oncol 39:4–16.

181. Miklavčič D, Mali B, Kos B, et al (2014) Electrochemotherapy: from the drawing board into medical practice. Biomed Eng Online 13:29. doi: 10.1186/1475-925X-13-29

182. Bianchi G, Campanacci L, Ronchetti M, Donati D (2016) Electrochemotherapy in the

Treatment of Bone Metastases: A Phase II Trial. World J Surg 40:3088–3094. doi: 10.1007/s00268-016-3627-6

183. Hille B (1992) Ionic channels of excitable membranes, 2nd ed. Sinauer Associates, Sunderland, Mass

184. Garcia PA, Rossmeisl JH, Robertson JL, et al (2012) 7.0-T Magnetic Resonance Imaging Characterization of Acute Blood-Brain-Barrier Disruption Achieved with Intracranial Irreversible Electroporation. PLoS One 7:e50482. doi: 10.1371/journal.pone.0050482

185. Garcia PA, Pancotto T, Rossmeisl JH, et al (2011) Non-thermal irreversible electroporation (N-TIRE) and adjuvant fractionated radiotherapeutic multimodal therapy for intracranial malignant glioma in a canine patient. Technol Cancer Res Treat 10:73–83.

186. Hjouj M, Last D, Guez D, et al (2012) MRI Study on Reversible and Irreversible Electroporation Induced Blood Brain Barrier Disruption. PLoS One 7:e42817. doi: 10.1371/journal.pone.0042817

187. Linnert M, Iversen HK, Gehl J (2012) Multiple brain metastases - current management and perspectives for treatment with electrochemotherapy. Radiol Oncol. doi: 10.2478/v10019-012-0042-y

188. Sharabi S, Kos B, Last D, et al (2016) A statistical model describing combined irreversible electroporation and electroporation-induced blood-brain barrier disruption. Radiol Oncol 50:28–38.

189. Neal RE, Millar JL, Kavnoudias H, et al (2014) In vivo characterization and numerical simulation of prostate properties for non-thermal irreversible electroporation ablation: Characterized and Simulated Prostate IRE. Prostate 74:458–468. doi: 10.1002/pros.22760

190. Tschon M, Salamanna F, Ronchetti M, et al (2015) Feasibility of Electroporation in Bone and in the Surrounding Clinically Relevant Structures: A Preclinical Investigation. Technol Cancer Res Treat. doi: 10.1177/1533034615604454

191. Lavee J, Onik G, Mikus P, Rubinsky B (2007) A Novel Nonthermal Energy Source for Surgical Epicardial Atrial Ablation: Irreversible Electroporation. Heart Surg Forum 10:E162–E167. doi: 10.1532/HSF98.20061202

192. Neven K, van Driel V, van Wessel H, et al (2014) Myocardial Lesion Size After Epicardial Electroporation Catheter Ablation After Subxiphoid Puncture. Circ Arrhythmia Electrophysiol 7:728–733. doi: 10.1161/CIRCEP.114.001659

193. Xie F, Varghese F, Pakhomov AG, et al (2015) Ablation of Myocardial Tissue With Nanosecond Pulsed Electric Fields. PLoS One 10:e0144833. doi: 10.1371/journal.pone.0144833

194. Gehl J, Sørensen TH, Nielsen K, et al (1999) In vivo electroporation of skeletal muscle: threshold, efficacy and relation to electric field distribution. Biochim Biophys Acta - Gen Subj 1428:233–240. doi: 10.1016/S0304-4165(99)00094-X

195. Satkauskas S, Bureau MF, Puc M, et al (2002) Mechanisms of in Vivo DNA Electrotransfer: Respective Contributions of Cell Electropermeabilization and DNA Electrophoresis. Mol Ther 5:133–140. doi: 10.1006/mthe.2002.0526

196. Ayuni EL, Gazdhar A, Giraud MN, et al (2010) In Vivo Electroporation Mediated Gene Delivery to the Beating Heart. PLoS One 5:e14467. doi: 10.1371/journal.pone.0014467

197. Bulysheva AA, Hargrave B, Burcus N, et al (2016) Vascular endothelial growth factor-A gene electrotransfer promotes angiogenesis in a porcine model of cardiac ischemia. Gene Ther 23:649–656. doi: 10.1038/gt.2016.35

198. Li W, Fan Q, Ji Z, et al (2011) The Effects of Irreversible Electroporation (IRE) on Nerves. PLoS One 6:e18831. doi: 10.1371/journal.pone.0018831

199. Onik G, Mikus P, Rubinsky B (2007) Irreversible electroporation: implications for prostate ablation. Technol Cancer Res Treat 6:295–300.

200. Casciola M, Xiao S, Pakhomov AG (2017) Damage-free peripheral nerve stimulation by 12-ns pulsed electric field. Sci Rep 7:10453. doi: 10.1038/s41598-017-10282-5

201. Schoellnast H, Monette S, Ezell PC, et al (2011) Acute and subacute effects of irreversible electroporation on nerves: experimental study in a pig model. Radiology 260:421–427. doi: 10.1148/radiol.11103505

202. Nevian T, Helmchen F (2007) Calcium indicator loading of neurons using single-cell electroporation. Pflügers Arch - Eur J Physiol 454:675–688. doi: 10.1007/s00424-007-0234-2

203. van Driel VJHM, Neven K, van Wessel H, et al (2015) Low vulnerability of the right phrenic nerve to electroporation ablation. Hear Rhythm 12:1838–1844. doi: 10.1016/j.hrthm.2015.05.012

204. Arena CB, Davalos R V. (2012) Advances in Therapeutic Electroporation to Mitigate Muscle Contractions. J Membr Sci Technol. doi: 10.4172/2155-9589.1000e102

205. Golberg A, Rubinsky B (2012) Towards Electroporation Based Treatment Planning Considering Electric Field Induced Muscle Contractions. Technol Cancer Res Treat 11:189–201. doi: 10.7785/tcrt.2012.500249

206. Miklavčič D, Pucihar G, Pavlovec M, et al (2005) The effect of high frequency electric pulses on muscle contractions and antitumor efficiency in vivo for a potential use in clinical electrochemotherapy. Bioelectrochemistry 65:121–128. doi: 10.1016/j.bioelechem.2004.07.004

207. Županič A, Ribarič S, Miklavčič D (2007) Increasing the repetition frequency of electric pulse delivery reduces unpleasant sensations that occur in electrochemotherapy. Neoplasma 54:246–250.

208. Ball C, Thomson KR, Kavnoudias H (2010) Irreversible Electroporation: A New Challenge in “Out of Operating Theater” Anesthesia. Anesth Analg 110:1305–1309. doi: 10.1213/ANE.0b013e3181d27b30

209. Deodhar A, Dickfeld T, Single GW, et al (2011) Irreversible electroporation near the heart: ventricular arrhythmias can be prevented with ECG synchronization. AJR Am J Roentgenol 196:W330-335. doi: 10.2214/AJR.10.4490

210. Mali B, Gorjup V, Edhemovic I, et al (2015) Electrochemotherapy of colorectal liver metastases - an observational study of its effects on the electrocardiogram. Biomed Eng Online 14:S5. doi: 10.1186/1475-925X-14-S3-S5

211. Mali B, Jarm T, Corovic S, et al (2008) The effect of electroporation pulses on functioning of the heart. Med Biol Eng Comput 46:745–757. doi: 10.1007/s11517-008-0346-7

212. Jiang N, Cooper BY (2011) Frequency-dependent interaction of ultrashort E-fields with nociceptor membranes and proteins. Bioelectromagnetics 32:148–163. doi: 10.1002/bem.20620

213. Nene D, Jiang N, Rau KK, et al (2006) Nociceptor activation and damage by pulsed E-fields. doi: 10.1117/12.665181

214. Spitzner M, Ousingsawat J, Scheidt K, et al (2006) Voltage-gated K+ channels support proliferation of colonic carcinoma cells. FASEB J 21:35–44. doi: 10.1096/fj.06-6200com

215. Wolff C, Fuks B, Chatelain P (2003) Comparative study of membrane potential-sensitive fluorescent probes and their use in ion channel screening assays. J Biomol Screen 8:533–543. doi: 10.1177/1087057103257806

216. Lalik PH, Krafte DS, Volberg WA, Ciccarelli RB (1993) Characterization of endogenous sodium channel gene expressed in Chinese hamster ovary cells. Am J

Physiol Cell Physiol 264:C803-9.

217. Skryma R, Prevarskaya N, Vacher P, Dufy B (1994) Voltage-dependent Ca2+ channels in Chinese hamster ovary (CHO) cells. FEBS 349:289–294.

218. Gamper N, Stockand JD, Shapiro MS (2005) The use of Chinese hamster ovary (CHO) cells in the study of ion channels. J Pharmacol Toxicol Methods 51:177–185. doi: 10.1016/j.vascn.2004.08.008

219. Kandel ER, Schwartz JH, Jessell TM, et al (2012) Principles of neural science, 5th ed. McGraw-Hill, Education

220. Frandsen SK, Kruger MB, Mangalanathan UM, et al (2017) Normal and Malignant Cells Exhibit Differential Responses to Calcium Electroporation. Cancer Res 77:1–14. doi: 10.1158/0008-5472.CAN-16-1611

221. Frandsen SK, McNeil AK, Novak I, et al (2016) Difference in Membrane Repair Capacity Between Cancer Cell Lines and a Normal Cell Line. J Membr Biol 249:569–576. doi: 10.1007/s00232-016-9910-5

222. Fairless R, Beck A, Kravchenko M, et al (2013) Membrane Potential Measurements of Isolated Neurons Using a Voltage-Sensitive Dye. PLoS One 8:e58260. doi: 10.1371/journal.pone.0058260

223. Rols MP, Delteil C, Golzio M, Teissié J (1998) Control by ATP and ADP of voltage-induced mammalian-cell-membrane permeabilization, gene transfer and resulting expression. Eur J Biochem 254:382–388.

224. Chen W, Zhongsheng Z, Lee RC (2006) Supramembrane potential-induced electroconformational changes in sodium channel proteins: A potential mechanism involved in electric injury. Burns 32:52–59. doi: 10.1016/j.burns.2005.08.008

225. Levin M, Stevenson CG (2012) Regulation of Cell Behavior and Tissue Patterning by Bioelectrical Signals: Challenges and Opportunities for Biomedical Engineering. Annu

Rev Biomed Eng 14:295–323. doi: 10.1146/annurev-bioeng-071811-150114

226. Dermol J, Miklavčič D (2014) Predicting electroporation of cells in an inhomogeneous electric field based on mathematical modeling and experimental CHO-cell permeabilization to propidium iodide determination. Bioelectrochemistry 100:52–61. doi: 10.1016/j.bioelechem.2014.03.011

227. Pucihar G, Kotnik T, Teissié J, Miklavčič D (2007) Electropermeabilization of dense cell suspensions. Eur Biophys J 36:172–185.

228. Susil R, Šemrov D, Miklavčič D (1998) Electric field induced transmembrane potential depends on cell density and organization. Electro- and Magnetobiology 17:391–399.

229. Čemažar M, Jarm T, Miklavčič D, et al (1998) Effect of electric-field intensity on electropermeabilization and electrosensitivity of various tumor-cell lines in vitro. Electro- and Magnetobiology 17:263–272.

230. Moen EK, Ibey BL, Beier HT, Armani AM (2016) Quantifying pulsed electric field-induced membrane nanoporation in single cells. Biochim Biophys Acta - Biomembr 1858:2795–2803. doi: 10.1016/j.bbamem.2016.08.007

231. Muller KJ, Sukhorukov VL, Zimmermann U (2001) Membrane Biology Reversible Electropermeabilization of Mammalian Cells by High-Intensity , Ultra-Short. J Membr Biol 184:161–170. doi: 10.1007/s00232-001-0084-3

232. Satkauskas S, Ruzgys P, Venslauskas MS (2012) Towards the mechanisms for efficient gene transfer into cells and tissues by means of cell electroporation. Expert Opin Biol Ther 12:275–286. doi: 10.1517/14712598.2012.654775

233. Kinosita KJ, Tsong TY (1977) Voltage-induced pore formation and hemolysis of human erythrocytes. Biochim Biophys Acta 471:227–242.

234. Sale AJH, Hamilton WA (1968) Effects of high electric fields on micro-organisms: III. Lysis of erythrocytes and protoplasts. Biochim Biophys Acta - Biomembr 163:37–43.

doi: 10.1016/0005-2736(68)90030-8

235. Yang M, Brackenbury WJ (2013) Membrane potential and cancer progression. Front Physiol 4:1–10. doi: 10.3389/fphys.2013.00185

236. Voets T, Owsianik G, Janssens A, et al (2007) TRPM8 voltage sensor mutants reveal a mechanism for integrating thermal and chemical stimuli. Nat Chem Biol 3:174–182. doi: 10.1038/nchembio862

237. Fernández JA, Skryma R, Bidaux G, et al (2011) Voltage- and cold-dependent gating of single TRPM8 ion channels. J Gen Physiol 137:173–195. doi: 10.1085/jgp.201010498

238. Raddatz N, Castillo JP, Gonzalez C, et al (2014) Temperature and Voltage Coupling to Channel Opening in Transient Receptor Potential Melastatin 8 (TRPM8) *. J Biol Chem 289:35438–35454. doi: 10.1074/jbc.M114.612713

239. Belehradek M, Domenge C, Luboinski B, et al (1993) Electrochemotherapy , a New Antitumor Treatment First Clinical Phase I-II Trial. Cancer 72:3694–3700.

240. Falk H, Matthiessen LW, Wooler G, Gehl J (2017) Calcium electroporation for treatment of cutaneous metastases ; a randomized double- blinded phase II study , comparing the effect of calcium electroporation with electrochemotherapy. Acta Oncol (Madr) 1–9. doi: 10.1080/0284186X.2017.1355109

241. Gehl J, Geertsen PF (2000) Efficient palliation of haemorrhaging malignant melanoma skin metastases by electrochemotherapy. Melanoma Res 10:585–589.

242. Boinagrov D, Loudin J, Palanker D (2010) Strength-Duration Relationship for Extracellular Neural Stimulation: Numerical and Analytical Models. J Neurophysiol 104:2236–2248. doi: 10.1152/jn.00343.2010

243. Brunel N, Van Rossum MCW (2007) Quantitative investigations of electrical nerve excitation treated as polarization. Biol Cybern 97:341–349. doi: 10.1007/s00422-007-0189-6

244. Chen W, Han Y, Chen Y, Astumian D (1998) Electric field-induced functional reductions in the K+ channels mainly resulted from supramembrane potential-mediated electroconformational changes. Biophys J 75:196–206. doi: 10.1016/S0006-3495(98)77506-X

245. Chen W (2004) Supra-physiological membrane potential induced conformational changes in K+ channel conducting system of skeletal muscle fibers. Bioelectrochemistry 62:47–56. doi: 10.1016/j.bioelechem.2003.10.006

List of publications during Ph.D. candidature

Journal articles

1. **Burke RC**, Bardet SM, Carr L, et al (2017) Nanosecond pulsed electric fields depolarize transmembrane potential via voltage-gated K+, Ca2+ and TRPM8 channels in U87 glioblastoma cells. BBA - Biomembr 1859:2040–2050. doi: 10.1016/j.bbamem.2017.07.004

2. Carr L, Bardet SM, **Burke RC**, et al (2017) Calcium-independent disruption of microtubule dynamics by nanosecond pulsed electric fields in U87 human glioblastoma cells. Sci Rep. doi: 10.1038/srep41267

3. Moreau D, Lefort C, **Burke R**, et al (2015) Rhodamine B as an optical thermometer in cells focally exposed to infrared laser light or nanosecond pulsed electric fields. Biomed Opt Express 6:713–718. doi: 10.1364/BOE.6.004105

4. Dermol, Janja, Miklavcic, Damijan, Rebersek, Matej, et al (2017) Plasma membrane depolarization and permeabilization due to electric pulses in cell lines of different excitability. Bioelectrochemistry (in review)

Presentations at International Conferences

1. **Burke R**., Romanenko S., Moreau D., Arnaud-Cormos D., Leveque P., O'Connor R.P. "Application of a voltage sensitive dye to study the effect of nanosecond pulsed electric fields (nsPEF) on membrane potential in human U87 glioblastoma cells." In *BioEM 2015, Joint Meeting of the BioElectroMagnetics Society and the European BioElectromagnetics Association,* Pacific Grove, CA, USA, 14 - 19 June 2015

2. **Burke, R**., Moreau, David., Arnaud-Cormos, Delia., Leveque, Philippe., O'Connor, Rodney. "Voltage-gated ion channel antagonists inhibit nsPEF-induced membrane depolarization in U87 glioblastoma cells." In EBTT 2015 proceedings, Ljubljana, Slovenia, November 15 – 21, 2015.

3. Moreau, David., Lefort, Claire., **Burke, Ryan**., Leveque, Philippe., O'Connor, Rodney. "Thermal effect of nanosecond pulsed electric fields." In EBTT 2015 proceedings, Ljubljana, Slovenia, November 15 – 21, 2015.

4. Moreau, David., Lefort, Claire., **Burke, Ryan**., Leveque, Philippe., O'Connor, Rodney. "Thermal imaging with Rhodamine B in cells exposed to electromagnetic radiation." In BioEM 2016, joint meeting of the Bioelectromagnetics Society and the European Bioelectromagnetics Association, Ghent, Belgium, June 5 – 10, 2016.

5. Dermol, Janja., Arnaud-Cormos, Delia., Bardet, Sylvia., **Burke, Ryan**., Leveque, Philippe., Mekuc, Primoz., Miklavcic, Damijan. "Cell membrane depolarization and permeability of three cell lines of different excitability." In BES 2017, XXIV International symposium on Bioelectrochemistry and Bioenergetics of the Bioelectrochemical Society, Lyon, France, July 3 – 7, 2017.

6. Frandsen, Stine., **Burke, Ryan**., Arnaud-Cormos, Delia., Bardet, Sylvia., Leveque, Philippe. “Effect of *in vitro* calcium-electroporation on mitochondrial membrane potential.” WC2017, 2nd World Congress on Electroporation and pulsed electric fields in biology, medicine and food & environmental technologies, Norfolk, Virginia, USA, September 24 – 28, 2017.